UCLouvain

FACULTE DES SCIENCES

Faculté des sciences

Elaboration of interconnected mixed oxides nanotubes as photocatalytic materials

Author: Romain WEYDISCH

Supervisors: Prof. S. HERMANS, Prof. S. DEMOUSTIER, Dr. F. DRAULT

Jury members: Prof. C. APRILE, Prof. O. RIANT, Prof. L. TROIAN-GAUTIER

Academic year 2023-2024

Master [120] en sciences chimiques, à finalité approfondie

Acknowledgements

Avant tout, j'aimerais remercier sincèrement mes promotrices, les Prof. Sophie Demoustier et Sophie Hermans. Je leur suis vraiment reconnaissant pour leur implication, tous leurs conseils avisés, leur soutien, leur accessibilité et leur bonne humeur m'ayant facilité la réalisation des recherches dans leur laboratoire. Merci pour votre confiance, c'était un plaisir de travailler avec vous et merci également pour l'aide précieuse dans la rédaction de ce mémoire, les relectures et corrections.

Je tiens tout particulièrement à exprimer ma profonde gratitude à mon encadrant, Fabien Drault, qui m'a épaulé tout au long de cette aventure. Merci de m'avoir transmis tant de choses, que ça soit des connaissances sur les matériaux, la photocatalyse,… mais également pour les compétences que j'ai pu acquérir durant cette année. Merci pour les moments de partage, ta disponibilité, tes encouragements, ta rigueur m'ayant permis d'évoluer. Merci pour tes nombreuses relectures. J'espère que nous continuerons à travailler ensemble à l'avenir !

Ensuite, j'adresse mes remerciements au Prof. Carmela Aprile, Prof. Olivier Riant et Prof. Ludovic Troian-Gautier, les membres de mon jury, pour avoir accepté le rôle de lecteurs.

Merci également à notre technicien de laboratoire, Jean-François Statsyns, pour ta bonne humeur et ton aide quotidienne (et la course à pied !). Je remercie Delphine Magnin de m'avoir formé au SEM-EDX, François Devred à la DRX et à l'UV, Cécile D'Haese d'avoir réalisé les analyses XPS et Pierre Eloy de m'avoir appris à utiliser le logiciel Casa XPS ainsi qu'Elodie Devos d'avoir réalisé les analyses ICP. Je tiens également à remercier le Prof. Ludovic Troian-Gautier m'ayant permis d'utiliser son laboratoire pour réaliser les tests photocatalytiques.

Enfin, je tiens à remercier l'ensemble du groupe MOST, Zoé et Grégoire avec qui j'ai eu la chance de partager le bureau durant notre année de mémoire (et les squatteurs du fauteuil : Garance, Estelle, Céline, Loïc, …), Lauraleen, Louise et Antonin qui nous ont aidé au quotidien grâce à leur expérience du doctorat ! En outre, merci plus généralement à toutes les personnes que j'ai pu rencontrer durant mes études, à mes amis qui m'ont accompagné et soutenu, tout comme mes parents, mon frère, mes grands-parents et autres membres de ma famille.

Et de manière plus générale, merci à toutes les personnes qui ont, de près ou de loin, participé à la réussite de mon cursus et de mon mémoire.

Résumé

Le rejet croissant d'eaux usées contenant des molécules organiques persistantes polluantes par les industries est un véritable désastre environnemental. Pour faire face à ce problème, des recherches sont menées pour dégrader les molécules persistantes de manière catalytique. Une approche consisterait à utiliser des photocatalyseurs nanostructurés actifs dans la partie la plus intense du spectre solaire qu'est le visible. La nanostructuration en réseau 3D de nanotubes interconnectés photoactifs permettrait une dégradation en flux continu des polluants. Le TiO_2 est un photocatalyseur abondant et peu coûteux mais ayant l'inconvénient d'absorber dans le domaine ultra-violet, ne représentant que 5% du spectre solaire. La formation d'un oxyde mixte SiO_2-TiO_2 pourrait être l'une des solutions pour déplacer l'absorption dans le visible. De plus, au-delà de son activité photocatalytique intrinsèque, grâce à sa nanostructuration en nanotubes, il peut également servir de support à des complexes ou des nanoparticules également photoactives, et amener des synergies.

Dans ce contexte, l'objectif de ce travail était de synthétiser, de manière contrôlée, des réseaux 3D de nanotubes interconnectés photocatalytiques composés d'oxyde mixte de SiO_2-TiO_2 et de les utiliser en flux continu pour la dégradation du bleu de méthylène, un polluant organique qui peut être considéré comme molécule-modèle. Cette étude s'inscrit dans le cadre du projet CaScadOS, dont le but ultime est de développer des photocatalyseurs nanostructurés multifonctionnels pour réaliser des réactions en cascade complexes en flux continu. Dans un premier temps, les conditions d'une synthèse permettant d'obtenir des nanotubes 1D en TiO_2 dans un « template » en alumine au moyen d'une imprégnation dans un sol-gel ont été optimisées pour utiliser des « templates » en polycarbonate. Grâce à l'optimisation de ces conditions, des nanotubes 1D en TiO_2 de dimensions correspondant aux caractéristiques du « template » utilisé ont été obtenus. En combinant cette synthèse du TiO_2 avec la synthèse du SiO_2 élaborée préalablement sur le projet, et en contrôlant les rapports molaires engagés, différents oxydes mixtes ont été obtenus : SiO_2:TiO_2=10:90, 25:75, 50:50 et 75:25. Les échantillons ont été analysés par XPS et ICP afin de vérifier si la proportion de Si et de Ti incorporés dans les nanotubes était similaire au rapport molaire en Si et Ti introduit dans les solutions de précurseurs. L'effet de la calcination sur la structure cristalline ou amorphe des oxydes obtenus a également été investiguée. Toutes ces synthèses ont été transposées pour obtenir des réseaux 3D de nanotubes interconnectés. Finalement, des tests photocatalytiques de dégradation du bleu de méthylène en flux et en batch ont été réalisés avec les nanotubes 1D de

SiO_2, de TiO_2 et avec des oxydes mixtes de différentes compositions. Bien que les bandes interdites mesurées en UV n'aient pas été déplacées, une amélioration de l'activité photocatalytique a été observée avec un optimum pour un oxyde mixte de composition SiO_2:TiO_2comprise entre 75:25 et 50:50.

Abstract

The increasing discharge of wastewater containing polluting persistent organic molecules by industries is a real environmental disaster. To address this problem, research is being conducted on the catalytic degradation of persistent molecules. One approach involves using nanostructured photocatalysts that are active in the visible part of the solar spectrum, which is the most intense. Nanostructuring photocatalytic materials in a 3D network of interconnected nanotubes would enable pollutants to be degraded in a continuous flow. TiO_2 is an abundant and inexpensive photocatalyst but, has the disadvantage of absorbing in the ultra-violet range, which represents only 5% of the solar spectrum. The formation of a mixed oxide SiO_2-TiO_2 could be one of the solutions for shifting absorption into the visible range. In addition to its intrinsic photocatalytic activity, thanks to nanostructuring into nanotubes, it can also serve as a support for complexes or nanoparticles that are also photoactive, and give synergistic effects.

In this context, the aim of this work was to synthesise, in a controlled way, 3D networks of interconnected photocatalytic nanotubes composed of SiO_2-TiO_2 mixed oxide and to use them in continuous flow for the degradation of methylene blue, an organic pollutant that can be considered as a model-molecule. This study is part of the CaScadOS project; the ultimate aim of this project being to develop multifunctional nanostructured photocatalysts to carry out complex cascade reactions in continuous flow. Initially, the synthesis conditions for obtaining 1D TiO_2 nanotubes in an alumina template by means of sol-gel impregnation were optimised for the use of polycarbonate templates. Thanks to the optimisation of these conditions, 1D TiO_2 nanotubes with dimensions corresponding to the characteristics of the template used were obtained. By combining this TiO_2 synthesis with the SiO_2 synthesis developed earlier in the project, and by controlling the molar ratios engaged, various mixed oxides were obtained: SiO_2:TiO_2=10:90, 25:75, 50:50 and 75:25. Samples were analysed by XPS and ICP to verify if the Si and Ti content incorporated in the nanotubes was similar to the Si:Ti ratio in the precursor solutions. The effect of calcination on the crystalline or amorphous structure of the obtained oxides was also investigated. All these syntheses were transposed to obtain 3D networks of interconnected nanotubes. Finally, flow and batch photocatalytic tests for methylene blue degradation were carried out on 1D SiO_2 nanotubes, TiO_2 nanotubes and different compositions of mixed oxide nanotubes. Although the bandgaps measured by UV-vis spectroscopy did not shift, an improvement in photocatalytic activity was observed with an optimum for the mixed oxides with a SiO_2:TiO_2 composition between 75:25 and 50:50.

List of abbreviations

Ω	Ohm
∅	Diameter
µA	Microampere
µm	Micrometer
°C	Celsius degrees
A	Ampere
Å	Angström
Aq.	Aqueous
a.u.	Arbitrary Unity
AAO	Anodic Aluminium Oxide
ACAC	Acetylacetone
AES	Atomic Emission Spectroscopy
AOP	Advanced Oxidation Process
ARC	Actions de Recherche Concertées
C_B	Conduction Band
CIF	Crystallographic Information File
cm	Centimeter
CVD	Chemical Vapor Deposition
DCM	Dichloromethane
e^-	Electron
EDX	Energy-Dispersive X-ray spectroscopy
E_g	Bandgap
EtOH	Ethanol
eV	Electronvolt
g	Gram
GC	Gas chromatography
h	Hour
H	Height
h^+	Hole
H^+	Proton
H_2O_2	Hydrogen peroxide
HCl	Chloridric acid
ICP	Inductively Coupled Plasma spectroscopy
ICSD	Inorganic Crystal Structure Database
IR	Infrared
K	Kelvin
kV	Kilovolt
L	Litre
M	$mol.l^{-1}$
MB	Methylene Blue

mg	Milligram
min.	Minutes
ml	Milliliter
mm	Millimeter
MO	Mixed Oxide
nm	Nanometer
NO_x	Nitrogen Oxides
NP(s)	Nanoparticles
NR(s)	Nanorod(s)
NT(s)	Nanotube(s)
$O_2^{-\bullet}$	Superoxide radical anion
OH^-	Hydroxide
$^\bullet OH$	Hydroxyl radicals
Pa	Pascal
PC	Polycarbonate
PET	Polyethylene terephthalate
PI	Polyimide
PMMA	Poly(methyl methacrylate)
ppm	Parts Per Million
PPy	Polypyrrole
PVC	Polyvinyl chloride
PVD	Physical Vapour Deposition
PVP	Polyvinylpyrrolidone
(P)XRD	(Powder) X-Ray Diffraction
rpm	revolutions per minute
RSF	Relative Sensitivity Factors
RT	Room temperature
s	Second
SEM	Scanning Electron Microscopy
SiO_2	Silicon dioxide
T	Temperature
TEM	Transmission Electron Microscopy
TEOS	Tetraethyl orthosilicate
TiO_2	Titanium dioxide
TTIP	Titanium isopropoxide
UV(-vis)	Ultraviolet(-visible)
V_B	Valence Band
VOC(s)	Volatile Organic Compound(s)
W	Watt
wt.	Weight
XPS	X-ray Photoelectron Spectroscopy
ZnO	Zinc oxide

Table of contents

CHAPTER I:
Introduction

1.1. Generalities

1.1.1. Environmental challenges

1.1.1.1. Pollutant degradation

The increase in world population and worldwide development is leading to a massive progress in industrial activities. This escalation has undesirable side-effects, particularly the pollution of the biosphere. One of the most polluting industries is the dye industry, which regularly generates wastewater that is harmful to ecosystems. Dyes are used in colouring paper, cosmetics, leather, food and pharmaceutical products, but predominantly in textile fibres.[1] Approximately 15% of the world's dye production is lost during processing and discharged in textile effluents.[2] The release of coloured wastewater containing synthetic persistent dyes in the ecosystem results in significant non-aesthetic pollution, eutrophication and disruption of aquatic life.[1,2] This contamination can disrupt food chains and endanger the health of living organisms, including humans. Therefore, it is crucial to develop methods for degrading these pollutants before discharge to preserve aquatic biodiversity and comply with discharge regulations.[2]

Various methods are available to remove persistent organic pollutants from water including physical methods like adsorption, biological methods such as biodegradation, or chemical methods involving chlorination or ozonation.[3–5] An emerging approach is the use of heterogeneous photocatalysts, which enable the complete mineralisation of most organic pollutants.[2,6] The application of photoactive semiconductors as catalysts, harnessing the inexhaustible and clean energy source provided by the sun (see solar spectrum in **Figure 1**), makes photocatalysis an attractive method for achieving a sustainable and clean future.[7]

Figure 1 shows the solar spectrum, where the ultraviolet (UV) domain represents around 5%, the visible (vis) domain around 50% and the infrared (IR) domain the rest of the light emitted by the sun.

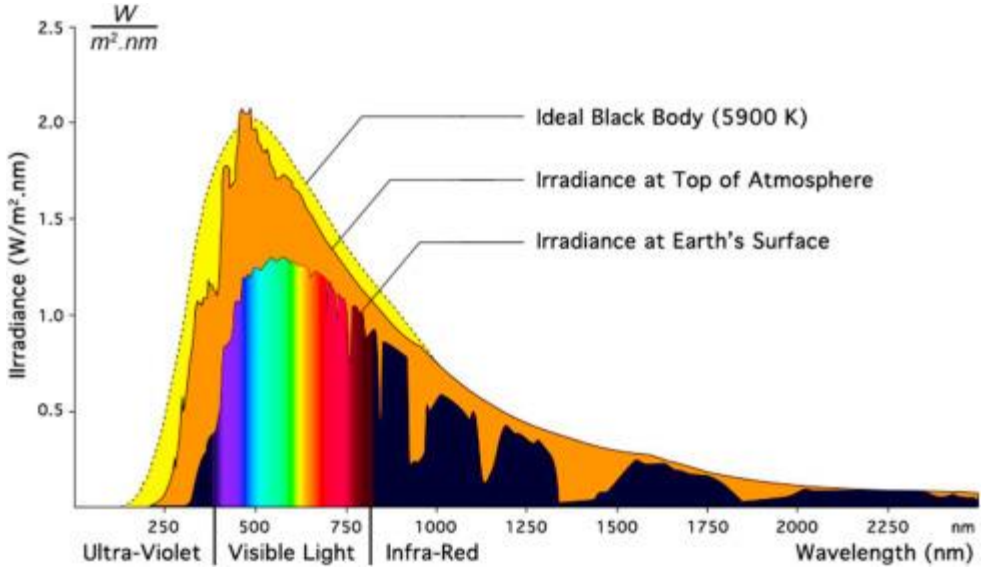

Figure 1*: Theoretical black body spectrum (yellow) and full solar spectrum at earth's surface (black) and the top of atmosphere (orange). Divisions into UV, Visible and IR ranges.*[8]

1.1.1.2. Photocatalytic materials

As previously mentioned, inorganic semiconductors are promising candidates to be used as photocatalytic materials. Inorganic semiconductors have a valence band (V_B) containing electrons and an empty conduction band (AOP). The conduction of the material is determined by the ease with which electrons can transition from the C_B to the V_B. The energy difference between the C_B and the V_B, known as the band gap, determines the minimum energy required to create of electron(e^-)-hole(h^+) pairs (e^--h^+) when the material is photoexcited (if undoped). This can be modulated by hybridation with other materials. Three types of semiconductors are therefore defined: (i) intrinsic, (ii) positive extrinsic (p-type: addition of an e^- acceptor in the band gap) and negative extrinsic (n-type: addition of an e^- donor in the bandgap).[9]

The electron-hole pairs (e^--h^+), known as charge carriers, can migrate towards the surface of the material's particles and generate redox reactions. However, to be effective, the semiconductor must meet certain criteria: (i) absorb over a wide wavelength range in the visible spectrum, (ii) facilitate efficient charge separation and migration and (iii) have energy levels appropriately aligned with the redox potentials of the targeted reactions.

Inorganic semiconductors photocatalysts can be used for various applications, including hydrogen production through water splitting[10,11], carbon dioxide reduction[12], selective compound synthesis (*e.g.* selective oxidation or reduction of aromatics, alkanes and olefins, or

selective C-C or C-N bond formation)[13], disinfection[14] and wastewater treatment. Heterogeneous photocatalysis for the complete degradation of polluting persistent organic molecules is one of the so-called AOP processes, *i.e.* advanced oxidation processes.[2,15,16] In this study, wastewater treatment will be targeted to study the photocatalytic efficiency of our materials. One of these persistent organic pollutants is methylene blue (MB), widely used, as its name suggests, to give the blue colour, primarily in the textile industry.

The MB photodegradation reaction has been extensively studied in the literature and will serve as a model reaction for assessing the photoactivity of the various materials that will be synthesised. MB is a cationic thiazine dye, which contains a phenazonium nucleus as its chromophore, with amino groups functioning as auxochrome groups (**Figure 2**).[17,18]

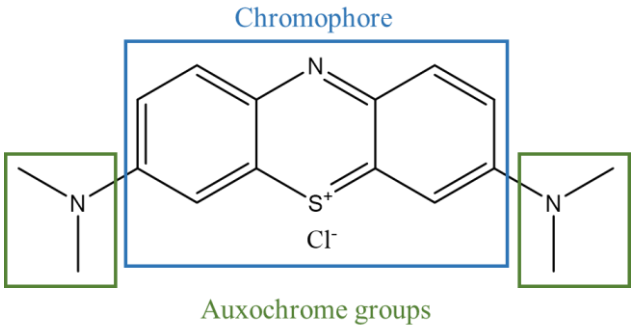

***Figure 2**: Structure of methylene blue.*

The inorganic semiconductor titanium dioxide (TiO_2) is a material of choice for this reaction as photocatalyst due to its long-term stability, good redox efficiency, low cost, non-toxicity.[19,20] The only drawback of TiO_2 is its bandgap requiring relatively high-energy UV light to excite an electron from the catalyst's valence band (V_B) to its conduction band (C_B), as shown in **Figure 3**.[21] Since TiO_2 mainly absorbs in the UV range, much research focused on shifting its absorption into the visible range to more effectively exploit the solar spectrum. TiO_2 properties will be discussed in 1.3.1., after giving some insight into photocatalytic mechanisms.

1.1.1.3. Photocatalytic mechanism

Methylene blue degradation in aqueous media using inorganic semiconductors such as TiO_2 is already well-studied for the reasons outlined in section 1.1.1.2. To reiterate, the primary drawback of TiO_2 is its bandgap, which necessitates a relatively high-energy light beam in the UV range (**Figure 3**).[21] This electronic transition occurs if the energy of the light used for photoexcitation is sufficient, resulting in the creation of an electron/hole pair (e^--h^+).[2,16] These charge carriers then can migrate to the surface of the catalyst and facilitate redox reactions, as depicted in **Figure 3**.

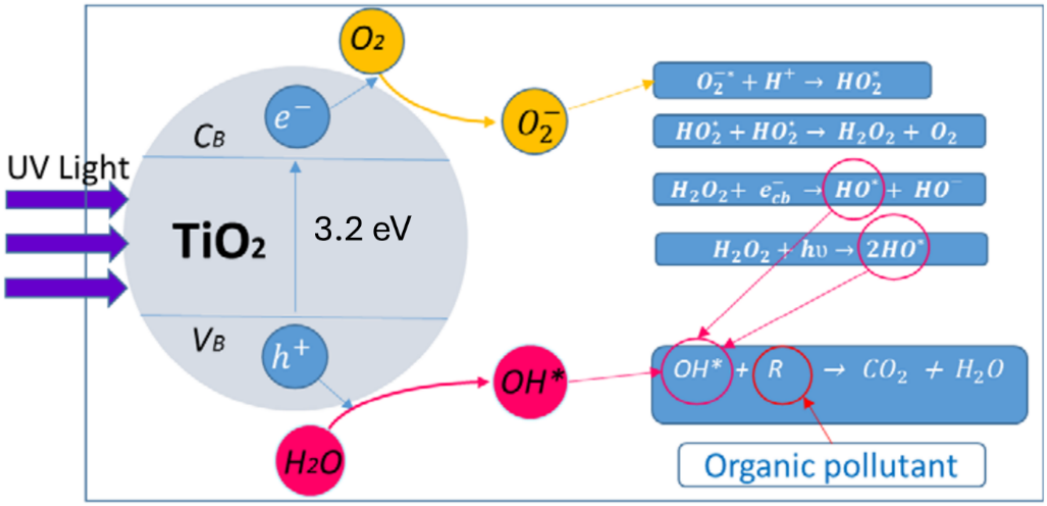

***Figure 3**: Photocatalytic mechanism of TiO_2 for organic molecules degradation.*[21]

In details, the photo-induced electron in the C_B could reduce the surrounding oxygen (O_2) to the superoxide radical anion ($O_2^{-\bullet}$), which subsequently generates hydroxyl radicals ($HO^\bullet$). Superoxide radicals ($O_2^{-\bullet}$) interact with water to produce hydrogen peroxide (H_2O_2). This hydrogen peroxide (H_2O_2) can react with a photoinduced electron from the C_B to produce hydroxyl radicals ($HO^\bullet$). Additionally, hydrogen peroxide (H_2O_2) can be converted into two hydroxyl radicals ($HO^\bullet$) by reacting with the light (hν). At the same time, the photo-induced hole in the V_B will also form hydroxyl radicals ($HO^\bullet$) by reacting with water.[2,16,21] As hydroxyl radicals are highly reactive oxidising species, they can lead to the degradation of the MB into CO_2 and H_2O as well as other by-products. This degradation is not perfect because it releases CO_2, a greenhouse gas. To avoid its release, CO_2 capture and storage can be envisaged.[22]

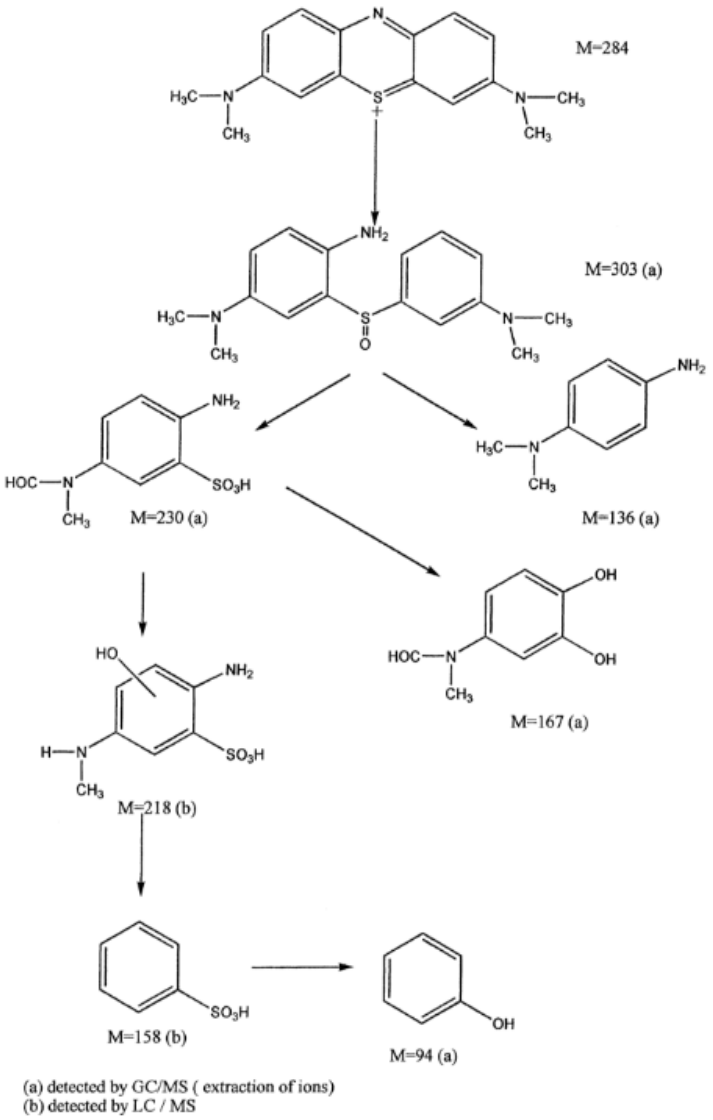

***Figure 4**: Photocatalytic degradation pathway of MB.*[2]

Figure 4 illustrates a probable pathway for MB degradation. The initial step involves an $HO^{\bullet}$ attacking the C-S^{+}=C functional group of the MB. This transition from C-S^{+}=C to C-S(=O)-C necessitates the preservation of the double bond conjugation, resulting in the opening of the central aromatic ring that includes the two heteroatoms, sulfur (S) and nitrogen (N). The sulfoxide group can undergo a subsequent attack by $HO^{\bullet}$ radicals, resulting in the separation of the two benzoic rings. This separation can occur through two distinct mechanisms. The various functional groups are then oxidised. The sulphonic acid (R-SO_3H) is transformed into SO_4^{2-}, the primary amine (R-NH_2) into NO_3^- and the tertiary amines (R-$N(CH_3)_2$) into R-NH_2 (**Figure 5.(a)**). The remaining aromatic rings undergo hydroxylation to open the rings (**Figure 5.(b)**). The end products of MB degradation are much less polluting compounds: CO_2, SO_4^{2-}, NH_4^+ and NO_3^-.[2]

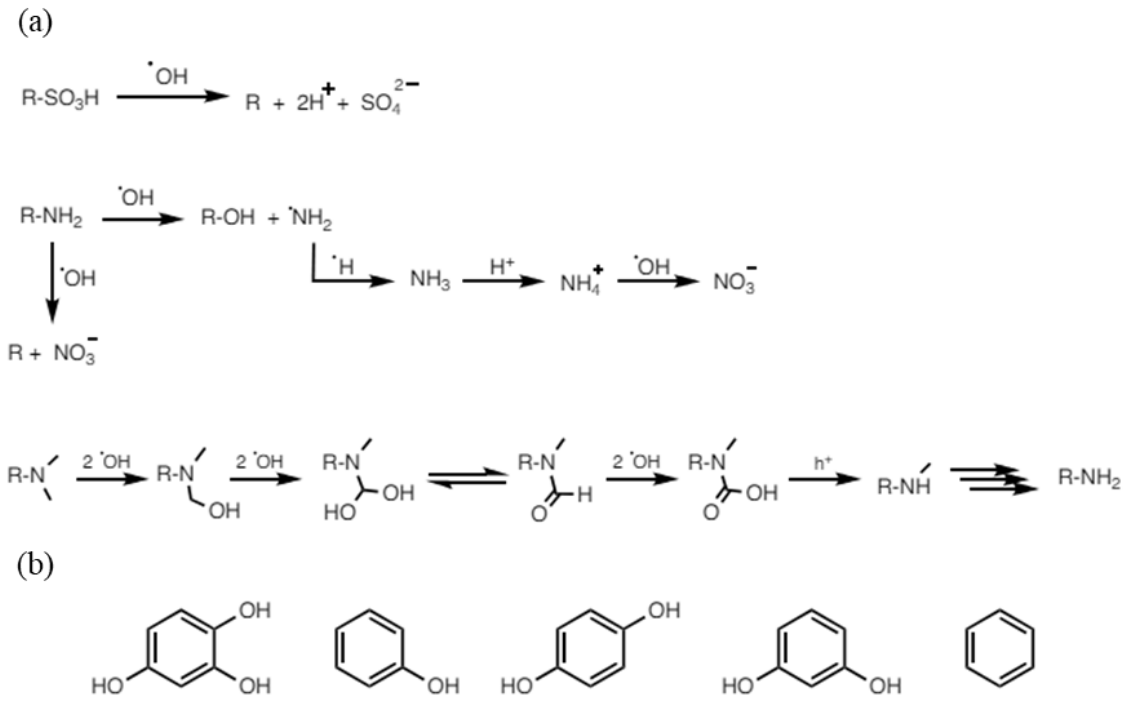

***Figure 5**: (a) Probable reaction pathway for the degradation of the various functional groups in MB and (b) aromatic rings remaining after the last hydroxylations in MB degradation.*[23]

Furthermore, the degradation must take place in a neutral or alkaline environment. In a basic medium, hydroxide (OH^-) ions can be converted into $HO^\bullet$ at the hole (h^+) in the V_B, leading to faster degradation due to the increased concentration of $HO^\bullet$ in solution. Conversely, in an acidic environment, degradation is slowed down due to recombination of $H^\bullet$ radicals (formed when proton (H^+) ions are reduced by an electron present in the C_B) with $HO^\bullet$ radicals, resulting in the formation of H_2O.

1.2. Nanostructuration of materials

Nanostructuring materials imparts unique or enhanced properties compared to their bulk counterparts, including increased strength and durability, greater conductivity and improved catalytic activity. A material is considered nanostructured if at least one of its dimensions is in the nanometre range, *i.e.* from 1 to 100 nm. The advantage of such structures in catalysis lies in their higher surface-to-volume ratio compared to larger particles. Since heterogeneous catalysis is a "surface" chemistry, a higher specific surface area significantly enhances catalytic performance.

Nanomaterials technology offers the ability to control the size and shape of catalytic nanoparticles (NPs), maximising accessibility as well as reactivity and regulating the selectivity of the active sites, thereby improving further the overall performance of the catalysts.[24,25]

Among various nanostructures, nanotubes (NTs) offer major advantages due to their hollow structures, which further increase the specific surface area. This characteristic makes them highly suitable for applications in photocatalysis, electrocatalysis and enzymatic, homogeneous or heterogeneous catalysis.[25]

Replication of the nanoporosity of templates for the elaboration of nanostructures present several advantages, in particular, a precise control over morphology such as well-defined size, shape and configuration. Synthesis of nanostructured materials using a template involves three main steps: (i) preparation of the template, (ii) synthesis of the material of interest using the template and (iii) extraction of the material from the template (if necessary). Almost any material with nanostructured characteristics can serve as a template for nanoscale synthesis. These templates can be soft materials, such as molecular assemblies, or hard materials, such as colloidal particles, patterned solid surfaces or porous membranes.[24]

Nanoporous membranes such as polycarbonate (PC), polyethylene terephthalate (PET) or polyimide (PI) are regularly used as templates for the synthesis of anisotropic nanomaterials with controlled dimensions and aspect ratios, a method known as “hard templating”. These membranes are obtained by irradiating thin films of PC, PET or PI with high-energy particles to form tracks, which are then converted into pores through specific chemical treatments. This technique, called "track-etching" leads to polymer membranes with cylindrical pores of uniform diameter and with tunable pore density over a wide range (10^5 to 10^{10} pores cm^{-2}). Using this

kind of membranes with well controlled and tunable characteristics has already lead to the elaboration of various monodisperse nanowires, nanorods (NRs) and nanotubes (NTs).[26,27]

The external diameter of the NTs is determined by the pore diameter of the membrane, which can range from 10 nm to a few micrometers, while the length of the NTs is governed by the thickness of the membrane and by the deposition conditions of the material. **Figure 6.(a)** shows the empty template, while **Figure 6.(b)** shows the membrane filled with the material of interest. Various synthesis methods within the template are possible: dip-coating[28], electrodeposition[27], chemical synthesis, physical or chemical vapor deposition (PVD or CVD)[29] or sol-gel deposition[30].

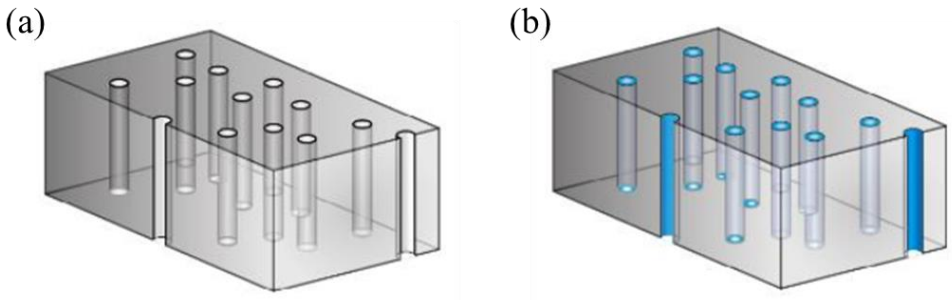

Figure 6*: Illustration of the 'hard-templating' model (a) empty membrane with parallel cylindrical pores and (b) membrane after synthesis filled with the material of interest (depicted in blue).*

NTs feature openings at their ends and along their entire length, allowing access and potential functionalisation of the inner surface, as shown in **Figure 7.(a)**. To force internal functionalisation, this can be carried out before the NTs are released from the PC membrane. This method is described in the article by Drault F. *et al.*[31] for the functionalisation of silicon dioxide (SiO_2) NTs with gold NPs by electroless deposition as described by Kobayashi Y. *et al.*[32] External functionalisation as shown in **Figure 7.(b)** requires the NTs to be released from the PC template. The article by Kim, J. U. *et al.*[33] proposes functionalisation by $TiCl_3$-mediated solution treatment at 80 °C of the outer surface of TiO_2 NTs, producing TiO_2 nano-branch that increase the number of catalytic sites on the surface. If the material is non-porous, it allows for differential functionalisation of the internal and external surfaces (**Figure 7.(c)**). This separation is advantageous when the particles or complexes used for functionalisation are not compatible with each other. Consequently, cascade catalysis can be carried out, *i.e.* two or more reactions in sequence with incompatible catalysts, such as acids and bases or redox couples, or to carry out two different reactions in parallel (= "dual catalysis").

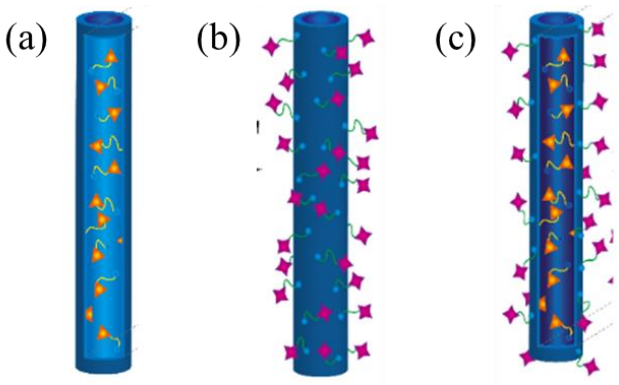

***Figure 7**: Representation of a nanotube with (a) internal, (b) external and (c) multiple functionalisation.*[23]

In the particular case of PC membranes, "track-etched" membranes, supplied by it$_4$ip, are also available with interconnected pores instead of straight ones (**Figure 8.(a)**). This design enables the fabrication of 3D networks of interconnected NRs or NTs (**Figure 8.(b)**). Such structures have been reported in the literature, notably for Au and polymers such as polypyrrole (PPy).[31,34] Or even to form large-area, mechanically stable networks of interconnected 3D nanowires in NiCo ferromagnetic alloys for their interesting magnetoresistive properties.[35] The advantage of these interconnected networks is that they can maintain a macroscopic structural organisation after removal of the template, allowing precise control over the diameter, length, shape, orientation and density of the pores during the synthesis. This type of coherent membrane-like structure of interconnected NTs can be handled and deposited on any substrate, including inside flow-through reactors, hence is highly suitable for applications in continuous flow chemistry and in particular photocatalysis (**Figure 8.(c)**).

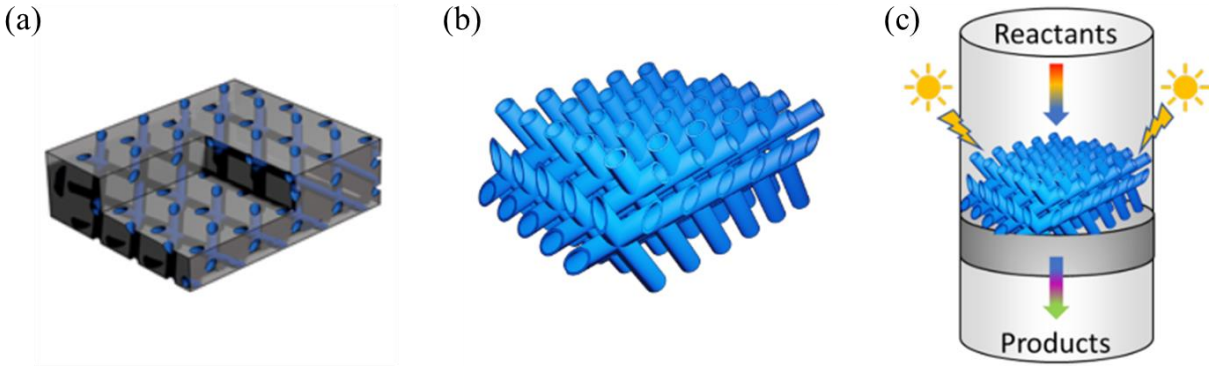

***Figure 8**: (a) "hard-template" to obtain 3D network of interconnected NTs filled with the material of interest (in blue), (b) 3D network of interconnected NTs of the material liberated from the template and (c) use of the 3D network of interconnected NTs in a flow process.*

The advantages of flow chemistry are numerous, particularly in photochemistry. Indeed, flow chemistry allows the photon flux to be focused and therefore higher and more homogeneous, which reduces reaction times and minimises the production of by-products that may result from prolonged irradiation. In addition, flow systems facilitate better heat and material exchange, enabling more efficient multi-phase reactions and preventing the accumulation of products in the reactor.[36] Over time, the productivity in certainly higher than with batch reactions, limited by the overall volume of the vessel and emptying steps.

1.3. Titanium oxide: TiO_2

1.3.1. History, structures, and properties

Titanium dioxide (TiO_2) was discovered in mineral form at the end of the 18th century by the German chemist Martin Heinrich Klaproth during his analysis of ilmenite, an ore with the formula Fe(II)TiO_3 (iron and titanium oxide) containing traces of magnesium, manganese and vanadium.[37] TiO_2 is a chemically stable, non-toxic, biocompatible, environmentally friendly, inexpensive semiconductor material with notable photocatalytic properties. Depending on its chemical composition, it has a wide range of electrical conductivities.[11,38]

TiO_2 exists in the environment in three different crystalline structures: rutile, anatase and brookite, shown in **Figure 9**.[39] These structures are all formed by corner-shared TiO_6 octahedra, where each Ti^{4+} ion is surrounded by an octahedron of O^{2-} ion, giving titanium a coordination number of 6 and oxygen a coordination number of 3. The crystal system of anatase and rutile are tetragonal ($a = b \neq c$, $\alpha = \beta = \gamma = 90°$), whereas brookite is orthorhombic ($a \neq b \neq c$, $\alpha = \beta = \gamma = 90°$).[39] Rutile has a third axis (c) that is smaller than the other two (a and b), while the third axis of anatase is larger than the other two. Each unit cell contains four TiO_2 units.[39]

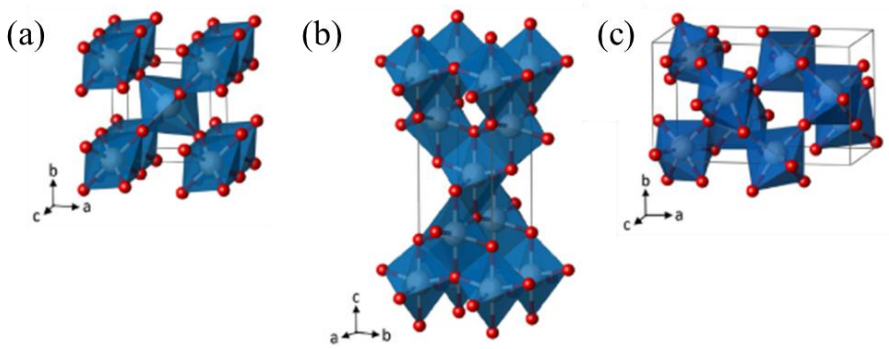

***Figure 9**: TiO_6 polyhedra structures for the TiO_2 phases: (a) rutile, (b) anatase and (c) brookite (Ti (white); O (red)), adapted from*[39].

Only two of the three crystalline structures of TiO_2 are stable: rutile and anatase. Brookite is rarer due to the more complex production conditions and lack of photocatalytic activity. Anatase is metastable at room temperature and irreversibly converts to rutile at around 1000 °C.

Table 1: Important properties of rutile and anatase, adapted from[38].

Polymorph	Rutile	Anatase
Density	4.25 g/cm³	3.89 g/cm³
Metal-to-metal distance (Ti-Ti)	2.69 Å	5.35 Å
Band gap at 10 K	3.05 eV (indirect)	3.46 eV (indirect)
Room temperature mobility in crystal	0.1-1 cm²/Vs	15 cm²/Vs
Room temperature mobility in polycrystalline thin film	0.1 cm²/Vs	0.1-4 cm²/Vs

Rutile is denser than anatase, which results in longer Ti-Ti bonds in anatase. This structural difference directly impacts the bandgap, which is higher for anatase. TiO_2 is, in these two forms, a semiconductor with a wide band gap (> 3 eV). However, the electrical conductivity of TiO_2 is made possible by O vacancies, interstitial Ti atoms or a reduction in the crystalline surface. TiO_2 is only photoactive in the UV range, given its bandgap.[40]

The bandgaps of the different crystalline structures of TiO_2 are called indirect. This means that the photo-induced transition must be assisted by a phonon in addition to the photon. Phonons provide a quantity of energy associated with the elastic vibration of the atoms in a crystal and transfers it to the electron, which modifies the energy and the quantity of movement of the pair e^--h^+.[39] The rutile form of TiO_2 requires less energetic irradiation than anatase (407 nm for rutile versus 388 nm for anatase). Nevertheless, to determine which phase is more active, the mobility of the charge carriers must also be considered. Anatase has significantly higher charge carrier mobility, making it the phase with superior photocatalytic activity.[38,39]

1.3.2. Applications

Up to 90% of the titanium (Ti) consumed to form TiO_2 is used as a white pigment in various applications such as paints, plastics, paper (opacifying agent), textiles, inks, asphalt (brighter pavement for tunnel interiors).[41] TiO_2 is also used as a white pigment in the food additive E171.[41] Additionally, Ti is used in other applications such as an electrode in arc welding, as a mild polishing agent, in sun creams, *etc*.[41]

In medical research, TiO_2 nanostructures are being investigated for various applications, including biosensors, local and controlled drug delivery, for example for cancer (in photodynamic or sonodynamic therapy as a sensitising agent, in computed tomography imaging and radiation therapy as an enhancement and contrast agent), as an antibacterial agent to prevent infections, in implants,...[42,43]

Thanks to these properties, research is also being carried out into the use of TiO_2 in dye-sensitised solar cells as cathode dye-sensitisers or in solar batteries.[44,45] Another major area of research on TiO_2 (and the list is not exhaustive) is its use as a photocatalyst. One application of TiO_2 as a photocatalyst is the use of this material as a photoanode in an electrochemical cell to produce hydrogen. The redox potentials of water are compatible with those of TiO_2, allowing the water splitting into O_2 and H_2.[46]

The photocatalytic property of TiO_2 can also be used to produce self-cleaning facades or glass by adding particles to the material, but also and above all to purify air and water of persistent organic molecules. The principle behind these applications is based on the degradation of organic molecules through the generation of radicals, as explained in section 1.1.1.3. Additionally, TiO_2 exhibits photo-induced superhydrophilicity, which enables rainwater to form a film instead of droplets, allowing it to slide off surfaces by gravity while cleaning them.[40,41,47,48]

1.3.3. Synthesis methods of TiO_2 NTs

One of the most widely used methods in the literature for obtaining titania nanotubes is a combination of sol-gel and hard templating techniques. Hard templating is the use of a preformed mold with nanoscopic cavities that can be removed afterwards to give the nanostructured material, while sol-gel refers to widespread techniques involving hydrolysis/condensation of molecular precursors in solution to form colloidal suspensions (sol) that further polymerise into a gel (reticulated material with entrapped solvent molecules) that precipitates or can be dried/calcined into a solid form (usually a powder) as shown in **Figure 10**.[49] However, other methods for the synthesis of TiO_2 NTs are also well described, such as electrochemical anodisation of a titanium metal sheet[50], electroless metal deposition[51], atomic layer deposition[20], hydrothermal treatment of TiO_2 NPs with an alkali solution[52], hydrolysis of TiF_4 under acidic conditions[53],...

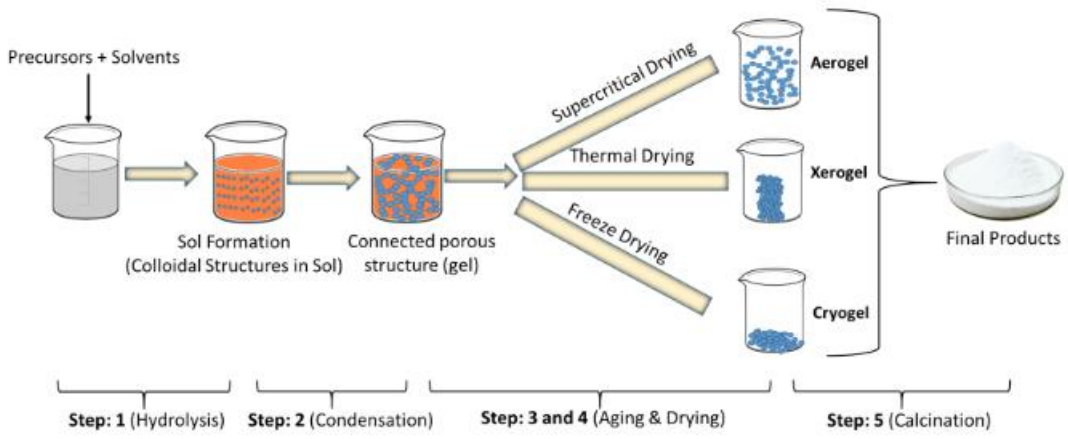

***Figure 10**: Steps involved in sol–gel process to synthesise metal oxide nanoparticles.*[49]

The use of PC templates for the synthesis of TiO_2 NTs to our knowledge has never been previously documented. It is by modifying the track-etched template and therefore the pore structure that we can obtain NTs or 3D networks of interconnected NTs. The advantage of the PC template over other types of templates such as Anodic Aluminium Oxide (AAO) membranes lies in the ease of extraction. Indeed, NTs/3D networks of interconnected NTs can be easily extracted from their PC template either by dissolving the PC in a solvent such as dichloromethane (DCM), if the material is resistant to the DCM, or by calcination.[31] Whereas the release of NTs from the template in AAO generally requires dissolution of the alumina membrane under difficult conditions (strongly basic or acidic solutions) and in an additional step after calcination.[31]

The synthesis of TiO_2 NTs by template impregnation (AAO membrane) combined with a sol-gel process has been reported by Zhang M. *et al.*[54] They obtained thin-walled TiO_2 NTs (not NRs) using the preparation of a typical sol-gel starting solution with molar ratio TI:ACAC(Acetylacetone):H_2O:EtOH(Ethanol)=1:1:3:20 where TI stands for titanium isopropoxide (TTIP).[54] ACAC, or acetylacetone, acts as a chelating agent and by bonding to the TiO_2 precursor (TTIP), it reduces the rate of hydrolysis of the Ti precursor, leading to the formation of smaller diameter particles.[55,56] The AAO membrane is then impregnated for 10 minutes (min.) in this sol-gel suspension, before being dried at room temperature (RT) for one day and then calcined at 400 °C for another day. The template is then removed by harsh basic treatment.[54] This method primarily produced broken NTs with wall thicknesses ranging from 15-20 nm (**Figure 11**). The authors reported that the wall thickness can be controlled by adjusting the quantity of ACAC in the initial solution. Decreasing the amount of ACAC results in thinner tubes.[54] Additionally, another way to control the wall thickness of the tubes is by modifying the template impregnation time, as reported by Hulteen J. and Martin R.[57]

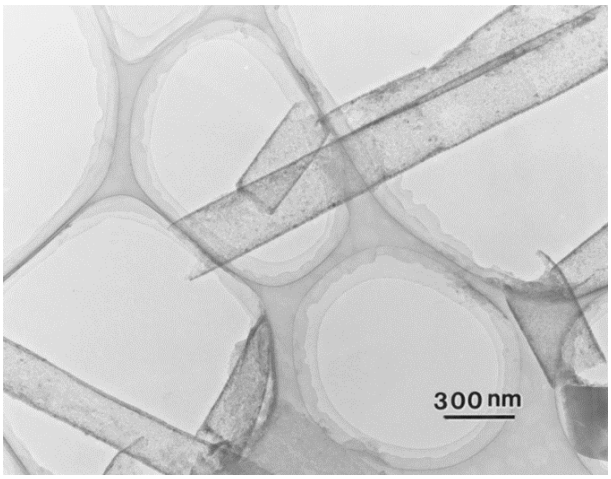

***Figure 11**: TEM images of broken TiO_2 nanotubes with a wall thickness of 15–20 nm obtained in AAO membrane.*[54]

As previously mentioned in section 1.1.1.2., the primary drawback of TiO_2 in photocatalysis is that it absorbs in the UV due to its bandgap around 3.2 eV, which represents only 5% of the solar spectrum. To address this limitation, various strategies have been proposed to shift its absorption towards the visible range, which represents almost half the solar spectrum. These strategies include doping with other elements such as N, V, Rb, Ni, and Fe, coupling with other semiconductors, and nanostructuring, among others. Additionally, these strategies can help to reduce the recombination of charge carriers and improve light absorption and conductivity.[58,59] By combining TiO_2 with SiO_2, it is possible to leverage the beneficial properties of both materials. SiO_2 can provide a high surface area and good thermal stability, while TiO_2 contributes its photocatalytic properties. The goal of this combination is to enhance photocatalytic activity by improving charge separation, increasing surface area, and potentially shifting the absorption towards the visible spectrum. This particular mixed oxide will therefore be introduced in the next section.

1.4. Mixed oxide: SiO_2-TiO_2

1.4.1. History, and interests

Mixed oxides naturally existed for a long time, but their in-depth study and technological applications developed mainly during the 20th century, with notable advances in the 1970s and 2000s for transition metal oxides.[60] SiO_2:TiO_2 mixed oxides can be used as low-thermal-coefficient glasses, materials for encapsulating catalysts such as in Ziegler-Natta polymerisation, for liquid-phase oxidation, and as heterogeneous catalysts for various selective oxidation reactions: H_2S, volatile organic compounds (VOCs) and nitrogen oxides (NO_x) reduction.[61,62] They can also be used, as in this work, to carry out photocatalytic reactions. This mixed SiO_2:TiO_2 oxide can be used as a photocatalyst for water splitting, as a photocatalytic antibacterial agent, and of course for the degradation of polluting organic molecules such as MB.[63–65]

1.4.2. Synthesis methods

Various synthesis methods can be employed to obtain mixed oxides such has impregnation, precipitation, reverse suspension but the most common is the sol-gel process.[66–68] The sol-gel process offers versatility and control over the composition and structure of the resulting mixed oxides. Among the various sol-gel methods, two main approaches are the non-hydrolytic and “classic” sol-gel methods.

The non-hydrolytic sol-gel method involves the mixing of the metal precursors of the different oxides in an organic solvent, in an autoclave and under an inert atmosphere to avoid the presence of water. The mixture is then heated under pressure and in an inert atmosphere, allowing the precursors to condense and form a wet gel, *i.e.* a three-dimensional network swollen with solvents and the by-products of the reaction. This gel is then dried under vacuum to obtain a dried gel, then calcined under a flow of dry air (leading to evacuation of organic residues) to obtain the oxide. While this synthesis favours the formation of Si-O-Ti bonds in the particular case of SiO_2:TiO_2 mixed oxides, it requires relatively long reaction times, such as four days in the autoclave, and the entire synthesis must be conducted without the presence of water hence under tight control.[61,69]

The second method is a "classic" sol-gel process. It involves reacting the metal precursors in a solvent, usually water, followed by drying and calcination to obtain the mixed oxide. This method is much faster than the first described above but carries a risk of obtaining single domains due to differences in hydrolysis rates of the two precursors. To avoid this risk and to obtain good homogeneity as well as numerous Si-O-Ti bonds, the pre-hydrolysis stage of the solution to form the gel is crucial.[61,62]

Combining the second synthesis method with the PC template could enable tube-shaped nanostructures to be obtained in a controlled manner. As mentioned previously, control of the ageing time of the two precursors to obtain Si-O-Ti bonds will be essential due to their different hydrolysis rates. As the hydrolysis rate of tetraethyl orthosilicate (TEOS, Si precursor) is much slower than that of TTIP (Ti precursor), one solution outlined in the article by Cheng P. *et al.*[70] is to first introduce TEOS into a mixture of pure ethanol, distilled water and hydrochloric acid with stirring and then, after hydrolysis of TEOS for 1 h, slowly add TTIP to the first mixture. The solution is then stirred for a further 2 h.[70] Different compositions of SiO_2:TiO_2 mixed oxides can be obtained by varying the initial molar ratios of TEOS:TTIP.[70–72] This method allows for precise control over the composition and structure of the mixed oxides, leading to tailored properties for specific applications. The article by Cheng P. *et al.*[70] investigates SiO_2:TiO_2 mass ratios ranging from 10:90 to 50:50, with an optimum of 30:70 as a photocatalyst. The paper by Anderson C. and Bard A. J.[72] also proved that the ratio SiO_2:TiO_2 of 30:70 has the highest photocatalytic activity, with tested ratios ranging from 10:90 to 75:25.

1.4.3. Structures and properties

Numerous articles in the literature report an enhanced photocatalytic activity for mixed oxide nanocomposites compared to pure TiO_2, which can be attributed to several factors. A first reason is the increase in thermal stability, which reduces the phase transformation of anatase to rutile and also prevents the formation of large grains of TiO_2.[73] Reduced crystallites size increase catalytic efficiency but if the quantity of SiO_2 becomes too large, the size of the TiO_2 crystallites becomes too small and recombination of charges on the surface is favoured.[11] Moreover, excessive SiO_2 content can also lead to phase separation, adversely impacting catalytic properties.[70] A second reason is the increase in adsorption of reagents close to the catalytic centres (TiO_2) and the increase in the specific surface area of the catalyst as well as an increase in the stability of the porous structure.[11,70,73] The formation of Si-O-Ti bonds and the presence of vacant oxygens in the structure facilitate the mobilisation of photogenerated oxidisers on the catalyst surface, including on SiO_2 sites.[72] This modification also positively affects the surface acidity from Brönsted to Lewis acid character with maximum acidity correlating with the maximum photocatalytic activity.[73] An important reason for the increase in photoactivity is the decrease in recombination of photogenerated electrons (e^-) and holes (h^+). Adding SiO_2 has the effect of increasing the rate of transfer of e^- and h^+ to species in solution. Moreover, strong adsorption of reagents facilitates rapid utilisation of hydroxyl radicals generated, thereby reducing the probability of recombination with an e^-.[72] These synergistic effects contribute to the overall enhancement of photocatalytic activity in mixed oxide nanocomposites.

A mechanism proposed in the literature for MB degradation in the presence of a mixed SiO_2:TiO_2 oxide is shown in **Figure 12**. According to the literature, the presence of Si-O-Ti bonds enables charges carriers (e^- and h^+) to be easily separated and transferred between TiO_2 and SiO_2. As a reminder, these charge carriers are generated when the catalyst is photoexcited with an energy equal or greater than the bandgap value.

The hole (h^+) induced in the V_B of TiO_2 will be able to migrate rapidly into the V_B of SiO_2, while the electron (e^-) photoinduced in the C_B of SiO_2 will be able to migrate rapidly into the C_B of TiO_2. This process is rapid due to the close potential differences between the C_B and V_B of the two oxides SiO_2 and TiO_2. The rapid transfer of charge carriers between TiO_2 and SiO_2 slows down the recombination of e^- with h^+. The overall process can be summed up as the

photoexcitation of an electron from the V_B of SiO_2 to the C_B of TiO_2. In a similar way to TiO_2 alone, the e^- in the C_B of TiO_2 and h^+ in the V_B of SiO_2 can generate $HO^\bullet$ which is used to degrade the MB (see **Figure 3**).[64,74]

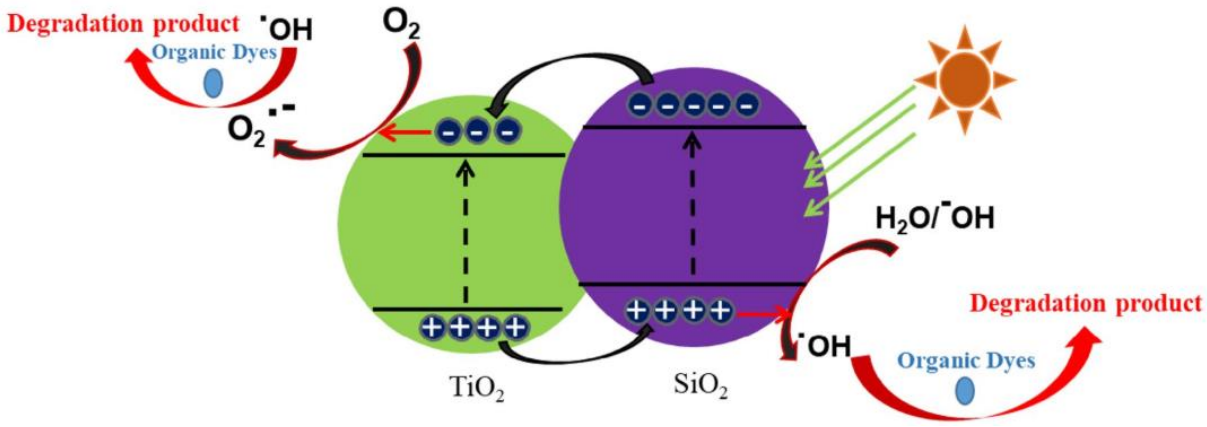

***Figure 12**: Schematic of the photocatalysis MB degradation mechanism on SiO_2:TiO_2 surface.*[74]

According to the paper by Ting P.K. *et al.*[66], the bandgap location of the SiO_2:TiO_2 nanocomposite is closer to the infrared and visible regions compared to SiO_2 and TiO_2 alone, indicating a decrease in bandgap.[66]

However, determining the bandgap (E_g) of modified semiconductors from UV-visible spectra can be challenging due to the presence of a shoulder in the UV spectra of hybrid materials, complicating the extrapolation of a linear part for bandgap determination. To address this, the article by Makuła, P. *et al.*[75] discusses of an alternative for more accurately determining the bandgap value from UV-visible spectra for modified semiconductors, particularly in the case of TiO_2 modified with SiO_2. The suggested method offers a more robust approach for determining E_g, as shown in **Figure 13**. This method consists of taking into account the observed shoulder and the main peak of the semiconductor. The extension of the shoulder as shown in **Figure 13** serves as baseline (blue dotted line). The linear portion of the main peak of the semiconductor is also traced, this is the red dotted line in **Figure 13**. The intersection between these two lines provides the bandgap value for the modified semiconductor in question. This method should be used in this work to determine the bandgap of synthesised SiO_2:TiO_2 mixed oxides as reliably as possible. As photocatalytic properties will directly be connected to bandgap values, and bandgaps values are connected to composition and characteristics of the materials, controlled through synthesis, determining the bandgap is useful to establish structure-activity relationships.

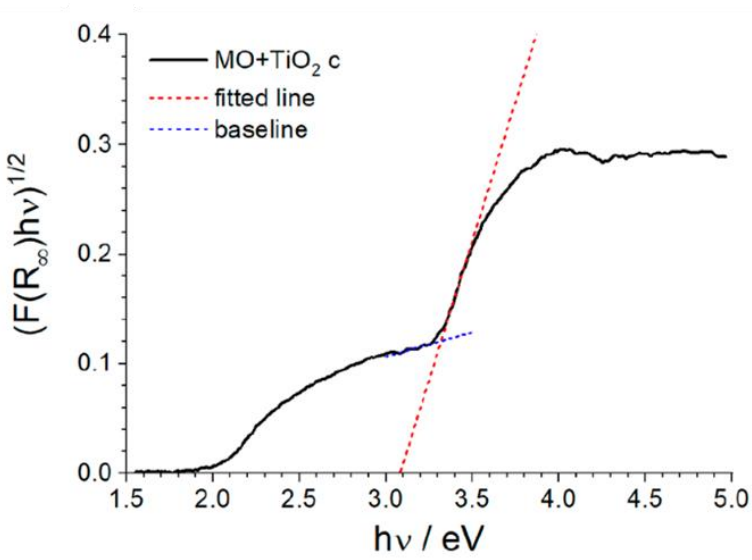

***Figure 13**: Illustration of the bandgap determination method for titania-based mixed oxides.*[75]

1.5. Master Thesis objectives

This Master Thesis is part of the ARC (Actions de Recherche Concertées/Concerted Research Actions) project entitled "Spatial compartmentalisation of multiple active sites on arrays of interconnected porous nanotubes for cascade catalysis - CaScadOS" led by Professor Sophie Demoustier-Champagne, Professor Olivier Riant and Professor Sophie Hermans. The general aim of this project is to prepare 3D networks of functional NTs, to enable the development of (photo-)catalytic membranes for cascade reactions in continuous flow reaction. This Master Thesis is based on the previous work carried out by Dr. F. Drault on the elaboration and characterisation of SiO_2 NTs by combining a sol-gel and a hard templating method as part of the CaScadOS project.[31,76]

The aim of this Master Thesis is to go one step further and to synthesise a new type of material, namely SiO_2:TiO_2 mixed oxide nanotubes, with a tight control on Si:Ti ratios and their structuration in 3 dimensions using porous polycarbonate membranes with straight or interconnected pores to develop a photocatalytically active support. To achieve this global objective, we aim to answer various research questions, as detailed below:

Firstly, is it possible to use polycarbonate membranes as a template to control the morphology of TiO_2 during synthesis? Which parameters of the synthesis are important for successful templating?

Then, is it possible to combine the synthesis method for obtaining SiO_2 NTs with the one for TiO_2 in order to obtain mixed oxide NTs? Is it possible to control the Si:Ti ratio in the obtained oxides and with which accuracy?

Next, is it possible to obtain 3D membranes made of interconnected TiO_2 NTs and mixed oxides NTs of different compositions, under conditions identical to those developed for 1D NTs? Are there any changes to be made in the protocol for synthesis to do so?

Finally, do the synthesised materials have photocatalytic activity? Are mixed oxides more active than TiO_2 alone in the visible range? Is there a shift from UV to visible light absorbance for mixed oxides compared with TiO_2?

1.6. Methodology

To achieve these specific objectives and answer the scientific questions, the work is divided into four experimental phases, corresponding to the four sections of the 'results' chapters in this manuscript. The first part consists in the optimisation of 1D TiO_2 NTs synthesis with a sol-gel process adapted to hard templating using track-etched PC membranes. The second part is the combination of the sol-gel SiO_2 and TiO_2 synthesis methods with hard templating to obtain mixed oxide 1D NTs with controlled SiO_2:TiO_2 ratios in the resulting materials. The third section involves the adaptation of the 1D NTs synthesis process to obtain 3D interconnected NTs. Finally, photocatalytic tests are performed on different materials to study their activity using the photodegradation of methylene blue as model reaction.

In more details, the first part consists in adapting a reported method for the synthesis of TiO_2 NTs using a sol-gel process combined with hard templating in an AAO membrane to our PC template.[54] All materials will be characterised by SEM (Scanning Electron Microscopy) and the most interesting ones by TEM (Transmission Electron Microscopy). (P)XRD ((Powder) X-Ray Diffraction) analysis will be carried out to determine the crystallinity and phases formed.

The second part of this project focuses on the synthesis of SiO_2:TiO_2 mixed oxides by controlling the ratios of Si:Ti in the mixed oxides produced and the desired NT morphology by means of hard templating. This synthesis step will be based on the combination of two well-established sol-gel synthesis techniques: the synthesis for obtaining SiO_2 NTs developed by Dr. F. Drault[31] and the synthesis for obtaining TiO_2 NTs developed in the first part of this master thesis, combined with the expertise in hard templating in PC membranes developed in the CaScadOS project. The molar ratios of the precursors involved, the use of HCl in the synthesis, the method of ageing the solution to form the gel from solution and the incorporation of Si and Ti into the final material will be investigated and optimised. The materials will be studied mainly by SEM-EDX (Energy-Dispersive X-ray spectroscopy) and occasionally by TEM. In order to quantify the SiO_2:TiO_2 ratios within the mixed oxides obtained, XPS (X-ray Photoelectron Spectroscopy) will be carried out and ICP-AES (Inductively Coupled Plasma spectroscopy - Atomic Emission Spectroscopy) will be used to confirm that the surface composition does reflect the composition of the material in the bulk. UV-vis measurements will be carried out to determine the bandgap of the photo-active materials so obtained.

The third part consists of synthesising 3D membranes made of interconnected NTs of TiO_2 and mixed oxides (SiO_2:TiO_2) with different ratios. To achieve this, a porous polycarbonate template with interconnected pores will be used and the reaction conditions adapted. The obtained materials will be studied by SEM-EDX. Additionally, UV-vis measurements will be carried out to determine the bandgap of the different materials.

Finally, continuous flow and batch photocatalytic tests under visible irradiation will be carried out for the methylene blue degradation reaction over the different materials prepared. The methylene blue degradation will be monitored by UV-visible analysis, measuring the area under the curve of absorbance peaks during 1 h.

This manuscript is divided into 4 different parts. After the first introductory part, an experimental section is developed, detailing the chemicals used, the experimental methods and the characterisation techniques employed. The results concerning the different materials synthesised and photocatalytic activities will be discussed in the third section. Finally, the last section will conclude on the work carried out through the year and give some perspectives for future exploration. The document closes with a list of references and Appendix.

CHAPTER II:
Experimental section

2.1. Solvents and reagents

All chemical reagents and solvents used during this project are listed below in alphabetical order with their purity and supplier under brackets. Unless otherwise specified, they were used without further purification.

Acetylacetone (for analysis EMSURE, Sigma-Aldrich, ACAC), Chlorohydric acid (Aq. 30%, Sigma-Aldrich), Dichloromethane (DCM, for analysis AnalR NORMAPUR Reag. Ph. Eur., VWR Chemicals), Ethanol absolute (for analysis AnalR NORMAPUR Reag. Ph. Eur., VWR Chemicals), H_2O Milli-Q (instrument VWR Puranity PU 15+), Tetraethyl orthosilicate (TEOS, ≥ 99.0% (GC, gas chromatography), Sigma-Aldrich) and Titanium Isopropoxide (for analysis Technipur, Sigma-Aldrich).

2.2. Templates

The syntheses of 1D and 3D nanotubes were performed using polycarbonate (PC) track-etched membranes supplied by it$_4$ip with straight and interconnected pores, respectively. Their characteristics are listed in the **Table 2**.

Table 2: Characteristics of the PC track-etched membranes used as templates.

Name	Pore diameter (µm)[a]	Pore density (cm^{-2})[b]	Thickness (µm)[c]	PVP treatment[d]
1D (M002)	0.4	$1.6x10^8$	25	Yes
3D (M007)	0.3	$2.8x10^8$	25	No

[a]Tube diameter
[b]Maximum number of tubes formed per cm^2
[c]Maximum tube length
[d]PVP (Polyvinylpyrrolidone) surface treatment increases the membrane hydrophilicity

2.3. Synthesis of simple oxides

2.3.1. Synthesis of pure TiO_2 nanotubes using PC templates

The formation of TiO_2 nanotubes (NTs) is performed by the combination of a sol-gel method and the dip-coating of a PC membrane, which is used as a hard template. This method is inspired from the literature where Zhang M. *et al.*[54] used the combination of AAO membranes and sol-gel methods for titania nanotubes elaboration (method described in section 1.3.3.).

Typically, to impregnate a PC template measuring 1 cm² (1 cm x 1 cm), 60 ml of sol-gel solution (volume required to immerse fully the membrane in our set-up) was prepared by adding 33.3-34.2 g ethanol, 3.6-3.8 g ACAC and 10.3-10.6 g TiO_2 precursor (as the quantities involved have been optimised, the masses depend on the molar ratios tested), namely titanium isopropoxide (TTIP), in that precise order. The volume (V) of Milli-Q water was then added drop by drop using a micropipette (p-1000) under magnetic stirring at 600 rpm (revolutions per minute). The solution was then left to mature without stirring during 0 min.-3 h (t_1) before immersing the PC membrane(s) in its Teflon holder (see Appendix 1) during 20 min.-1 h 30 (t_2) under gentle stirring at 600 rpm (the shape of the Teflon holder allows the magnetic stirrer to pass underneath the holder). In this sol-gel process, we considered that the gel was formed at the end of the ageing time and before that, it would be called a solution. The solution becomes increasingly viscous and turbid as it ages, to form the gel. After the impregnation step, the PC membrane surfaces were cleaned using a tissue (Kimtech) prior to a drying step at 100 °C for 24 h. The molar ratios of ACAC and H_2O will be optimised, as well as the times for ageing the solution to form the gel and for impregnating our template into the gel, in order to adapt the synthesis to the use of our porous PC membrane as a hard template.

For the synthesis in a template of 25 cm² (5 cm x 5 cm), the same protocol was used but with an increase in the volume of the initial solution to form the sol-gel. A 600 ml solution with the same molar ratio as the 60 ml solution was made up in order to completely immerse the larger PC template in its Teflon holder (see Appendix 2).

Some samples were calcined after the drying step to release the NTs from the PC membrane. For this, the PC membranes containing the NTs were introduced into a crucible measuring 9 x 4.5 mm (Ø × H) covered with its 9 mm diameter lid for 1 cm² PC membranes. For 25 cm² PC membranes, a crucible measuring 50 x 40 mm (Ø × H) covered with its 50 mm diameter cover was used. The assembly was introduced into a muffle furnace and positioned in the middle of the furnace. The oven was programmed to reach a temperature of 600 °C for 2 h with a temperature ramp of 10 °C/min. Subsequently, the oven was left to cool naturally to room temperature (RT). The powder was then recovered and stored away from light in a closed vial without any other special precautions.

2.3.2. Synthesis of pure SiO_2 nanotubes within a PC template

The formation of SiO_2 nanotubes is also performed by the combination of a sol-gel method and the dip-coating of a PC membrane, which is used as template. This method is a reproduction of a synthesis optimised in our lab and described in a publication by Drault F. *et al.*[31]

Typically, 60 ml of sol-gel solution (volume required to immerse fully the membrane in our set-up) is prepared by adding 34.19 g ethanol, 4.28 g water, 1.29 g HCl (1 $mol.L^{-1}$ (M)) and 10.52 g of the SiO_2 precursor, namely tetraethyl orthosilicate (TEOS), in that precise order. The solution was then left to age without stirring during 3 h at RT. The PC membrane(s) kept in its Teflon holder (see appendix 1) was then immersed in it for 1 h 30 at RT under stirring at 600 rpm. The polycarbonate membrane(s) was recovered and the excess of solution was removed using a Kimtech before being left to dry in an oven at 100 °C for 24 h.

2.4. Synthesis of mixed oxide nanotubes (SiO_2-TiO_2) within a PC template

2.4.1. Method 1: mixing of two differently aged solutions to form the gel

Typically, a first solution containing the SiO_2 precursor, TEOS, was prepared according to the method described by Drault F. *et al.*[31] A solution containing ethanol, water, chloridric acid (HCl) and TEOS was prepared and left to stand for 3 h so that the gel could form. The ratio of EtOH:H_2O:HCl:TEOS of this first solution is 14.7:4.7:0.7:1. In parallel, another solution containing the TiO_2 precursor, TTIP, was prepared using the method described in section 2.3.1. and adapted from the article by Zhang M. *et al.*[54] A solution containing ethanol, ACAC, TTIP and water was prepared and left to stand for 1h to allow the gel to form. The ratio of EtOH:ACAC:TTIP:H_2O in this second solution is 20:1:1:5.

The first solution was then added to the second one, giving a total volume of 60 ml, under stirring at 600 rpm for one minute to homogenise the resulting solution. The ratio between the two precursors can be varied, but the molar ratios within the two solutions must be respected.

The PC membrane in its Teflon holder was then immersed in it for 1 h 30 at RT under stirring at 600 rpm. The membrane(s) was then removed from the solution and the excess was eliminated using a Kimtech before being left to dry in an oven at 100 °C for 24 h.

Different Si:Ti molar ratios have been investigated: 25:75, 50:50 and 75:25, while maintaining constant the molar ratios of the different components within the solutions containing the precursors.

2.4.2. Method 2: Preparation of one solution containing the two precursors

Typically, a first solution containing the SiO_2 precursor, TEOS, was prepared according to the method previously described in section 2.3.2.[31] This solution containing ethanol, water, HCl and TEOS was prepared and left to stand for 2 h so that the gel could form. The ratio of EtOH:H_2O:HCl:TEOS of this first solution is 14.7:4.7:0.7:1. In parallel, another solution containing the TiO_2 precursor, TTIP, is prepared using the method described in the section 2.3.1. and adapted from the article by Zhang M. *et al.*[54] A solution containing ethanol, ACAC, TTIP and water was prepared with a ratio of EtOH:ACAC:TTIP:H_2O equal to 20:1:1:5. This solution was added under stirring at 600 rpm to the solution containing the SiO_2 precursor

(TEOS). The resulting mixed Si:Ti solution was then stirred for one minute to homogenise it and then left to stand for one hour to allow the gel to form. Note that the total volume of the two solutions together should be 60 ml. The ratio between the two precursors can be varied, but the molar ratios within the two solutions must be respected.

The PC membrane(s) in its Teflon holder were then immersed in the mixed gel suspension for 1 h 30 at RT under stirring at 600 rpm. The membrane(s) were then removed from the solution and the excess was eliminated using a Kimtech before being left to dry in an oven at 100 °C for 24 h.

Different Si:Ti molar ratios have been investigated: 25:75, 50:50, 75:25 and 90:10, while maintaining constant the molar ratios within the solutions containing the precursors.

2.5. Nanotubes release from the PC templates

The release of the materials from the PC template is an important step to characterise the nanotubes using analytical methods such as SEM, EDX, TEM, XPS, XRD or to carry out the photocatalytic tests. Two different methods, described below, were employed depending on the type of characterisation carried out.

2.5.1. Release of nanotubes in a solvent

The most common method to release the synthesised nanotubes from the polymer template consists of dissolving the PC membrane in DCM. Between 3 and 5 ml of DCM were used to dissolve approximately a quarter of a 1 cm^2 membrane. This release method is simple, fast and uses less solvent than other release methods. The only disadvantage of this method is that some undissolved or re-precipitated PC may remain and be visible during analysis. This method is used before SEM and TEM analysis.

2.5.2. Release of nanotubes on PET (Polyethylene terephthalate) membrane

A Millipore filtration system was used under vacuum using a Büchner system. A grid with 150 µm holes is used as a rigid support. A PET membrane , used as a holder for the material released from the PC membrane, was deposited above the metallic grid. The PC template filled with the inorganic oxide is then deposited on top. Up to 30 ml of DCM was gradually added on the membranes using a pipette. Then, the sample was left to dry on the Büchner under air flow. This technique has shown to be highly effective to eliminate the residual PC on the samples but was highly consuming in solvent. Nevertheless, this method allows the complete release of a 1 cm² membrane. It was used to release both 1D NTs and 3D networks of interconnected NTs before carrying out solid-state UV-vis analysis, XRD, XPS and photocatalytic tests.

2.6. Photocatalytic tests

2.6.1. Photodegradation of methylene blue

The photocatalytic activity of selected materials is studied for the (photo)degradation of methylene blue ($C_{16}H_{18}ClN_3S$, MB), an organic dye, in water.

The quantification of MB degradation for the photocatalytic flow tests was carried out using a liquid UV-visible spectrometer set-up with “Microplate Readers” (Molecular Devices, SpectraMax iD3) based on a calibration curve. In details, the integral of the area under the MB absorbance peak was taken between 420 and 750 nm for 5 different MB solutions of known concentration ranging from 2 $mg.L^{-1}$ to 12 $mg.L^{-1}$ (see section 3.4.1.).

The quantification for batch photocatalytic tests was carried out using a UV-visible spectrometer (Agilent technologies, Cary 60 UV-Vis spectrophotometer) based on a calibration curve. In details, the integral of the area under the MB absorbance peak curve was taken between 530 and 730 nm for 5 different MB solutions of known concentration ranging from 2 and 12 $mg.L^{-1}$ (see section 3.4.2.).

In this work, irradiation was carried out with Thorlabs OSL2IR lamps between 400 and 1800 nm to obtain irradiation in the visible range (spectrum of the lamp in Appendix 3). For some tests, a filter was used to cut off all wavelengths below 400 nm.

2.6.2. Continuous flow photocatalytic tests

The photocatalytic tests were carried out on a set-up comprising a Gilson peristaltic pump set at a flow rate of 0.05 ml.min^{-1}, a polycarbonate cell fitted with two rubber seals for positioning the membrane and sealing the cell, all connected by Polyvinyl chloride (PVC) tubing (Gilson F11793) and irradiated by the OSL2IR Fiber illuminator lamp (**Figure 14**).

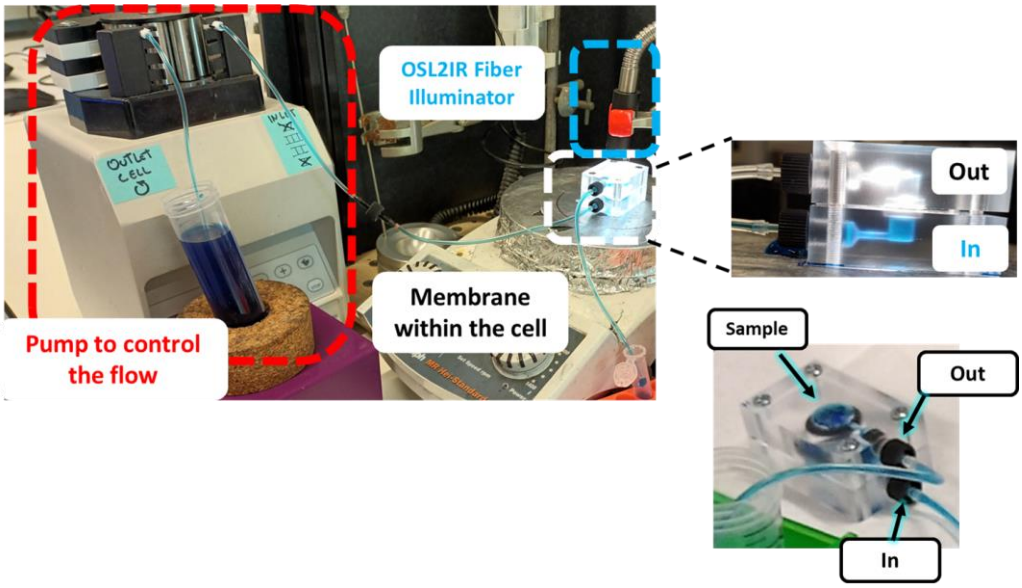

***Figure 14**: Continuous flow catalytic tests set-up.*

The PET membrane on which the catalyst is deposited was placed so that the catalyst faces upwards. The PET membrane has a diameter of 10 mm and the flow passes through a section of 6 mm in diameter (only a portion of the material is exposed). The pipes are positioned so that the flow is from bottom to top, meaning that the 5 mg.L^{-1} methylene blue solution first comes into contact with the PET membrane. Illumination is from the top of the cell at a power of 0.075 W/cm². The lamp is switched on when the MB solution made contact with the photocatalyst. The time t = 0 min. corresponds to the moment when the first drop of solution exited the sample tube. Aliquots of 0.5 ml were collected every 10 min. over a period of 1h as the flow rate is fixed at 0.05 ml.min^{-1}. 300 µl were then sampled and transferred to the wells of the plate changer grid (“96 wells Greiner clear”).

All samples were analysed by a liquid UV-visible spectrophotometer "Microplate Readers" (Molecular Devices, SpectraMax iD3) to obtain the UV spectra between 400 and 800 nm by measuring every 5 nm at RT. The area under the under the peak between 420 and 750 nm was then calculated and related to the MB concentration using a calibration line. Conversion in MB was then calculated using the following formula:

$$Conversion\ in\ MB\ (\%) = \frac{C_0 - C_t}{C_0} * 100 \quad (1)$$

Where C_0 is the initial concentration of the MB solution measured by the area under the curve of the UV-visible spectrum of the initial solution and C_t is the concentration measured at time "t" based on the area under the curve of the UV-visible spectrum obtained.

A reference blank test with a 5 µm PET membrane without catalyst was carried out on the set-up described above. This was done with and without a lamp to quantify MB absorption in the PET pores and to check that no conversion and therefore no photolysis was observed without the presence of a catalyst.

2.6.3. Batch photocatalytic tests

Into a 2 ml polymethyl methacrylate (PMMA) VWR spectroscopic cuvette, 1 ml of a 10 mg.L^{-1} MB solution was added together with 0.5 mg of photocatalyst and a small magnetic stirrer. The cuvette was closed with a lid and parafilm. The cuvette was then agitated and irradiated with the OSL2IR Fiber illuminator at a position to ensure a power of 0.075 W/cm². A filter was placed between the lamp and the cuvette to block all wavelengths below 400 nm (**Figure 15**). The spectra of the solution was recorded by a liquid single-beam cuvette UV-visible spectrometer (Agilent technologies, Cary 60 UV-Vis spectrophotometer) to obtain the spectra between 400 and 800 nm every 5 nm at RT. The concentration was determined using the area under the MB peak between 530 and 730 nm every 10 min. for 1 h.

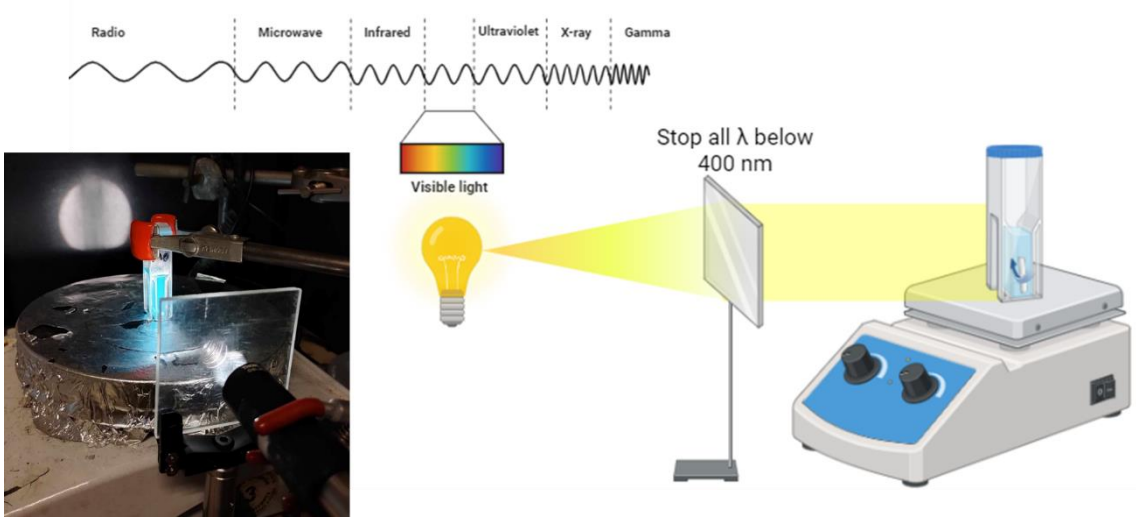

***Figure 15**: Batch photocatalytic tests set-up.*

A blank without catalyst was also run for this type of test to highlight any photolysis or thermal degradation of the MB.

2.7. Characterisation techniques

2.7.1. Scanning Electron Microscopy

Scanning electron microscopy was carried out on a JEOL JSM-7600F microscope operating at 40 kV and 8 µA, equipped with an EDX system. The sample was prepared by placing a piece of double-face adhesive tape on a sheet of aluminium foil. When the sample is a membrane (either a PC membrane used as a template, where the NTs are still inside, or a PET membrane on which the NTs have been released), the membrane is placed on the double-sided tape using precision tweezers. When the sample is suspended in a solvent (for instance dichloromethane for the release of 1D NTs or 3D interconnected NTs networks), a few drops of the solution were deposited, using a Pasteur pipette, onto a small piece of aluminium foil held in place by precision tweezers. Once the solvent has evaporated, the aluminium foil is stuck on the piece of double-face scotch tape previously applied to the aluminium foil.

To prevent the samples from charging under the electron beam, their surface was metallised with gold to make their layer conductive. The Sputter Metal (Sputter Coater Cressington 208HR & Thickness Controller Cressington mtm20) was used to deposit a 15 nm layer of gold on the surface of the prepared sample using a gold target (CODEX, 99.99%, 57 x 0.2 mm $\emptyset \times h$).

2.7.2. Transmission Electron Microscopy

Transmission electron microscopy imaging was carried out by Dr. F. Drault on the LEO 922 OMEGA Energy Filter microscope (Zeiss) operating at 120 kV. Sample preparation consisted of placing a few drops of the sample suspended in a solvent (dichloromethane for the release of NTs or NTs membranes) on a copper TEM grid (CF-1.2/1.3-2Cu-50, C-flatTM, Protochips USA) and allowing it to dry at room temperature prior to analysis.

2.7.3. X-ray photoelectron spectroscopy

XPS analyses were performed by Cécile D'Haese, on a FISONS SSI-X-probe 100/206 spectrometer (Surface Science Instruments), equipped with an electron beam (8 keV) for surface charge neutralisation. The samples analysed were 1D NTs released on PET. The PET membranes were deposited on a double-sided adhesive backing attached to a brass cup, then introduced into a Macor carousel topped with a nickel grid to avoid charging effects. The analyses were then carried out, without any further sample preparation, at room temperature with an analysis chamber pressure of 10^{-6} Pa.

The main peaks analysed in the different samples were C_{1s}, O_{1s}, N_{1s}, Si_{2p} and Ti_{2p}. Data processing was carried out with the CasaXPS software (Casa software Ltd, Japan) using Gaussian/Lorentzian decomposition processing (85/15) after subtraction of a Shirley type baseline. All XPS spectra were calibrated using the C-(C,H) component of the C_{1s} peak localised at 284.8 eV.

2.7.4. X-ray powder diffraction

Lab PXRD analyses were performed using a MAR345 diffractometer with X-rays generated by an Incoatec Microfocus Source ^{HIGHBRILLIANCE} (IμS ^{HIGHBRILLIANCE}) Mo ELM47 operating at 50 kV and 1000 μA (λ = 0.71073 Å). Powdered samples were loaded in glass capillaries (0.7 mm, Hilgenberg GmbH) and data were collected over a 2-day range from 1.14° to 40.78°, in increments of 0.02° and a time interval in increments of 1.5 s at room temperature. The diffraction data were integrated using the Fit2D software (a 0.1 mm diameter capillary filled with LaB_6 was used as a calibrant). All simulated powder patterns are sourced from CIF (Crystallographic Information File) files of structures simulated in the Vesta program with a mean wavelength of the Kα lines of Mo radiation at 0.71073 Å.

2.7.5. Solid UV-Visible spectroscopy

Analysis of solid-state samples by UV-visible spectroscopy was carried out on a Shimadzu 3600Plus UV/visible spectrophotometer. The PC membrane with NTs inside or tubes released on PET was positioned on a cylindrical support and positioned to be as flat as possible. The spectra were recorded between 300 and 800 nm in 0.5 nm increments, and the baseline was made with the reference sample: Teflon (Absorbance = 0% or Reflectance = 100%). Data were collected using UV-Probe software.

On the basis of the UV-vis spectra, the direct and indirect bandgaps of the samples can be estimated using the Tauc diagram and the Kubelka-Munk approximation, which describes light absorption and diffuse reflection when the particle size is greater than the radiation wavelength.[77] Consequently, the Kubelka-Munk function is described by the following equation:

$$F\,(R) = \frac{K}{S} = \frac{(1-R)^2}{2R} \quad (2)$$

where K is the absorption coefficient, S the scattering coefficient and R the reflectance fraction. Next, $(F\,(R).h\nu)^n$ is plotted as a function of $h\nu$ (eV) with n a constant describing the nature of the electronic transition (n = 2 if the gap is direct and n = 1/2 if the gap is indirect) and $h\nu = \frac{h.c}{\lambda}$ where $h = 4.135.10^{-15}\ eVs$, $c = 3.10^{8}\ m/s$ and $\lambda = 200\ to\ 800\ .10^{-9}\ m$. Finally, by extrapolating the linear part of the curve to the intersection of this line with the abscissa axis, we find the value of the bandgap E_g in eV because $(F\,(R).h\nu)^n = z.h\nu - z.E_g$ where z = constant.

2.7.6. Inductively coupled plasma - atomic emission spectrometry

The ICP analyses were performed by Elodie Devos on a Thermo Scientific (6000 Series) iCAP 6500 Duo ICP-AES instrument. A calibration line for Si and Ti was established using standards between 0.05 and 20 ppm (parts per million) in the same matrix as the sample. The measurements were carried out with axial alignment for greater sensitivity due to the low mass of the sample (NTs + PC template = 2.6 mg). The λ measured for Si: 212.4 nm ; 221.7 nm ; 251.6nm ; 288.1 nm and for Ti: 323.4 nm ; 336.1 nm ; 337.3 nm.

The sample was prepared by peroxide fusion. The first step consisted of placing the sample, 1 g of Na_2O_2 and 0.4 g of NaOH in a crucible and passing them through a flame to carry out the fusion. The sample was then diluted in 30 ml of HNO_3 before being reported to the volume of 500 ml. The final stage of preparation involved dilution by a factor of 2 before analysis.

For the data processing, an average was taken between the different λ and the final percentages were calculated on the basis of the fresh weight and the dilutions carried out.

The molar percentages were calculated on the basis of the atomic percentages obtained in the ICP-AES analysis. Firstly, the mass in X, where X = Si or Ti, was determined using the following formula:

$$m_X = \frac{m_{fresh} * wt.\%_X}{M_X * 100} \quad (3)$$

where m_X is the mass of X (g), m_{fresh} is the mass of the sample (g), $wt.\%_X$ is the mass percentage of X and M_X is the molar mass of X. The total mass (m_{tot}) was then calculated by summing the Si mass and the Ti mass ($m_{tot} = m_{Si} + m_{Ti}$). The mass percentage of X was then determined using the following formula:

$$Mol\ \%_X = \frac{m_X}{m_{tot}} * 100 \quad (4)$$

CHAPTER III:
Results and discussion

3.1. Synthesis of 1D TiO_2 NTs in a PC template

In this section, the optimisation of the parameters (molar ratio, aging and impregnation times) for the synthesis of pure TiO_2 NTs using a PC template is studied. Firstly, an interesting method of synthesis from the article of Lakshmi B. *et al.*[51] was initially tried due to its apparent fastness and simplicity. This sol-gel synthesis consists of preparing a first solution containing 25 ml EtOH and 5 ml TTIP and cooling it in an ice bath. A second solution containing 25 ml EtOH, 0.5 ml water and 0.5 ml 1 M HCl is then added slowly to the first one removed from the ice bath, keeping the temperature at 15 °C. After 60 seconds (s), the solution turns milky white and the AAO membrane is impregnated in it for durations between 5 and 60 s. It was then air-dried for 30 min. at RT. The membranes were then calcined at 400 °C for 6 h, with a ramp of 50 °C.h^{-1} to reach temperature.

Unfortunately, we were unable to obtain any tubes with this synthesis method. In the publication, the membrane used as template was an alumina AAO membrane with a pore diameter of 200 nm, while we used a PC membrane with a pore diameter of 400 nm. As the AAO membrane is hydrophilic whereas the PC membrane is hydrophobic, the diffusion of the precursor solution within the membrane is certainly impacted. As no tubes were obtained with the impregnation times reported in the article and, assuming that the problem was due to diffusion, longer impregnation times were tested. But, once again, no tubes were obtained. Another hypothesis is that the problem comes from the formed gel itself. In this synthesis, no additive was used to reduce the rate of hydrolysis of the precursor, known to be very fast with Ti, the aim being to have a rapid synthesis and therefore for the gel to form quickly. The reaction conditions are therefore more complex to control, particularly the temperature, which plays a very important role. The rapid hydrolysis rate can be seen when, after just one minute, the solution is completely milky white. The gel is then too advanced in its formation and does not diffuse into the pores of our template. This is because the size of the network formed and its polarity are incompatible with the hydrophobicity of the PC template.

A solution using a reagent that reduces the hydrolysis rate of our TiO_2 precursor, TTIP, seemed to be the best option for obtaining a gel that could diffuse into our template before being too reticulated.

The second synthesis studied therefore was the one described in the article of Zhang M. *et al.*[54] using also an AAO membrane as template (detailed in section 1.3.3.) but adding ACAC as a ligand to stabilise Ti in monomeric form for longer durations and delay the gel formation. In the objective of obtaining nanotubes of adequate length and strength, the conditions, *i.e.* the ratios of reagents in the initial solution and the times for ageing the solution to form the gel and for impregnating the template, had to be adapted for the use of the PC template. **Table 3** summarises the different synthesis parameters investigated.

Table 3: Summary of the synthesis parameters investigated to optimise the reagents ratios, the maturation and impregnation times for titania nanotubes formation.

Reaction name	Molar ratios				Aging time (t_1)	Impregnation time (t_2)
	EtOH	ACAC	TTIP	H_2O		
RW02	20	1	1	3	3h00	1h30
RW03	20	1	1	3	2h00	20 min
RW05	20	1	1	5	2h00	20 min
RW10	20	1	1	5	2h00	A: 1h00
						B: 1h30
RW11	20	1	1	5	1h00	A: 1h00
						B: 1h30
RW12	20	1	1	5	30 min	1h30
RW13	20	1	1	5	0 min	1h30

First, the effect of reagents ratios in the starting solution will be discussed in connexion with the quality of the nanotubes obtained as imaged by SEM analysis. The criteria used to select the best conditions were: (i) the length of the tubes, supposed to correspond to the thickness of the template (25 µm), (ii) the number of NTs and (iii) the quality of the NTs obtained (proportion of broken tubes or not). TEM analysis was then carried out for the samples obtained in the best conditions to confirm that the desired NTs morphology was obtained. The difference in structure between calcined and uncalcined tubes using XRD analysis will then be discussed.

Firstly, tests were carried out to determine the optimum ratios of reagents in the solution to form the gel. The tests consisted in determining the optimum ratio of ACAC and H_2O in the initial solution, as these two reagents influence the rate of hydrolysis of the TiO_2 precursor, TTIP. When the solution turns milky white, it means that the hydrolysis rate is too fast. When the solution remains translucent and yellow-orange but does not remain transparent, this means that the gel is forming and the solution is stable.

ACAC is used to chelate TTIP and reduce its hydrolysis rate, as suggested in the article by Siwińska-Stefańska K. *et al*.[55] ACAC therefore significantly slows down the hydrolysis rate. In the case of a TTIP:ACAC ratio greater than one, hydrolysis is immediate on addition of water and the solution changes from translucent yellow to milky white. Impregnation of the PC template is then not possible because the diffusion of the precursor solution within the pores is inhibited due to the gelification process which is already at a too advanced stage. It is therefore essential to have a stoichiometric ratio of 1:1 between the TiO_2 precursor (TTIP) and ACAC. In parallel, the molar ratio of water in the solution was increased from three to five in order to reduce the time required for the solution ageing step.

The order of addition is obviously very important as well, and water must be introduced in last position because it is when water is added that the gel formation is initiated. The speed at which the water is added is also very important, and it must be added drop by drop with stirring to avoid hydrolysis of the unchelated TTIP and its precipitation. In other words, equilibrium is not reached and the precursor precipitates if the addition of water is too fast since there is a competition between chelation and hydrolysis. Furthermore, when the water ratio is greater than five, immediate precipitation is also observed.

From all these observations, an ideal molar composition of EtOH:TTIP:ACAC:H_2O=20:1:1:5 was determined.

3.1.1. SEM imaging of formed titania NTs after release from the template

Figure 16 shows SEM images of samples RW02, RW05, RW13 and RW11A. These four reaction products represent extreme cases of short or long durations for the ageing and impregnation stages. This also demonstrates the importance of the water ratio for the hydrolysis rate.

The SEM images confirm that the tubes formed are NTs and not filled nanorods (NRs), as the objects obtained present an axial hollow cavity in all the cases.

For RW02 and 05 (**Figure 16.(a)** and **(b)**, respectively), few NTs are observed, and their morphology does not correspond to the templates used during their synthesis. It can be explained, respectively, by a too long ageing time (RW02) and a too short impregnation time (RW05). When the template is directly impregnated and the solution does not have time to age (RW13, **Figure 16.(c)**), the solution diffuses more easily into the pores of the PC template and some tubes of the correct length *i.e.* 25 µm, corresponding to the thickness of the template, are observed. Unfortunately, most of the NTs observed were the wrong length because the hydrolysis of the solution was in its early stages and the gel was not yet formed. The walls of the NTs were therefore probably not thick enough and the NTs were not complete because they were too fragile.

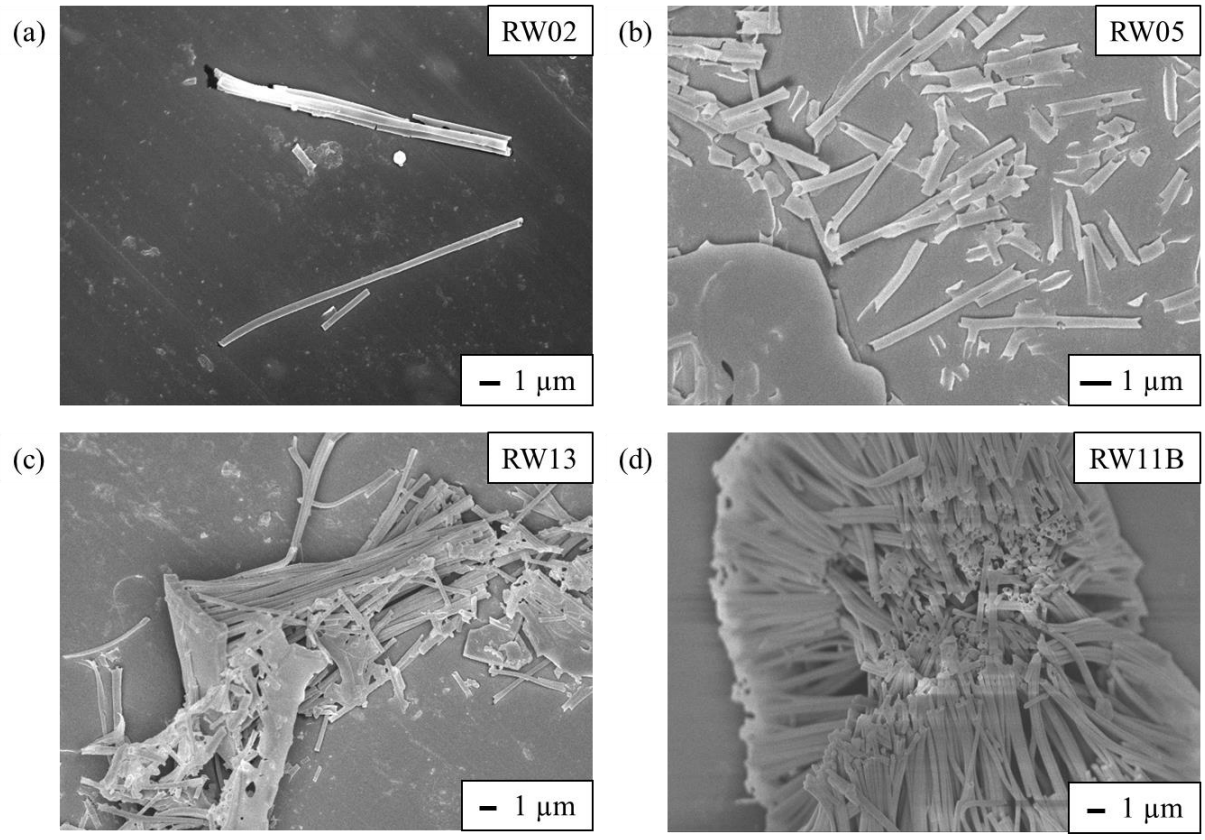

Figure 16*: SEM pictures of products obtained in the following conditions: (a) EtOH:TTIP:ACAC:H_2O=20:1:1:3, 3 h ageing and 1 h 30 impregnation, (b, c and d) EtOH:TTIP:ACAC:H_2O=20:1:1:5 with in the case of (b) 2 h ageing and 20 min. impregnation, (c) 0 min. ageing and 1 h 30 impregnation and (d) 1 h ageing and 1 h 30 impregnation.*

To summarise, both the ageing time of the sol-gel and the impregnation time of the PC template influence the quality of the obtained tubes. The longer the solution ageing time, the fewer and more fractured the tubes. This suggests that diffusion within the template is less efficient and, consequently, TiO_2 does not form on the entire length of the template pores. As described in the article by Zhang M. *et al.*[54], the longer the impregnation time, the thicker and therefore less fragile the tubes. This trend is also observed for our NTs. RW05, RW10A and RW10B are three reactions with a solution ageing time of 2 h but impregnation times of 20 min., 1 h and 1 h 30. The thicknesses were calculated based on SEM images of PC templates filled with the NTs (see Appendix 4) by subtracting the remaining hole diameter of the template pore size and dividing by two, as illustrated in **Figure 17**. NTs with a thickness of around 24 nm for 20 min., 47 nm for 1 h and 77 nm for 1 h 30 impregnation times were obtained.

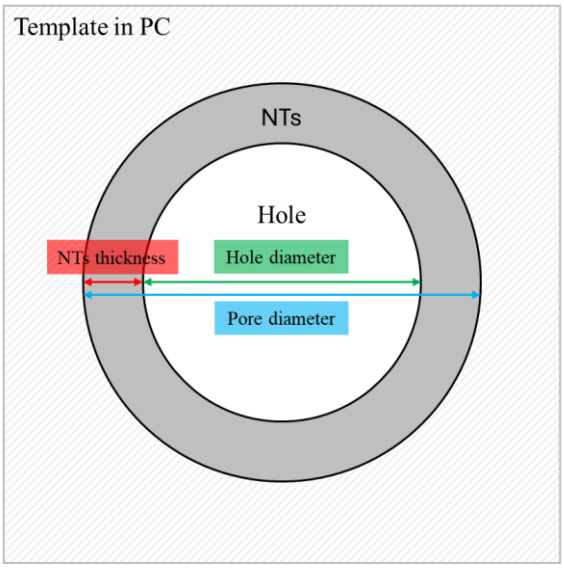

$$NTs\ thickness = \frac{Pore\ diameter - Hole\ diameter}{2}$$

***Figure 17**: Schematic illustration of the calculation of NT thickness in the template.*

The best conditions for obtaining well-formed titania NTs are therefore a solution ageing time of 1 h and an impregnation time of 1 h 30 for the PC template in the gel, as shown in **Figure 16.(d)**. Indeed, a large number of NTs with a length close to 25 µm were observed. Few of these NTs were broken, meaning that the template was perfectly filled. After 1 h of ageing, the gel was neither over- nor under-formed and 1 h 30 of diffusion is the optimum time to fill the PC template on its entire thickness.

3.1.2. TEM

TEM offers better resolution than SEM, but also has the advantage of being a transmission technique, permitting to see through the sample. **Figure 18** shows a TEM image of pure TiO_2 NTs before **(a)** and after **(b)** calcination.

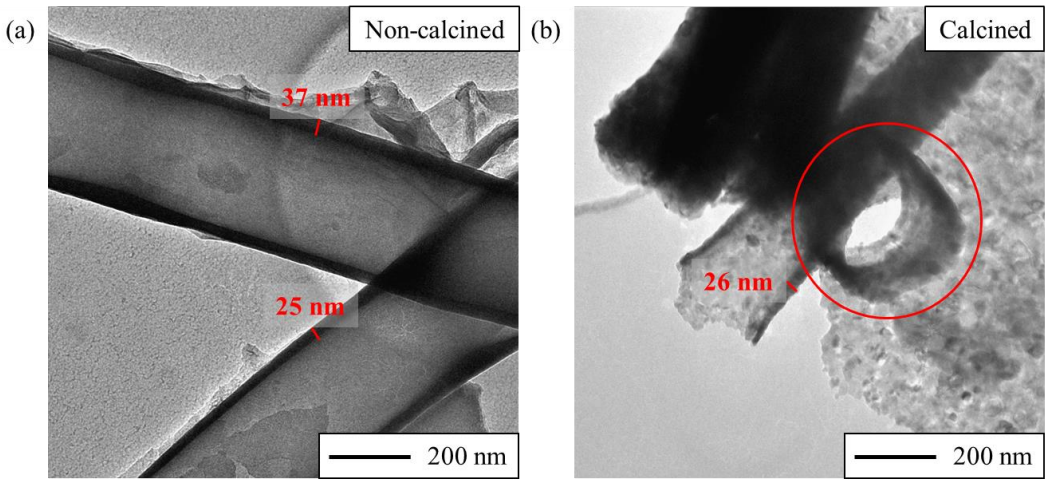

***Figure 18**: TEM image (a) NTs of pure non-calcined TiO_2 (b) NTs of pure calcined TiO_2 (TiO_2 synthesis conditions: EtOH:ACAC:TTIP:H_2O=20:1:1:5, 1 h ageing time and 1 h 30 impregnation time).*

TEM images confirm the presence of NTs as shown in **Figure 18**. The red circle (**Figure 18.(b)**) indicates a cross-section of a tube confirming that it is indeed hollow. The average diameter of TiO_2 NTs, whether calcined or not, is 340 nm, and the thickness is between 20 and 40 nm. This method of determination is more accurate than that based on SEM images of the PC template because it is based on the NTs itself and not on the membrane filling, but requires the use of TEM.

The TiO_2 NTs before (**Figure 18.(a)**) and after (**Figure 18.(b)**) calcination show a different aspect suggesting an effect of the thermal treatment on the material. In details, the surface of the non-calcined tubes looks smooth whereas the calcined tubes looks rougher. This change in appearance has also been observed in the literature by Wu L. *et al.*[78] The most likely hypothesis is a phase difference between the non-calcined and calcined tubes. To confirm this hypothesis, a powder XRD analysis has been carried out and is discussed in the following section 3.1.3.

3.1.3. Powder DRX analysis of titania NTs before and after calcination

As observed in TEM, significant changes in the material is obtained after the calcination step. Therefore, **Figure 19** shows the diffraction patterns obtained for calcined and non-calcined titania NTs powders and the theoretical diffractograms of anatase and rutile, the two major phases of TiO_2.

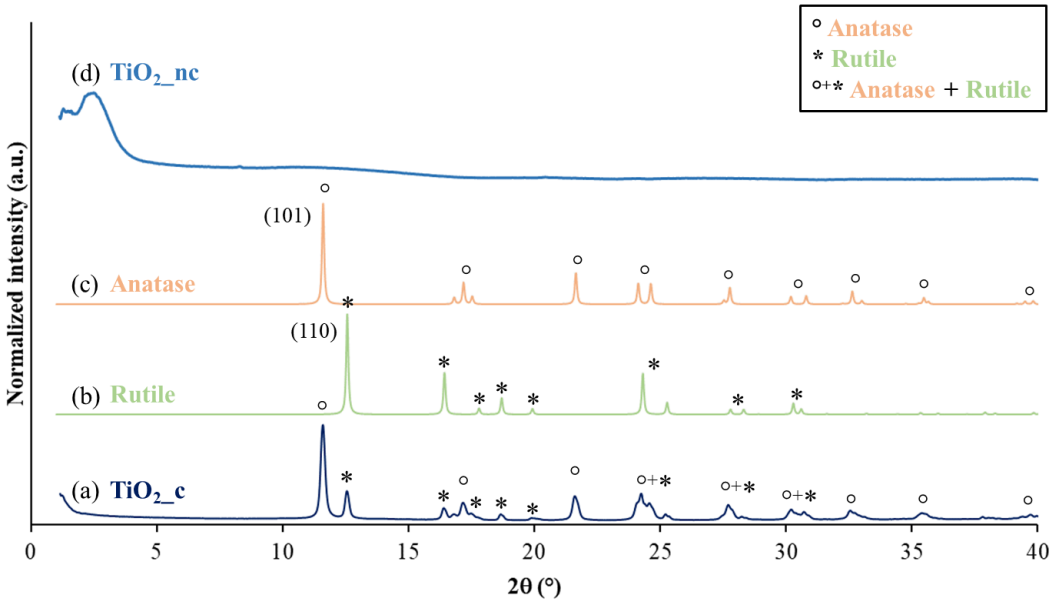

***Figure 19**: PXRD patterns of (a) TiO_2 calcined experimental (TiO_2_c), (b) rutile theoretical, (c) anatase theoretical and (d) TiO_2 non-calcined experimental (TiO_2_nc). TiO_2 synthesis conditions: EtOH:ACAC:TTIP:H_2O=20:1:1:5, 1 h ageing time and 1 h 30 impregnation time.*

As one can see on **Figure 19.(a)** and **(d)** the calcined TiO_2 is crystalline whereas non-calcined TiO_2 is amorphous. The characteristic peaks of rutile (Inorganic Crystal Structure Database (ICSD): 23697)[79] and anatase (ICSD: 92363)[80] TiO_2 type structure are observed in the diffraction pattern of the calcined TiO_2 NTs. Quantification to obtain the percentage of each phase in the material was carried out by G. Esser using FullProf software.[81] The refinement between the experimental pattern and the sum of the theoretical patterns for anatase and rutile are available in Appendix 5. The calculated percentage of anatase is 71.73% and that of rutile is therefore 28.27%. This ratio is practically equivalent to the commercial TiO_2 P-25 (a standard material in the field of photocatalytic reactions) which contains anatase and rutile phases in a ratio of about 3:1.[82]

Moreover, the difference in crystallinity could have an influence on the band gap of the material and therefore on its photocatalytic activity.

3.2. Synthesis of 1D SiO_2/TiO_2 mixed oxide NTs using PC template

In this section, the synthesis of SiO_2-TiO_2 mixed oxide NTs using PC porous membranes as hard template will be studied. Particular attention will be paid to the molar ratios of SiO_2 precursor, TEOS and TiO_2 precursor (TTIP) in the solution to form the gel and their incorporation into the final material obtained. Two different syntheses methods are studied to obtain mixed oxide NTs. They are based on the combination of the syntheses of SiO_2 NTs (described in the literature by Drault F. *et al.*[31]) and TiO_2 NTs (described in section 3.1. of this manuscript) using PC membranes as hard templates.

First of all, the SiO_2 synthesis described in the literature by Drault F. *et al.*[31] was reproduced with the aim to obtain SiO_2 NTs as reference system to compare its properties and catalytic performances with TiO_2 NTs and the different mixed oxides. This synthesis was performed successfully leading to the obtention of SiO_2 NTs of the right length, around 22 µm (corresponding to the thickness of the PC template used).

Then, the SiO_2 NTs synthesis method was adapted to obtain mixed oxide NTs. Indeed, the two monoxides synthesis processes have different ageing times to form the gel. Furthermore, the nominal molar ratios of both precursors had to be adapted in order to keep the same total volume of 60 ml to fully immerse the membranes in the gel. As a reminder, the gel is considered to be formed at the end of the ageing step given its viscous appearance and in order to simplify future discussions. The targeted molar ratios in the final mixed oxides are: SiO_2:TiO_2=75:25, 50:50, 25:75 and for the best of the two syntheses, the molar ratio SiO_2:TiO_2=10:90.

As shown and discussed in the section 3.1., the precursor of TiO_2, TTIP, hydrolyses very quickly, justifying the addition of ACAC to slow down this reaction. The solution ageing step took just 1 h in the TiO_2 NTs method. For the synthesis of SiO_2 NTs described in the literature by Drault F. *et al.*[31], the ageing time of the solution to form the gel was 3 h and HCl was added to catalyse the hydrolysis of the precursor. The ageing times in both methods are therefore very different, which must be taken into account in the synthesis of mixed oxides to ensure the formation of an adequate gel containing both precursors before the step of impregnation.

Two different synthesis methods of the mixed oxides were tested: in the first one, the two solutions were left to age separately before being mixed and, in the second one, the TiO_2 precursor, TTIP, was added to the solution containing the SiO_2 precursor, TEOS, to form a unified gel. The results obtained by both methods will be first reported before comparing them. Then a general discussion will focus on the determination of the best methodology to obtain mixed oxide NTs with targeted Si:Ti molar ratios.

3.2.1. Results for the first method of preparation of mixed oxides

In the first synthesis method, the two solutions containing the precursors are left to age separately according to the times described to obtain the simple oxides. Then, prior to the step of impregnation, both solutions are mixed together. The experimental protocol is described in experimental section 2.4.1.

Different Si:Ti molar ratios were investigated by such method: 25:75, 50:50 and 75:25. **Table 4** details the composition of both precursor solutions for the different investigated Si:Ti ratios.

Table 4: Different nominal molar ratios (TEOS:TTIP) investigated for mixed oxide production using the first synthesis method.

Nominal molar ratios TEOS:TTIP	Molar ratios							
	Solution A (SiO_2)				Solution B (TiO_2)			
	EtOH	H_2O	HCl	TEOS	EtOH	ACAC	TTIP	H_2O
25:75	3.675	1.175	0.175	0.250	15.000	0.750	0.750	3.750
50:50	14.700	4.700	0.700	1.000	20.000	1.000	1.000	5.000
50:50	14.700	4.700	/	1.000	20.000	1.000	1.000	5.000
75:25	11.025	3.525	0.525	0.750	5.000	0.250	0.250	1.250

3.2.1.1. Influence of HCl addition

Before discussing the different ratios investigated, the influence of the use of HCl in mixed oxide synthesis will be considered.

Two reactions for the TEOS:TTIP=50:50 ratio were carried out, one of them without HCl to see if this parameter has any influence on the synthesis of NTs. Indeed, having HCl in the solution of the SiO_2 could accelerated too much the hydrolysis of the TiO_2 precursor (TTIP) when the two solutions are mixed together and also affect the impregnation step. **Figure 20.(a)** shows a SEM image of mixed oxides TEOS:TTIP=50:50 NTs obtained with HCl and **Figure 20.(b)** without HCl. NTs of the expected length, *i.e.* practically 25 µm (size corresponding to the thickness of our PC template) were obtained for the synthesis with HCl, while we observed less well-shaped tubes for the synthesis without HCl. This is probably due to the fact that 3 h of aging of the SiO_2 precursor solution is not sufficient to properly form the gel. Chelation of the TiO_2 precursor (TTIP) by ACAC enables the precursor to be stabilised and HCl does not accelerate hydrolysis to such a point as to affect the impregnation step.

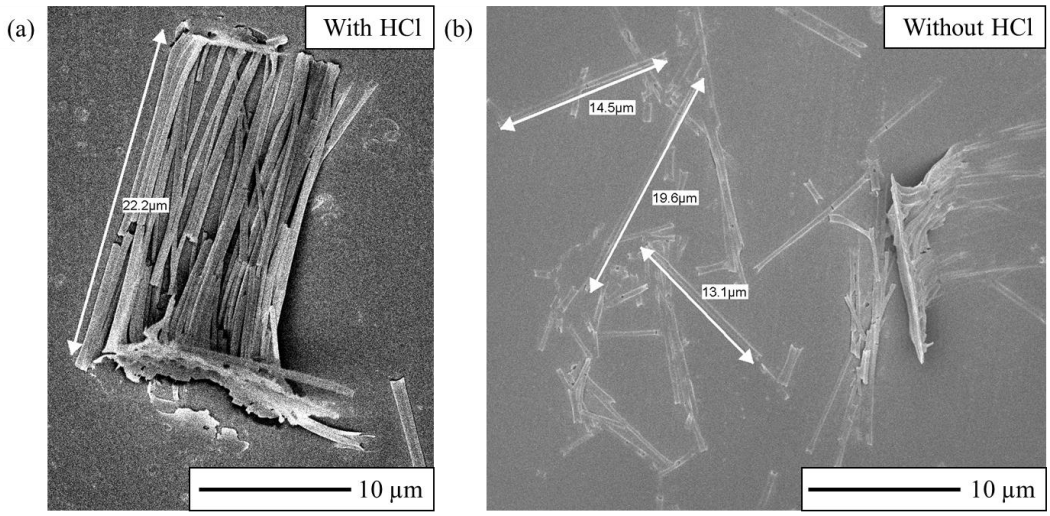

Figure 20*: SEM image of mixed oxide NTs TEOS:TTIP=50:50 obtained (a) with HCl and (b) without HCl in the TEOS solution.*

For the other molar ratios of mixed oxides explored, in agreement with these observations, HCl was therefore used in all cases to prepare the solution containing the SiO_2 precursor to form the gel.

3.2.1.2. Different SiO_2:TiO_2 ratios investigated

In this section, the first synthesis method will be discussed, and especially in terms of composition. To confirm that NTs were obtained, SEM analysis was carried out systematically. The SEM images obtained are shown in **Figure 21**. In these images, NTs are visible for the different ratios tested, meaning that the synthesis works even though most of the NTs do not have the expected length of 25 microns, but measure on average 12 to 14 µm. The reason why the NTs do not have the desired size, corresponding to the thickness of the template, is due to gel diffusion problems in the template, as the impregnation medium was very tick. As for TiO_2, this problem can be solved by optimising solution ageing or impregnation times to favour the diffusion of the gel into the PC template.

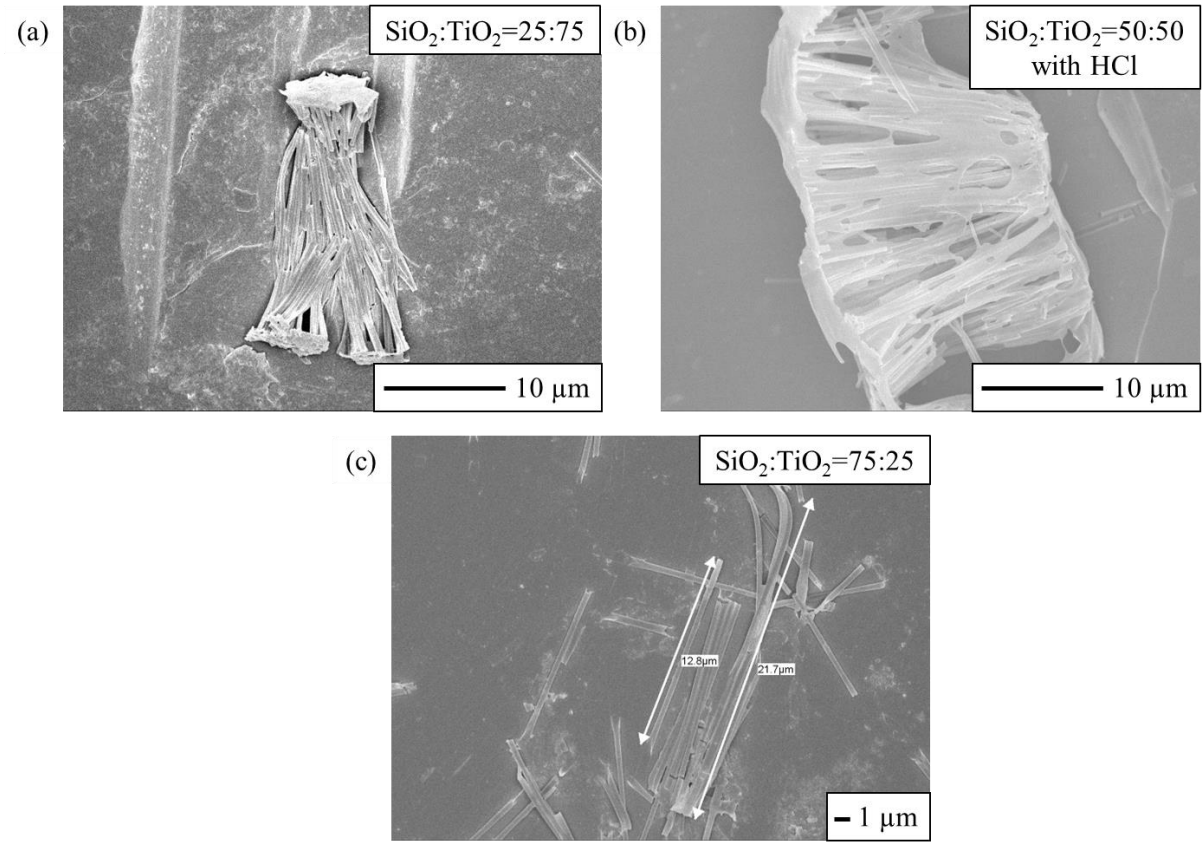

***Figure 21**: SEM images of different mixed oxides obtained via the first method: (a) SiO_2:TiO_2=25:75, (b) SiO_2:TiO_2=50:50 with HCl and (c) SiO_2:TiO_2=75:25.*

Prior to optimisation of the synthesis to obtain NTs with the expected morphology, it is necessary to determine if this synthesis method offers a control of the Si:Ti molar ratios in the final materials. Using EDX coupled with SEM, a quantification of the amount of each atom of interest was performed. **Figure 22** shows the EDX mapping analysis obtained for the three

different molar ratios Si:Ti of 25:75, 50:50 and 75:25, for the elements Si, Ti and O. A trend in colour intensity is observed, indicating that there is more Ti than Si in the 25:75 molar ratio (**Figure 22.(a)**), more Si than Ti in the 75:25 molar ratio (**Figure 22.(c)**) and a similar intensity for the 50:50 molar ratio (**Figure 22.(b)**). Oxygen is also detected where the NTs are located, confirming that the NTs are oxides. These observations are promising since the nominal molar ratios correspond to this trend of colours in the EDX maps (EDX spectra are available in Appendix 6).

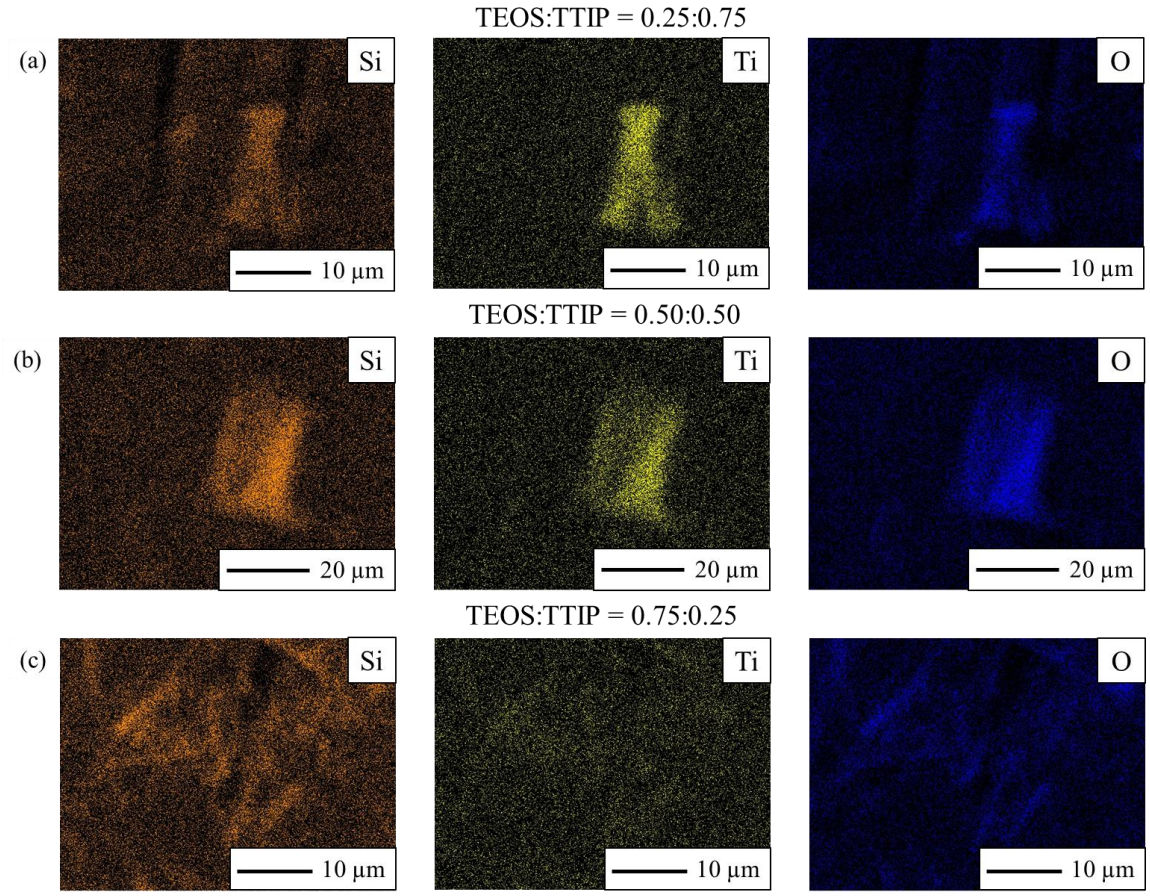

***Figure 22**: EDX mapping analysis obtained for different molar ratios of mixed oxides (Si:Ti): (a) 25:75, (b) 50:50 and (c) 75:25. Orange: Si map, yellow: Ti map and blue: O map.*

To obtain quantitative values of the molar ratios incorporated into our final material, XPS (surface analysis), possibly complemented by ICP (bulk analysis), was carried out. XPS must be complemented by ICP, at least once, to confirm that the surface composition reflects the composition of the bulk material. If the ICP confirms the XPS results, *i.e.* the surface ratios represent the bulk ratios, the XPS will be used for the quantitative analysis because the delays are shorter and it requires lower amounts of samples. The XPS results obtained will be described below in section 3.2.3. in order to compare the two synthesis methods.

3.2.2. Results for the second method of preparation of mixed oxides

In the second synthesis methodology, the solution containing the SiO_2 precursor, TEOS, was left to age for 2 h before adding the solution containing the TiO_2 precursor, TTIP, and then the resulting mixed solution was left to age for a further 1 h. In this way, the solution containing the SiO_2 precursor is left to age for a total of 3 h, while the one with the TiO_2 precursor is aged for just one hour. In addition, this procedure allows the two precursors to be both present during gel formation, increasing therefore the chance of obtaining a true mixed oxide, *i.e.* Si-O-Ti bonds and not Si-O-Si and Ti-O-Ti clusters in the final material. The experimental protocol is described in experimental section 2.4.2.

The same Si:Ti molar ratios as for the first synthesis method were studied: 25:75, 50:50 and 75:25. In addition, another molar ratio Si:Ti=10:90 was investigated. In this case, we could consider that it is not a mixed oxide, but rather TiO_2 doped with SiO_2. This material was synthetised since Zhang H. *et al.*[83] , Viet P. *et al.*[84] and Babyszko A. *et al.*[64] indicated that low doping of TiO_2 with 2-15% SiO_2 may significantly increase the photocatalytic activity. **Table *5*** summarises the molar composition of the reactants for the different ratios investigated in the formation of mixed oxides using the second method.

Table 5: Different nominal molar ratios (TEOS:TTIP) investigated for mixed oxide production using the second synthesis method.

Nominal molar ratios TEOS:TTIP	Molar ratios							
	Solution A (SiO_2)				Solution B (TiO_2)			
	EtOH	H_2O	HCl	TEOS	EtOH	ACAC	TTIP	H_2O
10:90	1.470	0.470	0.070	0.100	18.000	0.900	0.900	4.500
25:75	3.675	1.175	0.175	0.250	15.000	0.750	0.750	3.750
50:50	14.700	4.700	0.700	1.000	20.000	1.000	1.000	5.000
75:25	11.025	3.525	0.525	0.750	5.000	0.250	0.250	1.250

Figure 23 shows SEM images of the nanostructures obtained by this second synthesis method for the different TEOS:TTIP molar ratios tested: **(a)** 10:90, **(b)** 25:75, **(c)** 50:50 and **(d)** 75:25. NTs are obtained but some of them do not present the expected length, but have on average a length ranging between 14 and 24 µm. This is still more than the 12-14 µm observed for the first synthesis method. The fact that we observed some shorter NTs can be explained by a non-uniform diffusion of the precursor solution on the entire length of the PC template pores during the impregnation step. On some images, in cases **(a)** and **(c)**, we can see a layer holding the NTs together, unlike samples **(b)** and **(d)** where the NTs are more dispersed. This layer is probably an oxide layer that has been deposited on the surfaces of the PC template, and not removed efficiently during the cleaning step with the Kimtech. To remove this excess, a cotton bud soaked in water or in an acid such as HCl could be passed over the membrane to remove it. In sample **(b)**, some NTs appear to be covered by some remaining polycarbonate, which was not completely dissolved during release into DCM.

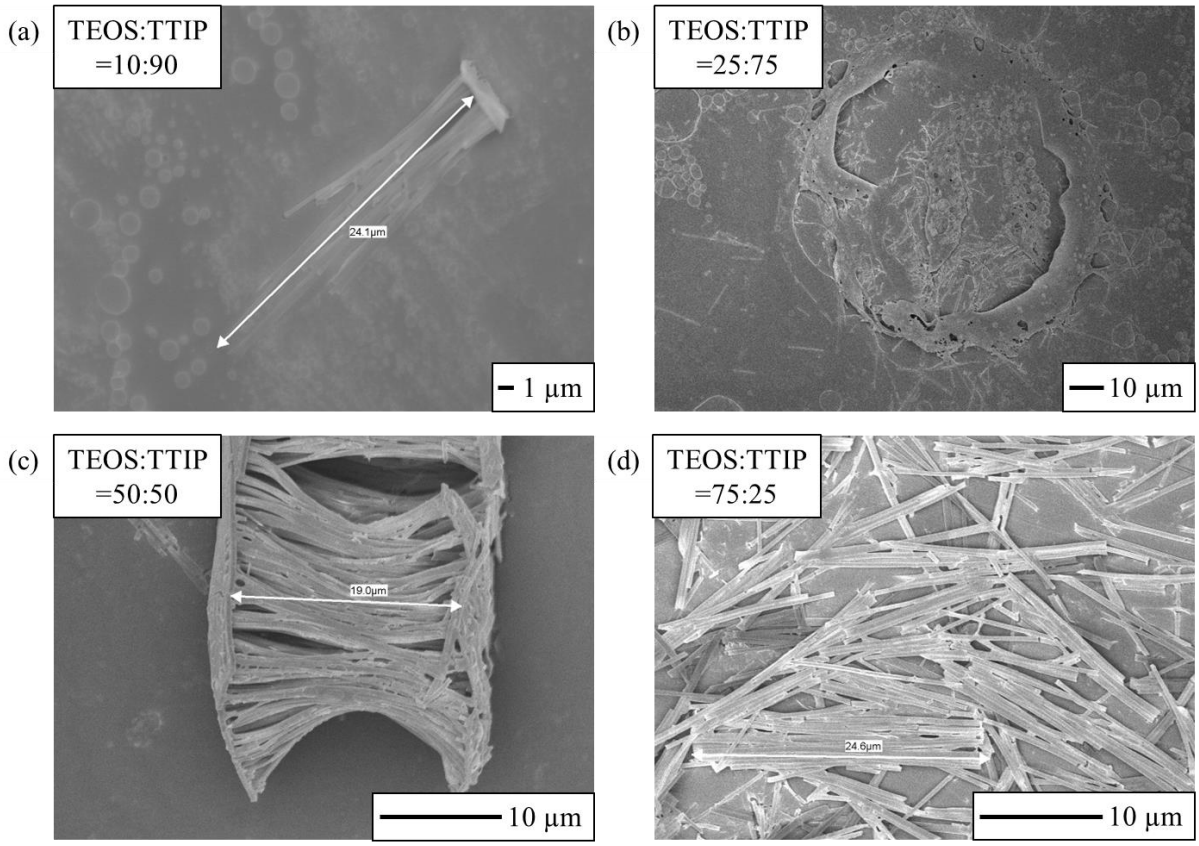

***Figure 23**: SEM images of NTs obtained for TEOS:TTIP molar ratios (a) 10:90, (b) 25:75, (c) 50:50 and (d) 75:25 using the second method.*

3.2.3. XPS and ICP analysis, comparing both methods

XPS is a surface analysis that was used to determine the Si:Ti molar ratios in the NTs obtained. ICP allows the same analysis but for the whole material, a so-called bulk analysis. First, the XPS results for the TEOS:TTIP=50:50 ratio are compared to determine which of the two synthesis methods is the best. In a second step, the NTs synthesised with other molar ratios are checked by XPS to verify if Si and Ti incorporation in the final material corresponds to the Si:Ti in the precursor solution. **Table 6** details the results obtained by XPS for both methods and different molar ratios. The survey spectra of the various samples and the deconvolutions for the peaks of certain relevant elements are presented in Appendix 7.

Table 6: Molar ratios in the final materials, calculated from XPS analysis.

Synthesis	In solution	In NTs	
	Nominal molar ratios TEOS:TTIP	%mol Si	%mol Ti
Method 1	50:50	62.05	37.95
Method 2	25:75	28.21	71.79
	50:50	53.83	46.17
	75:25	74.90	25.10

Using method 1, a 62:38 molar ratio of Si:Ti in the final material has been obtained by XPS, which does not fully correspond to the nominal ratio of 50:50 introduced in the precursor solution. Then, using the second method, a Si:Ti molar ratio in the final material of 54:46 has been obtained, which is much closer to the expected 50:50 molar ratio. In this case, the small variation may be due to experimental errors during the synthesis, in particular weighing and transferring the solution from one glassware to another (although the transfers are minimised with only the addition of the solution containing the TiO_2 precursor, TTIP, to the beaker containing the SiO_2 precursor, TEOS). Another possible source of error is the accuracy of the measurement in the XPS, given the small quantities of material at our disposal, the possible presence of PC template residues in addition to the material of interest, and the dispersion of NTs during the release step (*e.g.* some areas of the PET underlying support are not covered with NTs). In fact, when the tubes were released from the PC template onto a PET membrane, only 0.3 to 0.6 mg of material were collected. This a rather low amount, especially as some residual PC coming from the template may remain on the samples. Even with all these considerations, method 2 for the synthesis of mixed oxide NTs, in which the two precursors are aged together for 1 h, is the best method for obtaining the desired Si:Ti incorporation.

Subsequently, the mixed oxide NTs prepared by the second synthesis method with the 25:75 and 75:25 ratios were also analysed by XPS (**Table 6**, bottom). Molar Si:Ti ratios of 28:72 and 75:25 were obtained for initial molar TEOS:TTIP precursor ratios of 25:75 and 75:25, respectively. These results confirm that the second synthesis method of mixed oxides allows a quite good control on the incorporation of both SiO_2 and TiO_2, with a molar ratio almost equivalent to the one introduced in the precursor solution. Nevertheless, it needs to be verified if the composition of the material surface corresponds to the composition of the bulk material. To check this point, ICP was performed on the sample with molar ratio TEOS:TTIP= 75:25. A molar percentage of 74.9% for Si (1.55 wt.%) and 25.1% for Ti (0.88 wt.%) was obtained, which is in perfect agreement with the XPS results (the formula used to calculate the molar ratio based on the weight percentages is available in section 2.7.6.). It could therefore be concluded that the bulk and surface compositions are identical.

The second method for synthesising mixed oxide NTs with different Si:Ti ratios is therefore fully validated, as it enables us to control the molar ratios in our final materials.

3.2.4. TEM: effect of calcination

As with TiO_2, the mixed oxide with a Si:Ti molar ratio of 75:25 was calcined to see if this had any influence on NTs morphology. TEM was carried out on both calcined and non-calcined mixed oxide NTs. **Figure 24** shows TEM images obtained for **(a)** non-calcined and **(b)** calcined mixed oxides.

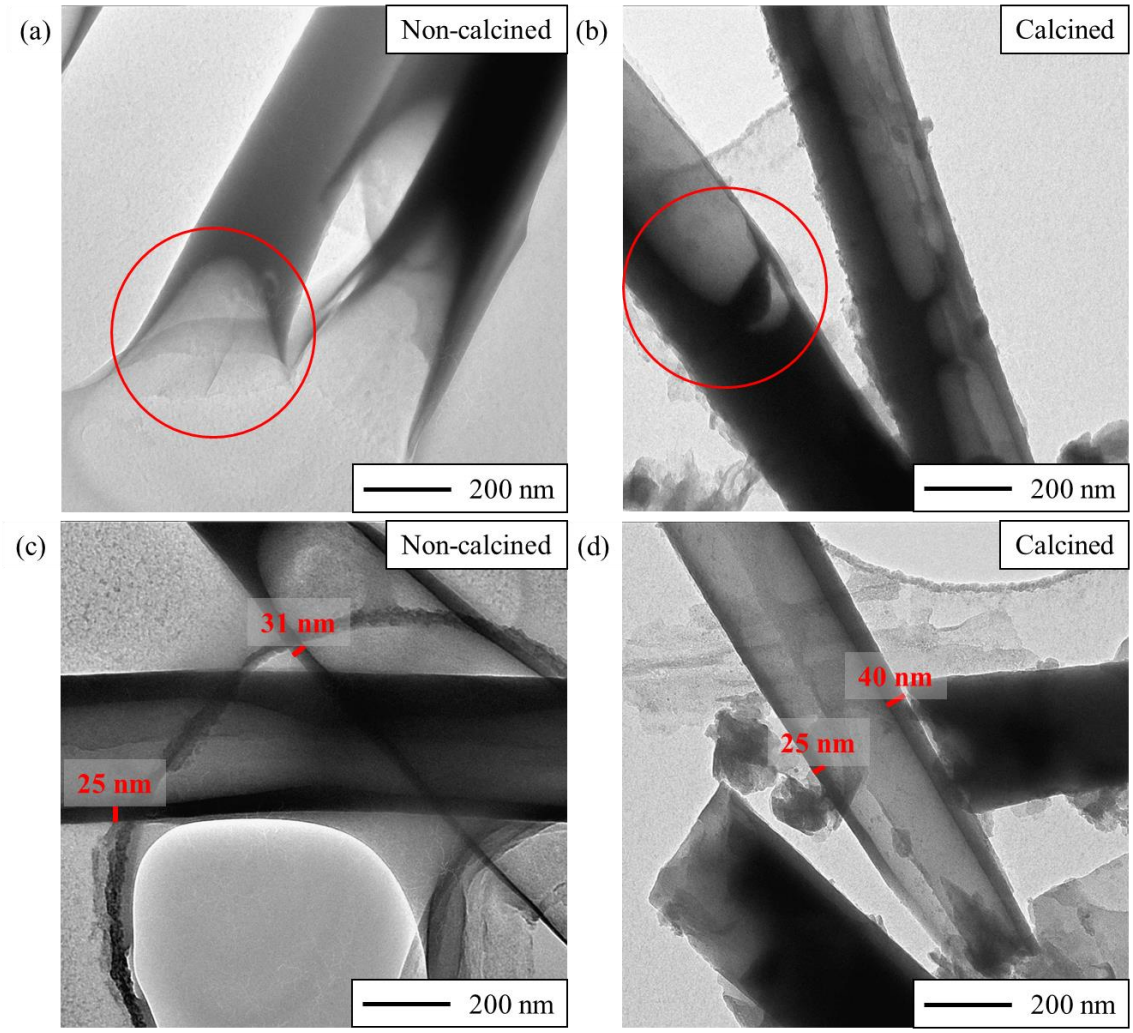

***Figure 24**: TEM images of the mixed oxide NTs with a Si:Ti molar ratio of 75:25 (a and c) non-calcined and (b and d) calcined.*

TEM images confirm that, in both cases, a hollow shape and therefore NTs and not NRs are obtained (see red circles on **Figure 24**). A difference in morphology similar to that pointed out for pure TiO_2 NTs is observable. Uncalcined NTs present a smooth surface, while calcined NTs appear much rougher. The wall thickness of the NTs obtained is difficult to determine on the two TEM images in **Figure 24**, but an average external diameter of around 300 nm has been measured on various TEM images. The difference of diameter between the NTs (300 nm) and

the pores of the used template (400 nm) can be explained by the dehydration of interlayered OH groups during calcination or drying, leading to shrunk NTs.[78]

In other images, see image **(c)** and **(d)** in **Figure 24**, the NT's wall thickness was measurable. The average thickness is between 15 and 40 nm whether the NTs are calcined or not (see red marks corresponding to NT wall thickness in **Figure 24.(c)** and **(d)**). This is similar to the thickness that was observed for TiO_2 NTs in TEM, which is consistent given that the impregnation time is identical (1 h 30) in the two syntheses.

3.2.5. Solid-state UV-visible spectroscopy characterisation of the 1D NTs

Absorption spectra of the different materials, pure TiO_2 and the various mixed oxides with different Si:Ti ratios were recorded by solid-state UV-visible analysis (**Figure 25**). These analyses were carried out on non-calcined materials released on PET membrane.

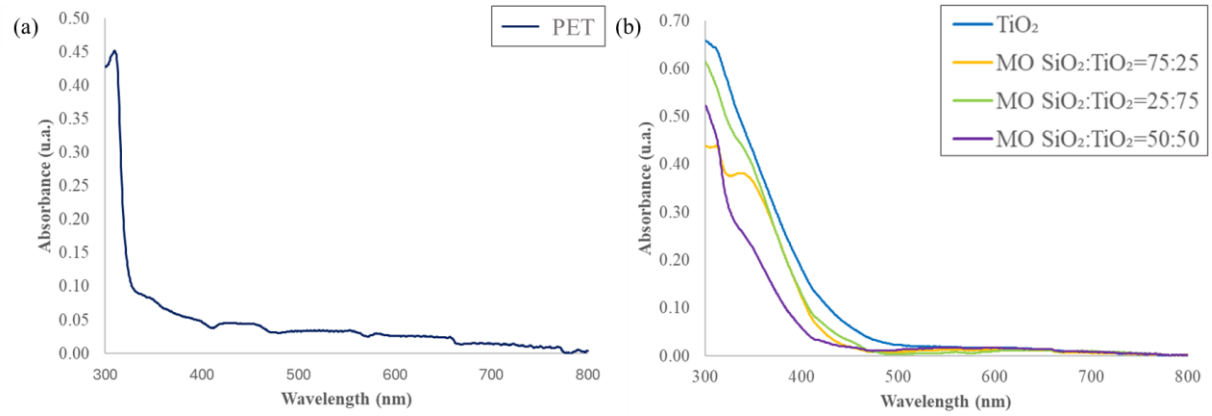

***Figure 25**: Solid-state UV-visible spectra of (a) PET membrane and (b)1D TiO_2 and mixed oxides SiO_2:TiO_2= 25:72, 50:50 and 75:25.*

First, given the small quantities of material (< 0.4 mg), it does not cover the entire PET membrane uniformly, and as PET absorbs from 325 nm with an intense peaks at around 300 nm, as observed in **Figure 25.(a)**, there is an overlap with the spectrum of TiO_2.

Figure 25.(b) shows the spectrum obtained for TiO_2 and the 3 mixed oxides (TEOS:TTIP): 25:75, 50:50 and 75:25 prepared by the second method. The peak at 300 nm corresponds to the sum of the TiO_2 peak and the PET peak. Nevertheless, a trend can be seen in the intensity of this peak, directly related to the amount of TiO_2 found in the material as a function of the Si:Ti ratio. Indeed, the intensity of the peak at 300 nm follows: TiO_2 > MO (Mixed Oxide) SiO_2:TiO_2=25:75 > MO SiO_2:TiO_2=50:50 > MO SiO_2:TiO_2=75:25, corresponding to the Si:Ti ratio in the material.

Determining amorphous nanomaterial bandgaps based on a UV-vis spectrum can be complex, as many factors can impact the measure. Indeed, Maryama, H. & Abbassi, A.[85] demonstrated that the increase of the thickness of amorphous ZnO decreased the transmittance maximum and the bandgap energy. They showed that increasing the thickness of a ZnO monolayer by a factor of three (from 393 nm to a 1,165 nm) lead to a significant change of the bandgap from 3.8 to 3.1 eV, respectively. The NTs synthesised in this work vary in thickness, which can have an impact on the band gap.

Another possible factor of variations is the orientation of our sample during analysis.[75] Indeed, our material in the shape of nanotube is anisotropic, which influence the reflectance measurements. In order to reduce this error, the measurement could have been carried out several times changing the position of the sample and the results obtained could have been averaged. However, modifying the orientation of the membrane is very complex in our setup since the material is slightly curved and the flattest possible part must be in the direction of the beam.

The size distribution of NTs can also have an impact on UV-visible absorption spectra. As nanoparticle size decreases, a blue shift is observed.[86,87] Depending on the orientation of the NT when incident UV radiation is reflected on their surface, the reflectance and thus absorbance will be different, which explains why the peak is not sharp. Indeed, if the NT is perfectly aligned with the beam, it exposes its entire length, *i.e.* around 25 µm, whereas if it is perfectly perpendicular to the beam, it exposes its width, *i.e.* around 300 nm. Taking into account that tubes are sometimes broken, never perfectly aligned or perpendicular (which explains the impact that orientation can have) and that some of them overlap, this creates a sort of absorbance continuum between 300 and 550 nm.

For all these reasons, it is difficult to determine the bandgaps of the synthesised materials with great precision. To determine the bandgaps more accurately, measurements could be taken on 3D membranes of interconnected NTs whose thickness would make the PET invisible. The measurements could also be performed on powders so that there is no PET and the surface is flat so that several different measurements can be carried out with several different orientations. But this would require scaling-up and further work on sample preparation for this analysis.

3.2.5.1. Bandgaps determination

Using the Kubelka-Munk approximation described in section 2.7.5., the Tauc diagram and using the method described in the article by Makuła, P. *et al.*[75] and detailed in section 2.7.5. as well, the bandgaps were calculated for the various mixed oxides. According to the literature, TiO_2 is an indirect semiconductor.[88] The Tauc graph of $(F\ (R).hv)^n$ (where n = 1/2 because TiO_2 has an indirect gap) as a function of hν (eV) can therefore be plotted (**Figure 26**).[77] The shoulder located around 3.5 eV before the TiO_2 peak for mixed oxides make linear extrapolation complex as is often the case with modified semiconductors. **Figure 26** shows the Tauc diagrams obtained for the different materials synthesised and the analogous graphical construction used in **Figure 13** (see section 1.4.3.) to determine the bandgaps.

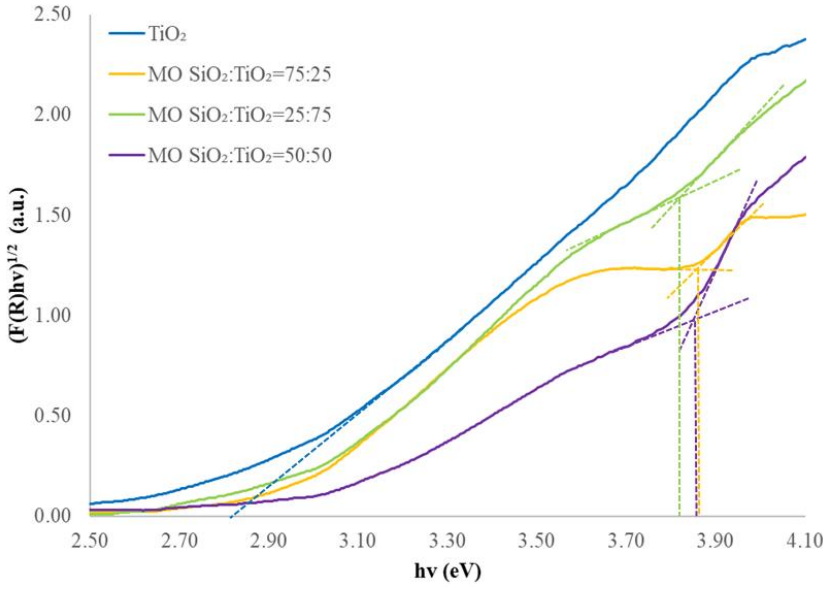

***Figure 26**: Transformed reflectance spectrum of TiO_2, MO SiO_2:TiO_2=25:75, MO SiO_2:TiO_2=50:50, MO SiO_2:TiO_2=75:25 samples and graphical construction for bandgap determination.*

As can be seen in **Figure 26**, TiO_2 was treated as a single oxide (prolongation of the linear portion of the spectrum) whereas the mixed oxides were treated with the graphical construction described in the article by Makula, P. *et al.*[75] The bandgaps obtained for the different mixed oxides are similar in value (3.82-3.87 eV) and higher than for TiO_2. The bandgap values obtained are presented in **Table 7**. The slight increase in bandgap as the amount of SiO_2 in the mixed oxide increases was also reported in the paper by Babyszko, A. *et al.*[64] but for low amounts of SiO_2 in the material (ranging from 2% to 17.2% for a bandgap going from 3.09 eV to 3.23 eV). The article by Fatimah, I. *et al.*[14] reports a slight decrease in bandgaps as the amount of Si in the mixed oxide increases, ranging from 40% SiO_2 (3.21 eV) to 80% SiO_2 (3.12 eV) in the material. The values obtained here tend to follow the trend described in the literature when small quantities of SiO_2 are present in the material, *i.e.* when TiO_2 is doped, whereas in our case the quantities of SiO_2 are higher and should therefore follow the opposite trend, a decrease in bandgap when the quantity of SiO_2 increases, as described in the article by Fatimah, I. *et al.*[14]

Table 7: Bandgaps obtained for the different 1D NTs oxides materials.

Samples	Eg (eV)
MO SiO_2:TiO_2=75:25	3.87
MO SiO_2:TiO_2=50:50	3.86
MO SiO_2:TiO_2=25:75	3.82
TiO_2	2.83

Due to the many parameters that can influence the measurement, which have been mentioned in section 3.2.5., the results should be treated with caution. The amorphous TiO_2 synthetised by our method has a bandgap of 2.83 eV, which is lower than the crystalline TiO_2 P-25 value of 3.20 eV reported in the literature.[88] As a reminder, to have good photoactivity, the material must have a dual function: good adsorption and be effective as a catalyst in the desired wavelength range.[40] The photoactivity of amorphous TiO_2 is due to its large specific surface area and its high adsorption capacity, but still theoretically weaker than the crystalline TiO_2. Indeed, the activity of amorphous TiO_2 is limited by the rapid recombination of photogenerated charge carriers due to the absence of an energy barrier for recombination.[40,89] To increase this barrier and reduce recombination, amorphous TiO_2 must be doped with heteroatoms or TiO_2-semiconductor hybrids must be formed.[90]

3.3. Synthesis of pure TiO_2 and mixed oxide SiO_2/TiO_2 3D NT networks

In order to move from 1D NTs (**Figure 27.(c)**) to a 3D membrane of interconnected NTs (**Figure 27.(d)**), the used template should be a PC membrane with tilted and interconnected pores (**Figure 27.(b)**) instead of PC membrane with straight pores (**Figure 27.(a)**). It should be noted that pore size is not identical in both cases, going from 400 nm for the 1D template to 300 nm for the 3D template, which may influence gel diffusion within the pores of the template.

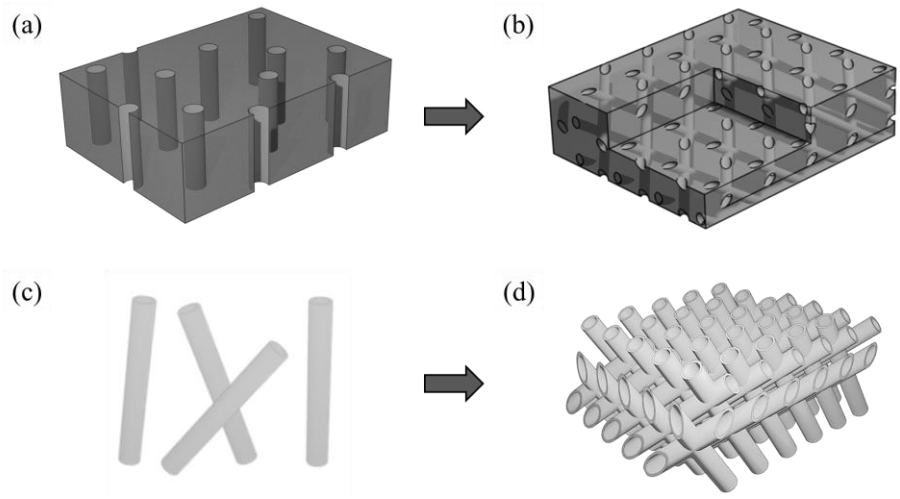

***Figure 27**: Representation of (a) PC template with straight pores, (b) PC template with tilted and interconnected pores, (c) 1D NTs and (d) 3D network of interconnected NTs.*

3.3.1. Synthesis of 3D interconnected NTs and SEM + EDX results

The synthesis of 3D networks of NTs in pure SiO_2 is described in the article by Drault F. *et al.*[31] and the solution composition as well as the durations are identical to those for the synthesis of SiO_2 1D NTs. This synthesis consists of preparing a 60 ml sol-gel solution by adding 34.19 g EtOH, 4.28 g water, 1.29 g HCl (1 M) and 10.52 g of SiO_2 precursor (TEOS), in that precise order. The solution was then left to age without stirring for 3 h at RT before the PC template in its Teflon holder was immersed for 1 h 30 at RT under stirring at 600 rpm. The PC membrane(s) was recovered and the excess of solution was removed using a Kimtech before being left to dry in an oven at 100 °C for 24 h. This synthesis was reproduced, and the 3D network of interconnected SiO_2 NTs was obtained, as shown in **Figure 28.**

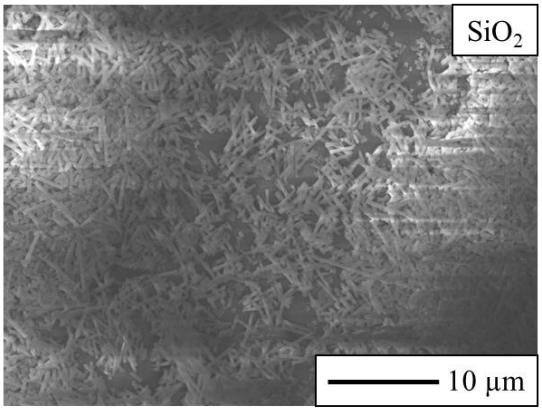

Figure 28*: SEM images of 3D network of interconnected nanotubes made of pure SiO_2.*

Since the synthesis transposition from 1D to 3D for the SiO_2 NTs system was successfully achieved, the same strategy was applied for the TiO_2 NTs. The composition of the precursor solution to create 3D NTs interconnected in TiO_2 was kept identical (ageing time: 1 h, impregnation time: 1 h 30) to the one used to obtain 1D NTs in pure TiO_2. However, as shown on **Figure 29**, no fully formed 3D network of interconnected TiO_2 NTs was obtained but only broken parts of NT network were observed. This probably results from a too far advanced hydrolysis of the precursor, leading to a diffusional problem into the PC template. This phenomenon could be accentuated by the smaller size of the pore diameter in the template with interconnected pores (300 nm) compared the one used to elaborate the 1D NTs (400 nm). Consequently, the formation of entire NTs, meaning around 25 µm of length, is partially inhibited.

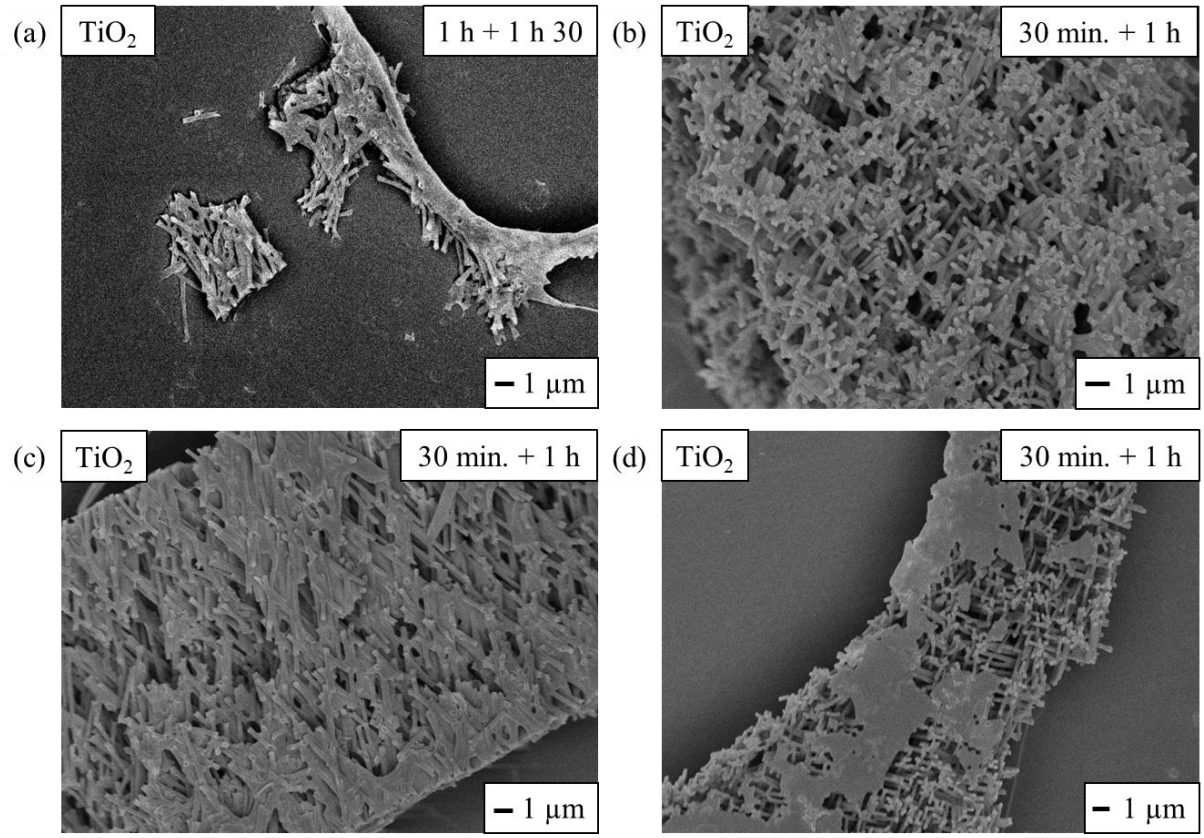

***Figure 29**: SEM image showing (a) parts of a 3D network of interconnected TiO_2 NTs before optimisation of ageing and impregnation times (1 h and 1 h 30 respectively) and (b-d) a 3D network of interconnected TiO_2 NTs after optimisation of ageing and impregnation times (30 min. and 1 h respectively). Conditions: solution ratio EtOH:ACAC:TTIP:H_2O=20:1:1:5.*

To improve the formation of the TiO_2 NTs network, the ageing and impregnation times were optimised. The reduction of the ageing time (from 1 h to 30 min.) could limit hydrolysis reaction and favours the penetration of the solution into the pores. The impregnation time (from 1 h 30 to 1 h) was also reduced to find an optimum. After several trials, the best conditions for obtaining a 3D network of interconnected TiO_2 NTs (see SEM image in **Figure 29.(b-d)**) are 30 min. of ageing of the solution to form the gel and 1 h of impregnation of the 3D PC template.

For the synthesis of 3D networks of mixed oxide NTs (TEOS:TTIP = 10:90, 25:75, 50:50 and 75:25), the same ageing time (30 min.) as previously optimised for the 3D network of interconnected TiO_2 NTs was used. In details, the solution containing the SiO_2 precursor, TEOS, was aged for 2 h 30 before adding the freshly prepared solution containing the TiO_2 precursor, TTIP. The resulting solution was then left to age for 30 min. to form the final gel. The impregnation time of the 3D PC template is set at 1 h 30, as for the synthesis of 3D networks of interconnected SiO_2 NTs. Using this synthesis protocol, 3D networks of interconnected NTs with different Si:Ti molar ratios (10:90, 25:75, 50:50 and 75:25) were successfully obtained as shown on SEM images in **Figure 30** (left column). EDX analysis was also performed on all these samples and the resulting mapping images of Si, Ti and O are presented in **Figure 30** (EDX spectra are available in Appendix 8).

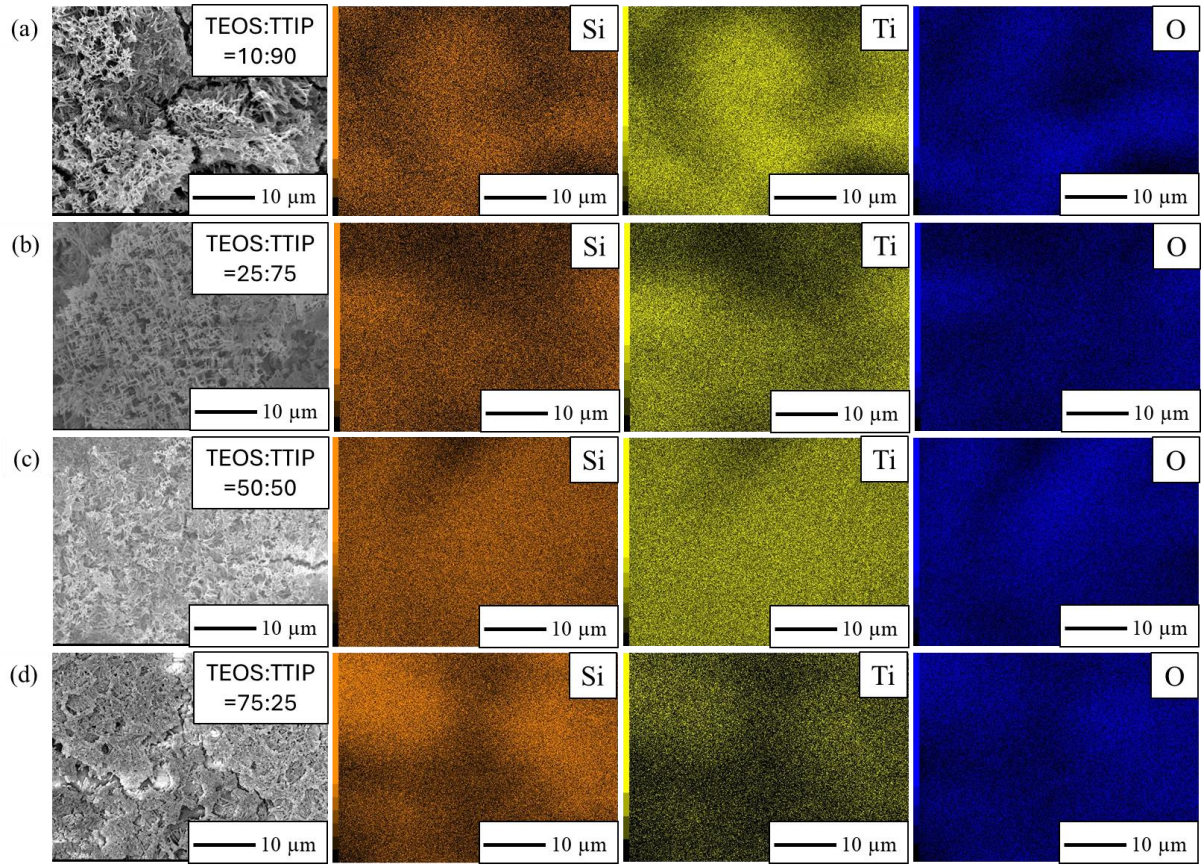

***Figure 30**: SEM images and EDX mapping analysis of interconnected 3D NT networks of mixed oxides with compositions: (a) SiO_2:TiO_2=10:90, (b) SiO_2:TiO_2=25:75, (c) SiO_2:TiO_2=50:50 and (d) SiO_2:TiO_2=75:25. Orange: Si map, yellow: Ti map and blue: O map.*

The presence of oxygen (blue) located at the same position than Si (orange) and/or Ti (yellow) confirms that SiO_2 and/or TiO_2 are very likely present. The differences in colour intensity between the Si and the Ti elements are less distinct than for the 1D NTs mixed oxides. Moreover, the colour intensity contrast between the different elements in each sample shows that MO SiO_2:TiO_2=50:50 are similar. For the MO SiO_2:TiO_2=75:25, the intensity for Si is significantly higher than that for Ti, which was expected. On the contrary, the intensity for Ti is significantly higher than that for Si for the MO SiO_2:TiO_2=10:90 and 25:75 samples, which was expected. This qualitatively confirms differences in the amount of Si and Ti elements incorporated in the final materials and could indicate as for the 1D MO NTs the desired trend corresponding to nominal ratios. Unfortunately, due to lack of time, no quantitative analysis was carried out (by XPS or ICP) as for the 1D materials to confirm and quantify this trend of ratios observed in EDX.

3.3.2. Solid state UV-visible spectroscopy characterisation: determination of bandgaps

The thickness of the 3D network of interconnected NTs (approximately 20 µm) suggests that improved results might be obtained by solid-state UV-visible analysis for bandgap determination. Interconnected 3D NT networks in pure SiO_2, TiO_2 and the mixed oxides (ratios SiO_2:TiO_2=10:90, 25:75, 50:50 and 75:25) were deposited onto PET and subsequently analysed by solid-state UV-visible spectroscopy. The absorbance spectra of the different materials are presented in **Figure 31.(a)**, while the corresponding Tauc diagrams for the determination of indirect bandgaps are shown in **Figure 31.(b)**.

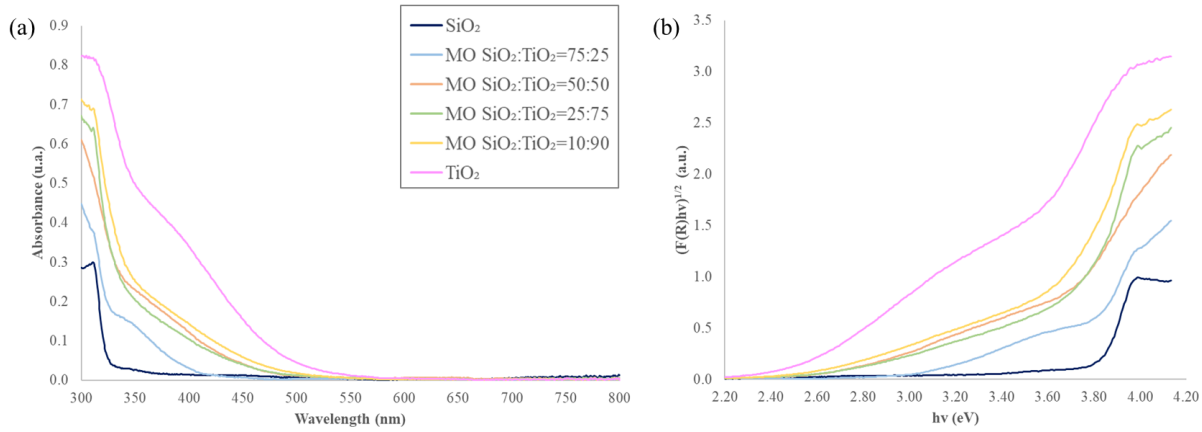

***Figure 31**: (a) Solid-state UV-visible spectra and (b) transformed reflectance spectra of SiO_2 (blue), MO SiO_2:TiO_2=75:25 (light blue), MO SiO_2:TiO_2=50:50 (orange), MO SiO_2:TiO_2=25:75 (green), MO SiO_2:TiO_2=10:90 (yellow) and TiO_2 (pink) 3D interconnected NTs samples.*

The 3D network of interconnected pure SiO_2 NTs appears to absorb from 325 nm with peaks at around 300 nm. This aligns precisely with the absorbance of PET, as discussed previously in section 3.2.5. for titania.

A similar trend was observed for the intensity of the peak located at 300 nm corresponding to TiO_2 as seen in 1D NTs (**Figure 31.(a)**). Absorbance at 300 nm is directly proportional to the amount of TiO_2 in the mixed oxides. The spectra also display a similar shoulder as observed in the spectra of 1D materials, located around 380 nm. This shoulder is visible for TiO_2, which is unexpected, as it was previously attributed to the modification of TiO_2 by SiO_2. Therefore, this shoulder might be explained by the fact that we have amorphous materials, the size of the nanotubes and their orientation, *etc.* as detailed in section 3.2.5. Unfortunately, there are no available solid UV-visible spectra of amorphous materials in the literature to compare to the results obtained in this study. Two different bandgaps were

determined for TiO_2 due to the presence of the shoulder and therefore two possible interpretations since the nature of the shoulder may be multiple and is not clearly identified. The first method consists of abstracting the shoulder and extrapolating the linear region of the peak to 300 nm (as for the pure 1D TiO_2 in **Figure 26.(b)** in section 3.2.5.).[75] This gives a bandgap of 3.25 eV, close to the 3.20 eV reported in the literature for P-25 TiO_2 used as a reference.[82] The second method involves taking account of the shoulder and using the graphical construction described in section 1.4.3., which is normally used for mixed oxides. A bandgap of 3.60 eV was determined by this method. The bandgap for SiO_2 was not calculated because it does not absorb visible light and its absorbance corresponded to PET. For mixed oxides, the determination method for bandgaps is identical to that used for 1D NTs, as presented in **Figure 26.(b)** in section 3.2.5.[75] The graphical determination of bandgap values is provided in Appendix 9 and the so-determined bandgaps are collected in **Table 8**.

The trend observed is similar for 3D materials as for NTs with the mixed oxides exhibiting higher bandgap than TiO_2. The values around 3.80 eV for MO correspond to those calculated for 1D NTs. However, the bandgap value for 3D TiO_2 NTs is found to be here 3.25/3.60 eV (depending on the method used to determine the bandgap), compared to 2.83 eV for 1D pure titania NTs. As the synthesis method was identical, the formed materials should be comparable, and such a significant discrepancy is unexpected. Unfortunately, it is not possible to verify the accuracy of these results, so they should be interpreted with caution, similarly than for 1D materials.

Table 8: Bandgap determined for the different 3D materials.

Samples	Eg (eV)
SiO_2	/
MO SiO_2:TiO_2=75:25	3.84
MO SiO_2:TiO_2=50:50	3.73
MO SiO_2:TiO_2=25:75	3.79
MO SiO_2:TiO_2=10:90	3.76
TiO_2	3.25[a]/3.60[b]

[a]Value determined by prolonging the linear part of the peak at 300 nm corresponding to the absorption of TiO_2
[b]Value determined by considering the observed shoulder and using the graphical construction of Makula, P. *et al.*[75]

3.4. Catalytic tests

The degradation of methylene blue in water is a commonly used model reaction described in the literature for evaluating the effectiveness of photocatalysts, providing additional characterisation for the various synthesised materials, enabling to compare them.[2,40,64]

Two types of photocatalytic tests were carried out: continuous flow tests and batch tests. The flow tests were used to compare the activity of the different synthesised mixed oxides with different Si:Ti ratios, while the batch tests were performed to study the effect of calcination. All catalytic tests were carried out using 1D NTs. Unfortunately, due to constraints in time and the incomplete characterisation of the 3D networks of interconnected NTs, photocatalytic tests have not yet been conducted on these materials. However, the potential for these 3D networks is very promising, and future research in this area is expected to be highly exciting.

3.4.1. Continuous flow photocatalytic tests

Continuous flow photocatalytic tests were carried out on the amorphous materials, *i.e.* not calcined, deposited on a PET membrane with 5 µm diameter pores. Herein, the objective is to compare the photocatalytic efficiency of the different synthesised 1D NTs: SiO_2, TiO_2 and MO SiO_2:TiO_2=75:25, 50:50, 25:75 and 10:90 in continuous flow. This process is the ultimate objective of this work, as it offers continuous degradation and allows full valorisation of the interconnected 3D networks of NTs. Initially, the tests were performed using 1D NTs, which in theory should give similar results than the 3D network of interconnected NTs and enable the best MO to be selected for futures works and applications.

To quantify MB degradation, a calibration curve was first established using UV-visible "Microplate Readers" spectrophotometer. This involves calculating the area under the absorbance peaks in the spectra between 420 and 750 nm for five calibration solutions of MB with known concentrations of 2, 3, 5, 10 and 12 $mg.L^{-1}$ (**Figure 32**).

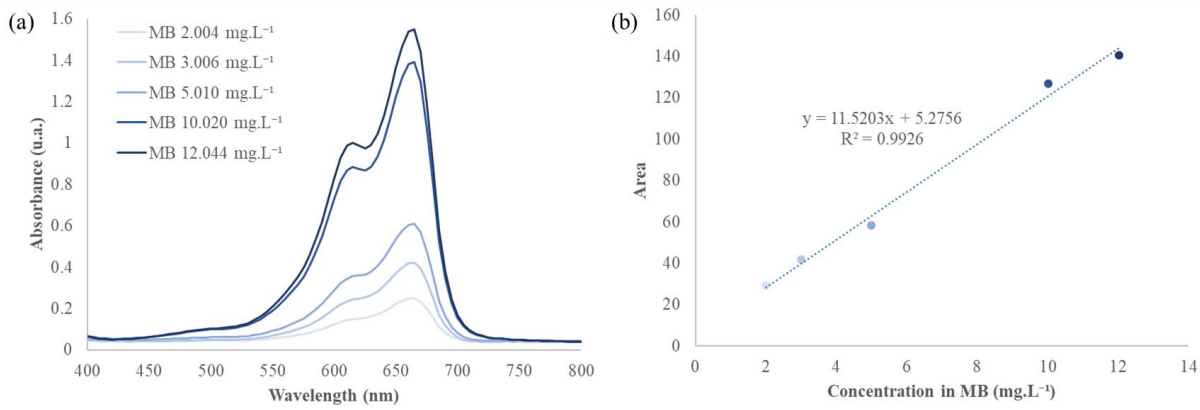

***Figure 32**: (a) UV-visible spectra of different solutions with known MB concentrations and (b) plot of the area under the curve between 420 and 750 nm as a function of MB concentration with the blue dots representing experimental values and the dotted line representing the linear regression with its equation.*

The continuous flow photocatalytic tests were carried out by placing the PET membrane on which the NTs were deposited inside a specially designed PC cell (see **Figure 14**). Once hermetically closed, the cell was connected to a peristaltic pump to generate a flow rate of 0.05 $ml.min^{-1}$ of 5 $mg.L^{-1}$ MB solution. Illumination was applied from the top of the cell at a power of 0.075 W/cm^2. Aliquots of 0.5 ml were collected every 10 min. over a period of 1 h and UV-visible analysis of the solutions was carried out to determine the concentration and subsequent conversion to MB was then calculated using formula (1) given in section 2.6.2.

The results of the catalytic tests on the different 1D NTs examined have been ordered from left to right in **Figure 33**: SiO_2, MO SiO_2:TiO_2=75:25, MO SiO_2:TiO_2=50:50, MO SiO_2:TiO_2=25:75, MO SiO_2:TiO_2=10:90, TiO_2. A blank test (at the extreme left of **Figure 33**) was performed first with a virgin PET membrane and under irradiation using the same conditions as the catalyst tests, to account for absorption in the PET pores and possible photolysis of the MB solution in homogeneous phase. It is therefore important to compare the results with the blank to identify photocatalytic activity due to our solid materials.

One test with pure TiO_2 was reproduced two times and similar results were obtained (see Appendix 10), meaning that the reproducibility of the test is good. As the deposition of NTs on PET is not homogeneous and only a 6 mm diameter circle (PET membrane diameter = 10 mm) is exposed to the flow, the quantity of catalyst exposed may slightly differ from one test to another and therefore explain slight variations in the results.

The data after 10 min. (the first bar for each sample of **Figure 33**) is attributed to the absorption of the MB solution in the PET support and in the material. This data varies accordingly to the amount of 1D NTs deposited on PET and the affinity of the material for MB.

When comparing the samples, it can be noted first that the conversion values obtained with pure SiO_2 are close to those of the 5 µm PET used as a blank (the first two samples at the left of **Figure 33**), meaning that the only effects present are absorption and homogeneous photolysis. Second, most degradations rates are stable over time in flow conditions (samples MO SiO_2:TiO_2=50:50, 25:75 and 10:90 of **Figure 33**), meaning that photocatalytic activity is constant. A decrease in conversion overtime, like for TiO_2 (on the very right of the **Figure 33**), could be due to the catalyst detaching from the PET support and being carried away by the flow, or deactivation of the photocatalytic material. On the contrary, an increase in conversion, like for MO SiO_2:TiO_2=75:25, is more complex to explain, but could be due to the lamp reaching its maximum power, a slight thermal effect, or slight differences in irradiation due to the position of the photocatalytic cell. At first sight, the MO SiO_2:TiO_2=50:50 appears to be the most active catalyst. In addition, it has good stability because the degradation of the MB is constant.

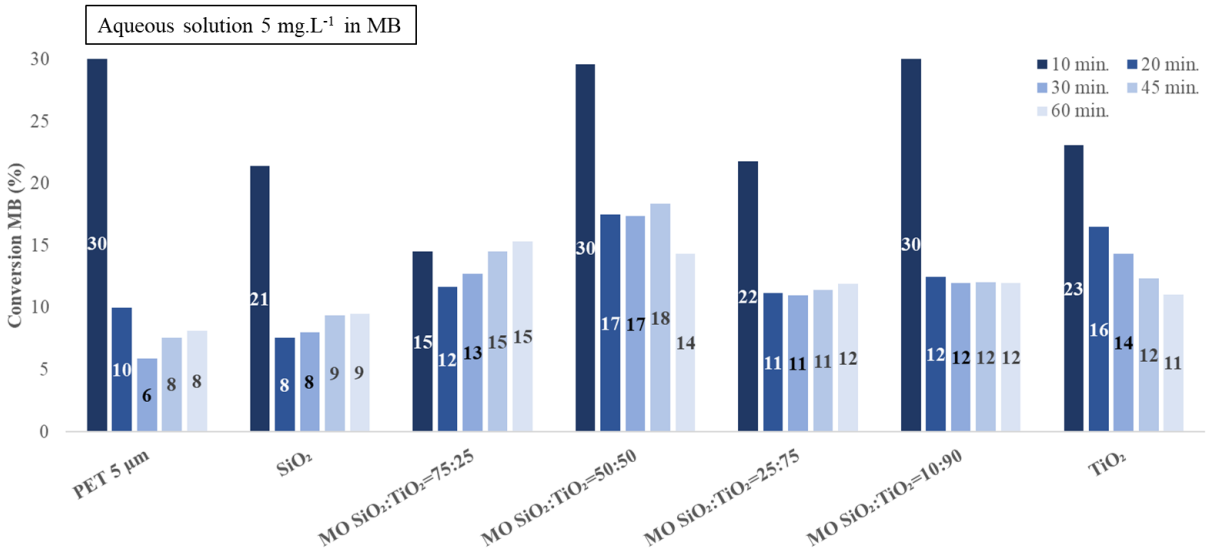

***Figure 33**: MB conversion (%) after 10, 20, 30, 45 and 60 min. for tests carried out in continuous flow on: the 5 µm PET membrane alone, 1D NTs in pure SiO_2, MO SiO_2:TiO_2=75:25, MO SiO_2:TiO_2=50:50, MO SiO_2:TiO_2=25:75, MO SiO_2:TiO_2=10:90 and pure TiO_2 released on PET and with an aqueous MB solution of 5 mg.L^{-1}.*

To facilitate the comparison of the results obtained for the different samples, in **Figure 34**, we only present the MB conversion (%) after 45 min. The theoretical conversions of mixed oxides were calculated based on the activity of the pure monoxide silica and titania NTs with a linear relationship. The results indicate that only two mixed oxides exhibit significant photocatalytic effects above these calculated values: MO SiO_2:TiO_2=75:25 and 50:50. The photocatalytic effect due to light exposure, can be determined using the following formula:

$$Photocatalytic\ efficiency\ (\%) = \frac{Conv._{45\ min.} - Conv._{th}}{Conv._{th}} * 100 \quad (5)$$

Where $Conv._{45\ min.}$ is the conversion after 45 min. and $Conv._{th}$ is the theoretical conversion calculated on the basis of the SiO_2 and TiO_2 conversions as explained above.

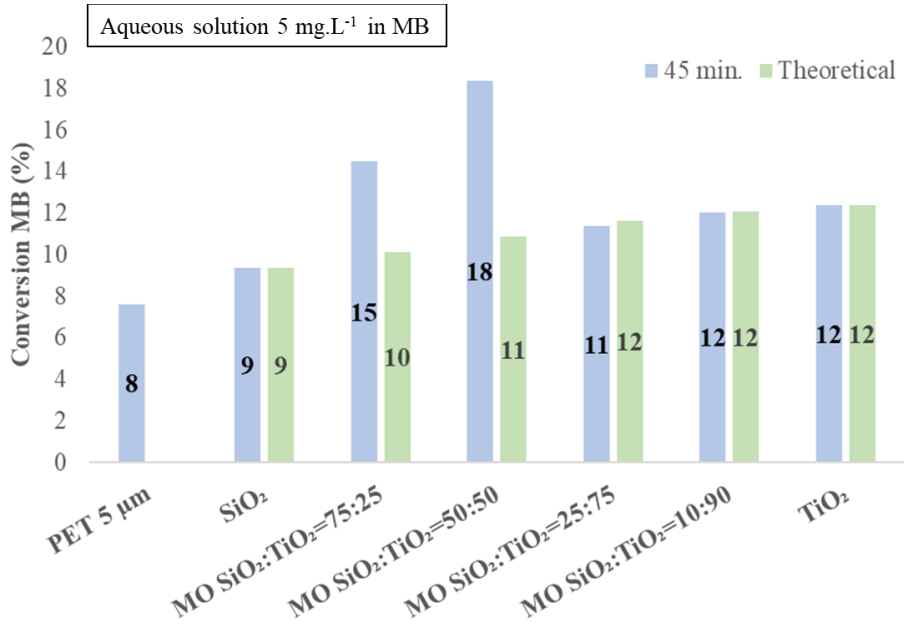

***Figure 34**: MB conversion (%) after 45 min. (blue) and theoretical (green) for 5 µm PET alone, pure SiO_2, MO SiO_2:TiO_2=75:25, MO SiO_2:TiO_2=50:50, MO SiO_2:TiO_2=25:75, MO SiO_2:TiO_2=10:90 and pure TiO_2 released on PET and with an aqueous MB solution of 5 mg.L^{-1}.*

The calculated photocatalytic effect is 43.50% for MO SiO_2:TiO_2=75:25 and 68.99% for MO SiO_2:TiO_2=50:50. Thus, the best synthesised catalyst appears to be the MO SiO_2:TiO_2=50:50. To confirm this, further experiments with intermediate ratios should be conducted. This would help identify any potential quadratic relationship between the conversion and the molar ratio in order to find the optimum SiO_2:TiO_2 molar ratio. In the article by Fatimah I. *et al.*[91], the mixed oxide samples with ratios SiO_2:TiO_2=40:60 and 60:40 were the only two cases to exhibit a better photodegradation than pure TiO_2, which is consistent with the results obtained in our study. The importance of silica is multiple, even though it is not

photoactive: (i) it offers a large specific surface area, (ii) it increases the hydrophobicity of the mixed oxide (promoting the adsorption of organic molecules and their proximity to the TiO_2 reactive centres) and (iii) it reduces the rate of charge carrier recombination.[15] Therefore, the optimum balance has to be found between the quantity of active phase, *i.e.* TiO_2, and SiO_2 whose properties enable the catalyst to be improved.

In the literature, Rasalingam S. *et al.*[15] reported that the large number of defects found in amorphous materials increases the recombination of charge carrier and therefore reduces catalyst activity. However, the article by Klein S. *et al.*[71] reported catalytic activity for amorphous mixed oxides. As in the last article, two of our catalysts: MO SiO_2:TiO_2=75:25 and 50:50, have demonstrated photoactivity. However, an improvement in photoactivity is expected for calcined and therefore crystalline materials, but this remains to be confirmed by synthesising and testing these materials.

The MO sample prepared with a ratio SiO_2:TiO_2=75:25 was also tested in the dark to verify that the degradation of the MB was due to photoactivity of our catalyst. The results obtained are shown in **Figure 35**. As one can see, in the dark, conversion is only observed over the first 20 min. This period corresponds to what has previously been identified as the absorption of methylene blue in PET as well as in our material. For times greater than 20 minutes, the conversion observed was practically inexistent, confirming that the catalyst is inactive in the absence of irradiation and therefore that the conversion observed under the lamp is due to the photoactivity of our catalyst.

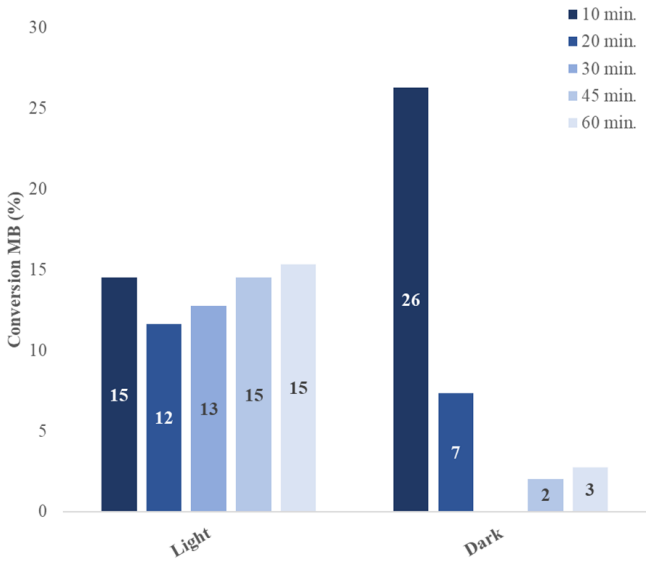

***Figure 35**: MB conversion (%) after 10, 20, 30, 45 and 60 min. for tests carried out in continuous flow under irradiation and in the dark with MO SiO_2:TiO_2=75:25 released on PET and with an aqueous MB solution of 5 mg.L^{-1}.*

The problem with flow catalytic testing is its incompatibility with our calcined catalysts in powder form. In a test, a calcined powder was placed on a 5 µm PET membrane and DCM was passed over it in an attempt to stick it to the membrane. Unfortunately, during catalytic flow test, the powder was detached from the membrane by the flowing MB solution. As the powder was positioned on top of the PET membrane, large quantities of catalyst were progressively lost during the test. This issue did not arise for non-calcined (amorphous) NTs, as deposition on PET occurred when the NTs were released from their PC template on PET using DCM. Although DCM solubilises the PC, it likely does not completely dissolve it, and the remaining PC acts as a "glue" attaching the NTs onto the PET.

As a result, batch photocatalytic tests were conducted to investigate the difference between calcined and non-calcined NTs. Experiments still need to be carried out before any conclusions can be drawn regarding the results obtained.

3.4.2. Batch photocatalytic tests

Batch photocatalytic tests were carried out on calcined and non-calcined 1D NTs powders to observe potential differences in catalytic activity. These tests were carried out in a cuvette to enable kinetic monitoring of degradation by a UV-visible spectrophotometer. The lamp used was identical to that for the continuous flow catalytic tests, but a filter cutting wavelengths below 400 nm was employed. This filter allows investigating whether there is a shift in the visible range compared with TiO_2 (normally inactive above 400 nm). The cuvette was placed at a fixed distance to ensure the same power as that used for continuous-flow catalytic tests (0.075 W/cm²).

A preliminary blank test was performed with a solution of 10 $mg.L^{-1}$ MB solution, without catalysts and under irradiation. Significant degradation was observed, which can be linked to a photolysis and/or a slight thermal effects in homogeneous phase (*i.e.* without the assistance of solid catalyst). Therefore, the photocatalytic tests of our materials will have to be interpreted taking into account this effect observed without a catalyst.

The following NTs powders were tested, in addition to the blank, with the 10 $mg.L^{-1}$ solution: non-calcined TiO_2 (TiO_2_nc), calcined TiO_2 (TiO_2_c) and calcined MO SiO_2:TiO_2=75:25 (MO SiO_2:TiO_2=75:25_c). The aim was firstly to compare calcined and non-calcined TiO_2 NTs and then calcined TiO_2 NTs and calcined MO SiO_2:TiO_2=75:25 NTs.

In order to quantify MB degradation, a calibration curve was first established using the single-beam UV-visible spectrophotometer in liquid mode. To do this, the area under the absorbance spectra was recorded between 530 and 730 nm for five calibration solutions of MB with known concentrations of 2.0, 3.0, 5.0, 7.5 and 10.0 $mg.L^{-1}$ (**Figure 36**). The area under the curve was taken between 530 and 730 nm instead of between 420 and 750 nm due to the appearance of the spectra when the catalyst is suspended in the MB solution. Indeed, a deviation from the baseline is observed, probably due to scattering of the incident beam by the suspended NTs.

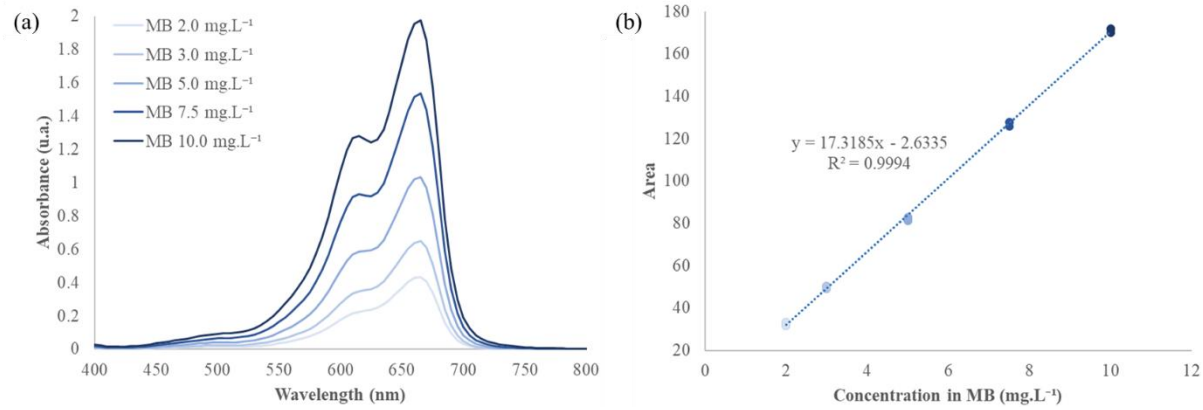

***Figure 36**: (a) UV-visible spectra of different solutions with known MB concentrations and (b) plot of the area under the curve between 530 and 730 nm as a function of MB concentration with the blue dots representing experimental values and the dotted line representing the linear regression with its equation.*

The results obtained for the photocatalytic tests in batch are gathered in **Figure 37**. The time t = 0 min. corresponds to the moment at which the illumination began. The cuvette was then left under the lamp for 10 min. before a new measurement, t = 10 min., was taken. This protocol was repeated six times (total duration of 1 h). The area under the peak was then recorded after baseline correction and related to the MB concentration using the calibration line (**Figure 36**). The conversion to MB was then calculated using formula (1) given in section 2.6.2.

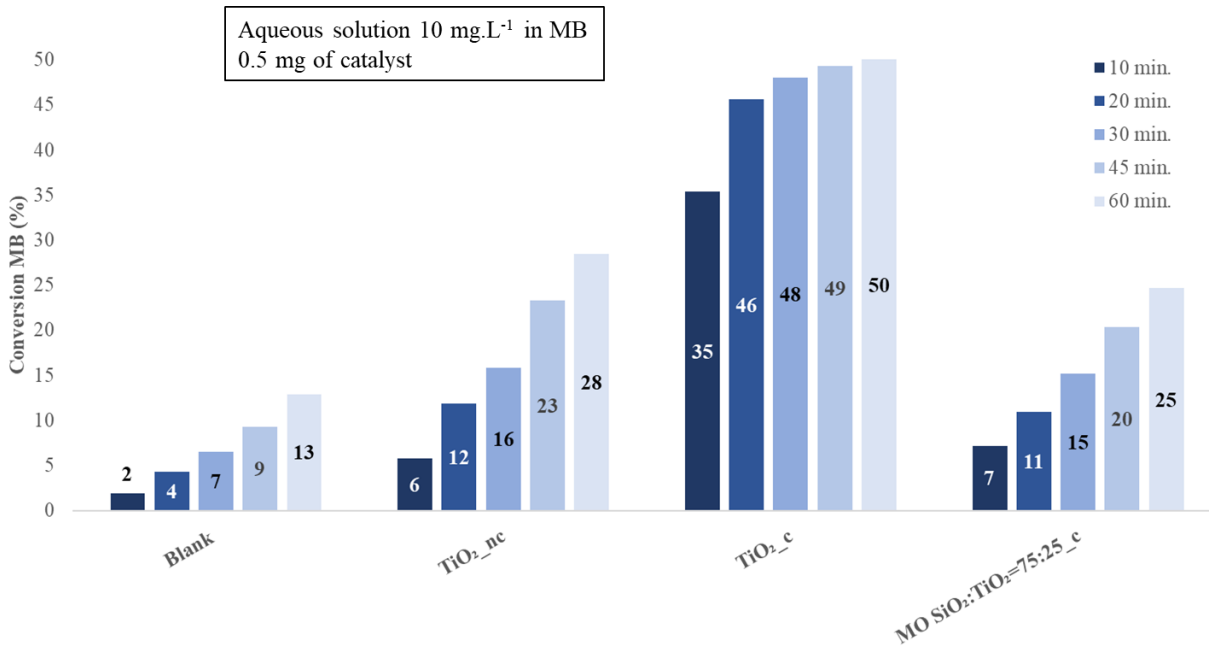

***Figure 37**: MB conversion (%) after 10, 20, 30, 45 and 60 min. for batch tests carried out with: a blank (without catalyst), TiO_2_nc (non-calcined), TiO_2_c (calcined) and MO SiO_2:TiO_2=75:25_c (calcined) with an aqueous MB solution of 10 mg.L^{-1}.*

The conversion to MB with calcined TiO_2 (TiO_2_c) as catalyst is significantly higher than that observed for non-calcined TiO_2 (TiO_2_nc) and the calcined mixed oxide SiO_2:TiO_2=75:25 (MO SiO_2:TiO_2=75:25_c) (**Figure 37**). The conversions obtained for calcined TiO_2, *i.e.* crystalline, were higher than those for non-calcined TiO_2, *i.e.* amorphous, suggesting that the calcined catalyst is more efficient. The article of Di Paola, A. *et al.*[92] confirms that the photocatalytic activity of TiO_2 powder increases with an increase in crystallinity. Nevertheless, the conversion obtained with both TiO_2 samples, calcined and non-calcined, are surprising since TiO_2 with a bandgap around 3.2 eV should be photoactive only in the UV range and tests were performed using a filter to cut wavelengths below 400 nm.

Moreover, the plateau observed from 20 min. for calcined TiO_2 could be interpreted as saturation of the number of MB molecules adsorbed or an almost complete deactivation of the catalyst. Both phenomena are not observed in the other batch tests, which makes it complex to treat these results. Actually, to thoroughly understand the observed photocatalytic behaviour, several additional tests would be necessary. Firstly, to reduce the effects of photolysis in homogeneous phase, the tests could also have been carried out on larger volumes, though it would require more catalyst. Secondly, it is essential to carry out tests in the dark in order to confirm the photoactive effect of the catalysts. In parallel, the photoactivity of photocatalysts could be demonstrated by increasing catalyst loadings, lamp power, catalytic test times, allowing time for the MB to be absorbed into the materials before starting the irradiation, or by irradiating at other wavelengths (by possibly cutting at certain wavelengths). Tests for comparing calcined and non-calcined TiO_2 could be carried out using UV irradiation (< 400 nm) to check whether there is a difference in photoactivity induced by the phase change under such wavelengths. It is also necessary to understand which phase out of the SiO_2 or TiO_2 contributes to the adsorption and how, to understand the difference in adsorption of the MB on the surface of the catalyst if the phase is amorphous or crystalline, and a pure or a mixed oxide, *etc*. and to correctly interpret the results. Answers could be provided by carrying out surface analyses such as nitrogen physisorption analysis to obtain the specific surface area of our catalysts.

These tests and analyses mark only the beginning of the catalytic investigation. They are designed to address specific questions raised by initial experiments, leading to a deeper understanding of the catalysts functioning. Further experiments will be required to draw definitive conclusions and optimise the photocatalytic system for practical applications.

Chapter IV:
Conclusions and outlook

4.1. Conclusions

The aim of this Master's Thesis was to synthesise mixed oxide nanotubes with different molar ratios SiO_2:TiO_2 (10:90, 25:75, 50:50 and 75:25) in three dimensions using the combination of hard templating and sol-gel methods.

The first part of this Master's Thesis was dedicated to adapting and optimising a procedure reported in the literature for the synthesis of 1D TiO_2 nanotubes by sol-gel process using an AAO membrane as a hard template to the use of a polycarbonate (PC) membrane as template.[54] Understanding the role of acetylacetone (ACAC) in stabilising the TiO_2 precursor (TTIP), which has a high hydrolysis rate and the role of water in initiating hydrolysis, permitted the composition adjustment of the solution to obtain an optimum molar ratios of: EtOH:ACAC:TTIP:H_2O=20:1:1:5. Using this precursor solution composition, we found that the optimum ageing and impregnation times were 1 h and 1 h 30, respectively to obtain NTs with the expected morphology (length and wall's thickness) by avoiding diffusional problems of the gel in the template. The formation of nanotubes thanks to the PC hard template was confirmed by SEM and TEM analysis. The difference of surface morphology observed in TEM between calcined and uncalcined nanotubes (rough and smooth, respectively) was also highlighted by XRD, since these materials were respectively crystalline and amorphous. Moreover, XRD data treatment revealed that the calcined TiO_2 nanotubes were composed of 71.73% anatase and 28.27% rutile, which corresponds closely to the TiO_2 P-25 commercial reference (75% anatase and 25% rutile).

The mastery of the 1D TiO_2 synthesis permitted then the focus on the synthesis of 1D mixed oxide nanotubes made of SiO_2 and TiO_2 with different molar ratio (10:90, 25:75, 50:50 and 75:25). For this purpose, we combined the synthesis protocol of SiO_2 nanotubes developed by Dr. F. Drault and the synthesis protocol of 1D TiO_2 nanotubes developed and optimised in this Master Thesis. Two sol-gel preparation methods with differences in the maturation step were studied and the addition of HCl during synthesis was demonstrated to be essential for obtaining well-formed nanotubes. Moreover, both synthesis methods produced nanotubes

composed of Si and Ti in oxide form, as demonstrated by SEM-EDX images. As for 1D TiO_2 nanotubes, TEM analysis revealed again a difference in morphology between calcined and non-calcined nanotubes, suggesting that the nanotubes are crystalline and amorphous in these two cases, respectively. The optimal method of maturation was with the addition of TTIP into the matured solution of TEOS after 2 h and then this mixed solution was aged for 1 h. Indeed, the Si:Ti ratio measured by XPS corresponded to the nominal molar ratios of each precursor in the initial solution used to form the gel. Quantitative incorporation was confirmed by ICP, meaning that the surface composition reflected the composition of the material as a whole, in the bulk. The bandgaps, measured by solid-state UV-visible spectroscopy for the various amorphous SiO_2:TiO_2 mixed oxides were higher than that of TiO_2 (~ 3.85 eV versus 2.83 eV for TiO_2) suggesting unfortunately that no shift from UV to visible absorption was induced by the addition of SiO_2 within TiO_2.

Then, 3D networks of interconnected nanotubes were synthetised using the achievements established in the two previous sections. However, the 1D template has 400 nm pores, while the 3D template has 300 nm pores, which means that the maturation time of the solution used to form the gel and the impregnation time of the polycarbonate template in this gel had to be adapted. Synthesis of a 3D network of interconnected TiO_2 nanotubes necessitated a reduction in the maturation time of the solution from 1 h to 30 min. and in the impregnation time of the template in the gel from 1 h 30 to 1 h. For mixed oxides, the solution containing the freshly prepared TiO_2 precursor is now added 2 h 30 after the beginning of the ageing of the solution containing the SiO_2 precursor. The resulting solution containing both precursors is then left to mature for a further 30 min., before impregnating the polycarbonate 3D template for 1 h 30 (this time was not varied and is based on the synthesis of interconnected SiO_2 nanotubes 3D membranes). SEM-EDX images confirmed the expected network structure and the qualitative incorporation of Si and Ti in oxide form in the SiO_2:TiO_2 mixed oxides. Solid-state UV-vis spectroscopy characterisation was also carried out, showing similar results to those obtained for 1D nanotubes in mixed oxides (bandgap ~ 3.78 eV for 3D versus 3.85 eV for 1D MO) but the bandgaps obtained for TiO_2 vary more significantly (bandgap ~ 3.20/3.60 eV for 3D versus 2.83 eV for 1D TiO_2).

Finally, continuous flow catalytic tests on the photodegradation of methylene blue were conducted with the various non-calcined (amorphous) mixed oxides as photocatalysts, using visible light. The photoactivity of two MO with the composition SiO_2:TiO_2=75:25 and 50:50, was above that of their corresponding monoxides. Batch catalytic tests were also carried out to study the influence of calcination on photocatalytic activity. These tests are still in their early stages and further tests need to be performed before any conclusions can be drawn on the results obtained. More striking results might be obtained if the bandgap could be significantly reduced in the mixed oxides. This would require further iterative loops, involving perhaps great synthetic efforts.

4.2. Outlook

Understanding and optimising the synthesis of 1D TiO_2 using track-etched polycarbonate template has opened the door to the synthesis of a new material, mixed oxide nanotubes of SiO_2 and TiO_2. Then, the synthesis of 3D membranes made of interconnected nanotubes also opens many doors, as they can be used directly for catalysis under continuous flow. In the future, XPS and ICP should be performed on these latter samples to confirm that the incorporation of Si:Ti into the 3D network of interconnected nanotubes is quantitative, as it was the case for the 1D mixed oxide nanotubes.

In addition, the effect of the calcination step on the materials could be studied further for the photodegradation of MB in batch mode since it is complicated to use powders in our flow setup. Furthermore, one or more new compositions of MO between the ratios SiO_2:TiO_2=75:25 and 50:50 could be synthesised in an attempt to determine the optimum ratio for maximum photocatalytic activity. For catalytic tests in general, longer test times, the use of filters and control tests in the dark are parameters that need to be carefully studied in the future in order to understand the adsorption of MB in the materials, as well as the catalytic efficiency spectrum of our photocatalysts in terms of wavelengths. If a mixed oxide is active in the visible range, its use for other, possibly more original, photocatalytic reactions could be studied.

Finally, longer-term perspectives might extend to the production of other mixed oxides by combining TiO_2 with ZnO or even materials such as gold or C_3N_4 already developed in the project CaScadOS, depending on potential applications. The possibility of creating core-shell nanotubes between different materials, enabling different internal and external functionalisation, inducing porosity to increase the specific surface area of the material, hybridisation of these nanotubes with other active phases (decoration by nanoparticles, grafting of organometallic complexes, *etc*.) would open the door to photocatalysed cascade reactions as ultimate goal of our project.

References

(1) Slama, H. Ben; Bouket, A. C.; Pourhassan, Z.; Alenezi, F. N.; Silini, A.; Cherif-Silini, H.; Oszako, T.; Luptakova, L.; Golińska, P.; Belbahri, L. Diversity of Synthetic Dyes from Textile Industries, Discharge Impacts and Treatment Methods. *Applied Sciences (Switzerland)* **2021**, *11* (14). https://doi.org/10.3390/app11146255.

(2) Houas, A.; Lachheb, H.; Ksibi, M.; Elaloui, E.; Guillard, C.; Herrmann, J.-M. Photocatalytic Degradation Pathway of Methylene Blue in Water. *Appl Catal B* **2001**, *31*, 145–157.

(3) DeJohn, P. B. , & H. R. A. Treatment of Dye Wastes with Granular Activated Carbon. *Textile Chemist & Colorist* **1976**, *8(4)*.

(4) Patil, S. S.; Shinde, V. M. Biodegradation Studies of Aniline and Nitrobenzene in Aniline Plant Wastewater by Gas Chromatography. *Environ Sci Technol* **1988**, *22* (10), 1160–1165. https://doi.org/10.1021/es00175a005.

(5) Slokar, Y. M.; Majcen Le Marechal, A. Methods of Decoloration of Textile Wastewaters. *Dyes and Pigments* **1998**, *37* (4), 335–356. https://doi.org/10.1016/S0143-7208(97)00075-2.

(6) Zhang, X.; Zhang, F.; Chan, K. Y. Synthesis of Titania-Silica Mixed Oxide Mesoporous Materials, Characterization and Photocatalytic Properties. *Appl Catal A Gen* **2005**, *284* (1–2), 193–198. https://doi.org/10.1016/j.apcata.2005.01.037.

(7) Hou, Y. D.; Wang, X. C.; Wu, L.; Chen, X. F.; Ding, Z. X.; Wang, X. X.; Fu, X. Z. N-Doped SiO2/TiO2 Mesoporous Nanoparticles with Enhanced Photocatalytic Activity under Visible-Light Irradiation. *Chemosphere* **2008**, *72* (3), 414–421. https://doi.org/10.1016/j.chemosphere.2008.02.035.

(8) Wang, L.; Yu, J. Principles of Photocatalysis. In *Interface science and technology*; **2023**; pp 1–52. https://doi.org/10.1016/B978-0-443-18786-5.00002-0.

(9) Gaya, U. I. *Heterogeneous Photocatalysis Using Inorganic Semiconductor Solids*; Springer Netherlands: Dordrecht, **2014**; Vol. 9789400777750. https://doi.org/10.1007/978-94-007-7775-0.

(10) Willkomm, J.; Orchard, K. L.; Reynal, A.; Pastor, E.; Durrant, J. R.; Reisner, E. Dye-Sensitised Semiconductors Modified with Molecular Catalysts for Light-Driven H_2 Production. *Chemical Society Reviews*. Royal Society of Chemistry January 7, **2016**, pp 9–23. https://doi.org/10.1039/c5cs00733j.

(11) Rungjaroentawon, N.; Onsuratoom, S.; Chavadej, S. Hydrogen Production from Water Splitting under Visible Light Irradiation Using Sensitized Mesoporous-Assembled TiO_2-SiO_2 Mixed Oxide Photocatalysts. *Int J Hydrogen Energy* **2012**, *37* (15), 11061–11071. https://doi.org/10.1016/j.ijhydene.2012.04.120.

(12) Abdullah, H.; Khan, M. M. R.; Ong, H. R.; Yaakob, Z. Modified TiO_2 Photocatalyst for CO_2 Photocatalytic Reduction: An Overview. *Journal of CO_2 Utilization* **2017**, *22*, 15–32. https://doi.org/10.1016/j.jcou.2017.08.004.

(13) Stroyuk, O. L.; Kuchmy, S. Y. Heterogeneous Photocatalytic Selective Reductive Transformations of Organic Compounds: A Review. *Theoretical and Experimental Chemistry* **2020**, *56* (3), 143–173. https://doi.org/10.1007/s11237-020-09648-0.

(14) Fatimah, I. Composite of TiO_2-Montmorillonite from Indonesia and Its Photocatalytic Properties in Methylene Blue and E.Coli Reduction Composite of TiO_2-Montmorillonite from Indonesia and Its Photocatalytic Properties in Methylene Blue and E.Coli Reduction. *J. Mater. Environ. Sci* **2012**, *3* (5), 983–992.

(15) Rasalingam, S.; Peng, R.; Koodali, R. T. Removal of Hazardous Pollutants from Wastewaters: Applications of TiO_2-SiO_2 Mixed Oxide Materials. *Journal of Nanomaterials*. Hindawi Publishing Corporation **2014**. https://doi.org/10.1155/2014/617405.

(16) Deng, Y.; Zhao, R. Advanced Oxidation Processes (AOPs) in Wastewater Treatment. *Current Pollution Reports*. Springer September 1, **2015**, pp 167–176. https://doi.org/10.1007/s40726-015-0015-z.

(17) Kizot Ambouckou Loïck Grâce. ETUDE DE LA DECOLORATION DU BLEU DE METHYLENE EN MILIEU AQUEUX, Université Badji Mokhtar-Annaba, Annaba, **2018**.

(18) SAIDI Fatima Zahra. Elimination Du Bleu de Méthylène Par Des Procédés d'Oxydation Avancée, Université Abou Bakr Belkaid, Tlemcen, **2013**.

(19) Ang, T. P.; Toh, C. S.; Han, Y. F. Synthesis, Characterization, and Activity of Visible-Light-Driven Nitrogen-Doped TiO_2-SiO_2 Mixed Oxide Photocatalysts. *Journal of Physical Chemistry C* **2009**, *113* (24), 10560–10567. https://doi.org/10.1021/jp9000658.

(20) Chang, W. T.; Hsueh, Y. C.; Huang, S. H.; Liu, K. I.; Kei, C. C.; Perng, T. P. Fabrication of Ag-Loaded Multi-Walled TiO2 Nanotube Arrays and Their Photocatalytic Activity. *J Mater Chem A Mater* **2013**, *1* (6), 1987–1991. https://doi.org/10.1039/c2ta00806h.

(21) Nasikhudin; Diantoro, M.; Kusumaatmaja, A.; Triyana, K. Study on Photocatalytic Properties of TiO_2 Nanoparticle in Various PH Condition. In *Journal of Physics: Conference Series*; Institute of Physics Publishing, **2018**; Vol. 1011. https://doi.org/10.1088/1742-6596/1011/1/012069.

(22) Yu, K. M. K.; Curcic, I.; Gabriel, J.; Tsang, S. C. E. Recent Advances in CO_2 Capture and Utilization. *ChemSusChem*. **2008**, pp 893–899. https://doi.org/10.1002/cssc.200800169.

(23) Lauraleen BARREMAECKER. Élaboration et Caractérisation de Nanotubes de C_3N_4 Photocatalytiques., UCLouvain, Louvain-la-Neuve, **2023**.

(24) Liu, Y.; Goebl, J.; Yin, Y. Templated Synthesis of Nanostructured Materials. *Chem Soc Rev* **2013**, *42* (7), 2610–2653. https://doi.org/10.1039/c2cs35369e.

(25) Prieto, G.; Tüysüz, H.; Duyckaerts, N.; Knossalla, J.; Wang, G. H.; Schüth, F. Hollow Nano- and Microstructures as Catalysts. *Chemical Reviews*. American Chemical Society November 23, **2016**, pp 14056–14119. https://doi.org/10.1021/acs.chemrev.6b00374.

(26) Zhu, C.; Du, D.; Eychmüller, A.; Lin, Y. Engineering Ordered and Nonordered Porous Noble Metal Nanostructures: Synthesis, Assembly, and Their Applications in Electrochemistry. *Chemical Reviews*. American Chemical Society August 26, **2015**, pp 8896–8943. https://doi.org/10.1021/acs.chemrev.5b00255.

(27) Roy, C. J.; Chorine, N.; De Geest, B. G.; De Smedt, S.; Jonas, A. M.; Demoustier-Champagne, S. Highly Versatile Approach for Preparing Functional Hybrid Multisegmented Nanotubes and Nanowires. *Chemistry of Materials* **2012**, *24* (9), 1562–1567. https://doi.org/10.1021/cm203279z.

(28) Ortel, E.; Sokolov, S.; Kraehnert, R. Influence of Steel Substrate Roughness on Morphology and Mesostructure of TiO_2 Porous Layers Produced by Template-Assisted Dip Coating. *Microporous and Mesoporous Materials* **2010**, *127* (1–2), 17–24. https://doi.org/10.1016/j.micromeso.2009.06.024.

(29) Kemell, M.; Härkönen, E.; Pore, V.; Ritala, M.; Leskelä, M. Ta_2O_5-and TiO_2-Based Nanostructures Made by Atomic Layer Deposition. *Nanotechnology* **2010**, *21* (3). https://doi.org/10.1088/0957-4484/21/3/035301.

(30) Liang, Z.; Susha, A. S. Mesostructured Silica Tubes and Rods by Templating Porous Membranes. *Chemistry - A European Journal* **2004**, *10* (19), 4910–4914. https://doi.org/10.1002/chem.200400005.

(31) Drault, F.; Ferain, E.; Lisboa, M. C.; Hermans, S.; Demoustier-Champagne, S. Tuning Au/SiO_2 Nanostructures from 1D to 3D Interconnected Nanotube Networks Using Polycarbonate Porous Templates. *Nanoscale* **2023**, *15* (36), 14981–14993. https://doi.org/10.1039/d3nr03783e.

(32) Kobayashi, Y.; Tadaki, Y.; Nagao, D.; Konno, M. Deposition of Gold Nanoparticles on Silica Spheres by Electroless Metal Plating Technique. *J Colloid Interface Sci* **2005**, *283* (2), 601–604. https://doi.org/10.1016/j.jcis.2004.09.002.

(33) Kim, J. U.; Han, H. S.; Park, J.; Park, W.; Baek, J. H.; Lee, J. M.; Jung, H. S.; Cho, I. S. Facile and Controllable Surface-Functionalization of TiO_2 Nanotubes Array for Highly-Efficient Photoelectrochemical Water-Oxidation. *J Catal* **2018**, *365*, 138–144. https://doi.org/10.1016/j.jcat.2018.06.022.

(34) Lefèvre, D.; Louvegny, J.; Naudin, M.; Ferain, E.; Dupont-Gillain, C.; Demoustier-Champagne, S. Biofunctionalized and Self-Supported Polypyrrole Frameworks as Nanostructured ECM-like Biointerfaces. *RSC Adv* **2018**, *8* (41), 22932–22943. https://doi.org/10.1039/c8ra00325d.

(35) da Câmara Santa Clara Gomes, T.; De La Torre Medina, J.; Lemaitre, M.; Piraux, L. Magnetic and Magnetoresistive Properties of 3D Interconnected NiCo Nanowire Networks. *Nanoscale Res Lett* **2016**, *11* (1). https://doi.org/10.1186/s11671-016-1679-z.

(36) Sambiagio, C.; Noël, T. Flow Photochemistry: Shine Some Light on Those Tubes! *Trends in Chemistry*. Cell Press February 1, **2020**, pp 92–106. https://doi.org/10.1016/j.trechm.2019.09.003.

(37) Juergen Heinrich Maar. Martin Heinrich Klaproth (1743-1817), a Great, Somewhat Forgotten, Chemist. *Substantia An International Journal of the History of Chemistry* **2023**, *7* (2), 2532–3997.

(38) Banerjee, A. N. The Design, Fabrication, and Photocatalytic Utility of Nanostructured Semiconductors: Focus on TiO_2-Based Nanostructures. *Nanotechnology, Science and Applications*. **2011**, pp 35–65. https://doi.org/10.2147/NSA.S9040.

(39) Landmann, M.; Rauls, E.; Schmidt, W. G. The Electronic Structure and Optical Response of Rutile, Anatase and Brookite TiO_2. *Journal of Physics Condensed Matter* **2012**, *24* (19). https://doi.org/10.1088/0953-8984/24/19/195503.

(40) Niu, L.; Zhao, X.; Tang, Z.; Lv, H.; Wu, F.; Wang, X.; Zhao, T.; Wang, J.; Wu, A.; Giesy, J. P. Difference in Performance and Mechanism for Methylene Blue When TiO_2 Nanoparticles Are Converted to Nanotubes. *J Clean Prod* **2021**, *297*. https://doi.org/10.1016/j.jclepro.2021.126498.

(41) L'Élémentarium. *Dioxyde de titane*. https://lelementarium.fr/product/dioxyde-de-titane/ (accessed 2024-05-25).

(42) Jafari, S.; Mahyad, B.; Hashemzadeh, H.; Janfaza, S.; Gholikhani, T.; Tayebi, L. Biomedical Applications of TiO_2 Nanostructures: Recent Advances. *International Journal of Nanomedicine*. Dove Medical Press Ltd. **2020**, pp 3447–3470. https://doi.org/10.2147/IJN.S249441.

(43) Çeşmeli, S.; Biray Avci, C. Application of Titanium Dioxide (TiO_2) Nanoparticles in Cancer Therapies. *Journal of Drug Targeting*. Taylor and Francis Ltd August 9, **2019**, pp 762–766. https://doi.org/10.1080/1061186X.2018.1527338.

(44) Choe, M. S.; Choi, S.; Lee, H. S.; Chon, B.; Shin, J. Y.; Kim, C. H.; Son, H. J.; Kang, S. O. Sustainable Carbon Dioxide Reduction of the P3HT Polymer-Sensitized TiO_2/Re(I) Photocatalyst. *ACS Appl Mater Interfaces* **2022**, *14* (45), 50718–50730. https://doi.org/10.1021/acsami.2c09924.

(45) Fitra, M.; Daut, I.; Irwanto, M.; Gomesh, N.; Irwan, Y. M. TiO_2 Dye Sensitized Solar Cells Cathode Using Recycle Battery. In *Energy Procedia*; Elsevier Ltd, **2013**; Vol. 36, pp 333–340. https://doi.org/10.1016/j.egypro.2013.07.038.

(46) Kochuveedu, S. T. Photocatalytic and Photoelectrochemical Water Splitting on TiO_2 via Photosensitization. *Journal of Nanomaterials*. Hindawi Limited **2016**. https://doi.org/10.1155/2016/4073142.

(47) *THÈSE DE DOCTORAT DE L'UNIVERSITÉ PIERRE ET MARIE CURIE Génie Des Procédés et Haute Technologie. Véronique SPAGNOL PROPRIÉTÉS SUPER-HYDROPHILES DE COUCHES DE TIO_2 NANO-COLONNAIRES. CARACTERISATION PAR MÉTHODES ÉLECTROCHIMIQUES*.

(48) Banerjee, S.; Dionysiou, D. D.; Pillai, S. C. Self-Cleaning Applications of TiO_2 by Photo-Induced Hydrophilicity and Photocatalysis. *Applied Catalysis B: Environmental*. Elsevier B.V. October 1, **2015**, pp 396–428. https://doi.org/10.1016/j.apcatb.2015.03.058.

(49) Parashar, M.; Shukla, V. K.; Singh, R. Metal Oxides Nanoparticles via Sol–Gel Method: A Review on Synthesis, Characterization and Applications. *Journal of Materials Science: Materials in Electronics*. Springer March 1, **2020**, pp 3729–3749. https://doi.org/10.1007/s10854-020-02994-8.

(50) Roy, P.; Berger, S.; Schmuki, P. TiO_2 Nanotubes: Synthesis and Applications. *Angewandte Chemie - International Edition*. March 21, **2011**, pp 2904–2939. https://doi.org/10.1002/anie.201001374.

(51) Lakshmi, B. B.; Dorhout, P. K.; Martin, C. R. Sol-Gel Template Synthesis of Semiconductor Nanostructures. *Chemistry of materials* **1997**, *9* (3), 857–862.

(52) Wang, K.; Wei, M.; Morris, M. A.; Zhou, H.; Holmes, J. D. Mesoporous Titania Nanotubes: Their Preparation and Application as Electrode Materials for Rechargeable Lithium Batteries. *Advanced Materials* **2007**, *19* (19), 3016–3020. https://doi.org/10.1002/adma.200602189.

(53) Liu, S. M.; Gan, L. M.; Liu, L. H.; Zhang, W. D.; Zeng, H. C. Synthesis of Single-Crystalline TiO_2 Nanotubes. *Chemistry of Materials* **2002**, *14* (3), 1391–1397. https://doi.org/10.1021/cm0115057.

(54) Zhang, M.; Bando, Y.; Wada, K. Sol-Gel Template Preparation of TiO_2 Nanotubes and Nanorods. *J Mater Sci Lett* **2001**, *20*, 167–170.

(55) Siwińska-Stefańska, K.; Zdarta, J.; Paukszta, D.; Jesionowski, T. The Influence of Addition of a Catalyst and Chelating Agent on the Properties of Titanium Dioxide Synthesized via the Sol–Gel Method. *J Solgel Sci Technol* **2015**, *75* (2), 264–278. https://doi.org/10.1007/s10971-015-3696-2.

(56) Lgaustic, A.; Babonneau, F.; Livage, J. Structural Investigation of the Hydrolysis-Condensation of Titanium Alkoxides $Ti(OR)_4$ (OR = OPri, OEt) Modified by Acetylacetone. 1. Study of the Alkoxide. *American Chemical Society* **1989**, *1* (9), 257.

(57) Hulteen, J. C. A General Template-Based Method for the Preparation of Nanomaterials. *J Mater Chem* **1997**, *7* (7), 1075–1087. https://doi.org/10.1039/a700027h.

(58) Choi, J.; Park, H.; Hoffmann, M. R. Effects of Single Metal-Ion Doping on the Visible-Light Photoreactivity of TiO_2. *Journal of Physical Chemistry C* **2010**, *114* (2), 783–792. https://doi.org/10.1021/jp908088x.

(59) Cheng, X.; Yu, X.; Xing, Z. Characterization and Mechanism Analysis of N Doped TiO_2 with Visible Light Response and Its Enhanced Visible Activity. *Appl Surf Sci* **2012**, *258* (7), 3244–3248. https://doi.org/10.1016/j.apsusc.2011.11.072.

(60) Natacha KRINS. Films Minces Mesoporeux d'oxydes Mixtes de Vanadium et de Niobium Comme Électrode Positive Pour Accumulateurs Au Lithium, **2009**.

(61) Brisou, A. Synthèse d'oxydes Mixtes Par Sol-Gel Non Hydrolytique : Vers Le Design de Nouveaux Catalyseurs Adaptés à La Conversion de Composés Biosourcés, **2017**. https://theses.hal.science/tel-01647124.

(62) Pabón, E.; Retuert, J.; Quijada, R.; Zarate, A. TiO_2-SiO_2 Mixed Oxides Prepared by a Combined Sol-Gel and Polymer Inclusion Method. *Microporous and Mesoporous Materials* **2004**, *67* (2–3), 195–203. https://doi.org/10.1016/j.micromeso.2003.10.017.

(63) Nguyen, T. V.; Yang, O. B. Photoresponse and AC Impedance Characterization of TiO_2-SiO_2 Mixed Oxide for Photocatalytic Water Decomposition. In *Catalysis Today*; **2003**; Vol. 87, pp 69–75. https://doi.org/10.1016/j.cattod.2003.10.014.

(64) Babyszko, A.; Wanag, A.; Sadłowski, M.; Kusiak-Nejman, E.; Morawski, A. W. Synthesis and Characterization of SiO_2/TiO_2 as Photocatalyst on Methylene Blue Degradation. *Catalysts* **2022**, *12* (11). https://doi.org/10.3390/catal12111372.

(65) Chen, Y.; Tang, X.; Gao, X.; Zhang, B.; Luo, Y.; Yao, X. Antimicrobial Property and Photocatalytic Antibacterial Mechanism of the TiO_2-Doped SiO_2 Hybrid Materials under Ultraviolet-Light Irradiation and Visible-Light Irradiation. *Ceram Int* **2019**, *45* (12), 15505–15513. https://doi.org/10.1016/j.ceramint.2019.05.054.

(66) Ting, P. K.; Hussain, Z.; Cheong, K. Y. Synthesis and Characterization of Silica-Titania Nanocomposite via a Combination of Sol-Gel and Mechanochemical Process. *J Alloys Compd* **2008**, *466* (1–2), 304–307. https://doi.org/10.1016/j.jallcom.2007.11.026.

(67) Li, Q.; Dong, P. Preparation of Nearly Monodisperse Multiply Coated Submicrospheres with a High Refractive Index. *J Colloid Interface Sci* **2003**, *261* (2), 325–329. https://doi.org/10.1016/S0021-9797(03)00060-2.

(68) Uguina, M. A.; Serrano, D. P.; Ovejero, G.; Van Grieken, R.; Camacho, M. Preparation of TS-1 by Wetness Impregnation of Amorphous SiO_2-TiO_2 Solids: Influence of the Synthesis Variables. *Appl Catal A Gen* **1995**, *124*, 391–408.

(69) Debecker, D. P.; Bouchmella, K.; Delaigle, R.; Eloy, P.; Poleunis, C.; Bertrand, P.; Gaigneaux, E. M.; Mutin, P. H. One-Step Non-Hydrolytic Sol-Gel Preparation of Efficient V_2O_5-TiO_2 Catalysts for VOC Total Oxidation. *Appl Catal B* **2010**, *94* (1–2), 38–45. https://doi.org/10.1016/j.apcatb.2009.10.018.

(70) Cheng, P.; Zheng, M.; Jin, Y.; Huang, Q.; Gu, M. Preparation and Characterization of Silica-Doped Titania Photocatalyst through Sol-Gel Method. *Mater Lett* **2003**, *57* (20), 2989–2994. https://doi.org/10.1016/S0167-577X(02)01409-X.

(71) Klein, S.; Thorimbert, S.; Maier, W. F. Amorphous Microporous Titania-Silica Mixed Oxides: Preparation, Characterization, and Catalytic Redox Properties. *J Catal* **1996**, *163*, 476–488.

(72) Anderson, C.; Bard, A. J. An Improved Photocatalyst of TiO_2/SiO_2 Prepared by a Sol-Gel Synthesis. *J. Phys. Chem* **1995**, *99*, 9882–9885.

(73) C L A R K , † Q I N G Y A N G , A N D M A R, S. A. Enhanced Photocatalytic Performance of Titania-Based Binary Metal Oxides: TiO_2/SiO_2 and TiO_2/ZrO_2. *Environ. Sci. Technol.* **1996**, *30*, 647–653.

(74) Nabih, S.; Shalan, A. E.; Serea, E. S. A.; Goda, M. A.; Sanad, M. F. Photocatalytic Performance of TiO_2@SiO_2 Nanocomposites for the Treatment of Different Organic Dyes. *Journal of Materials Science: Materials in Electronics* **2019**, *30* (10), 9623–9633. https://doi.org/10.1007/s10854-019-01296-y.

(75) Makuła, P.; Pacia, M.; Macyk, W. How To Correctly Determine the Band Gap Energy of Modified Semiconductor Photocatalysts Based on UV-Vis Spectra. *Journal of Physical Chemistry Letters*. American Chemical Society December 6, **2018**, pp 6814–6817. https://doi.org/10.1021/acs.jpclett.8b02892.

(76) Drault, F.; Eloy, P.; Demoustier-Champagne, S.; Hermans, S. Facile Fabrication of Au/SiO_2 Nanostructures from 1D to 3D Nanotubes Networks Using Templating Methods. *Catal Today* **2024**, *429*. https://doi.org/10.1016/j.cattod.2023.114472.

(77) Abdullahi, S. S.; Güner, S.; Musa, I. M. *Sımple Method For The Determınatıon of Band Gap of a Nanopowdered Sample Usıng Kubelka Munk Theory*; **2016**. https://www.researchgate.net/publication/305810656.

(78) Wu, L.; Yang, X.; Li, J.; Huang, Y.; Li, X. Fabrication of Titanium Dioxide Nanotubes with Good Morphology at High Calcination Temperature and Their Photocatalytic Activity. *Mater Chem Phys* **2017**, *202*, 136–142. https://doi.org/10.1016/j.matchemphys.2017.09.022.

(79) Abrahams, S. C.; Bernstein, J. L. Rutile: Normal Probability Plot Analysis and Accurate Measurement of Crystal Structure. *J Chem Phys* **1971**, *55* (7), 3300–3307. https://doi.org/10.1063/1.1676569.

(80) Weirich, T. E.; Winterer, M.; Seifried, S.; Hahn, H.; Fuess, H. Rietveld Analysis of Electron Powder Diffraction Data from Nanocrystalline Anatase, TiO_2. *Ultramicroscopy* **2000**, *81*, 263–270.

(81) Rodríguez-Carvajal, J. *Study of Micro-Structural Effects by Powder Diffraction Using the Program FULLPROF*.

(82) Ohno, T.; Sarukawa, K.; Tokieda, K.; Matsumura, M. Morphology of a TiO_2 Photocatalyst (Degussa, P-25) Consisting of Anatase and Rutile Crystalline Phases. *J Catal* **2001**, *203* (1), 82–86. https://doi.org/10.1006/jcat.2001.3316.

(83) Zhang, H.; Song, X.; Zhang, B.; Liu, G.; Hu, G.; Xiao, C.; Wei, Z.; Zheng, Y. The Research of Photocatalytic Activity on Si Doped TiO_2 Nanotubes. *Mater Lett* **2017**, *188*, 66–68. https://doi.org/10.1016/j.matlet.2016.10.097.

(84) Viet, P. Van; Huy, T. H.; You, S. J.; Hieu, L. Van; Thi, C. M. Hydrothermal Synthesis, Characterization, and Photocatalytic Activity of Silicon Doped TiO_2 Nanotubes. *Superlattices Microstruct* **2018**, *123*, 447–455. https://doi.org/10.1016/j.spmi.2018.09.035.

(85) Maryama, H.; Abbassi, A. Comparative Study of Accurate Experimentally Determined and Calculated Band Gap of Amorphous ZnO Layers. *Materials Letters*. Elsevier B.V. March 1, **2016**, pp 206–209. https://doi.org/10.1016/j.matlet.2015.12.073.

(86) De Mello Donegá, C. Nanoparticles: Workhorses of Nanoscience. *Nanoparticles: Workhorses of Nanoscience* **2014**, *9783662448236*, 1–299. https://doi.org/10.1007/978-3-662-44823-6.

(87) Vijayalakshmi, R.; Rajendran, V. Synthesis and Characterization of Nano-TiO_2 via Different Methods. *Scholars Research Library Archives of Applied Science Research* **2012**, *4* (2), 1183–1190.

(88) Reyes-Coronado, D.; Rodríguez-Gattorno, G.; Espinosa-Pesqueira, M. E.; Cab, C.; De Coss, R.; Oskam, G. Phase-Pure TiO_2 Nanoparticles: Anatase, Brookite and Rutile. *Nanotechnology* **2008**, *19* (14). https://doi.org/10.1088/0957-4484/19/14/145605.

(89) Gao, L.; Zhang, Q. EFFECTS OF AMORPHOUS CONTENTS AND PARTICLE SIZE ON THE PHOTOCATALYTIC PROPERTIES OF TiO_2 NANOPARTICLES. *Scripta mater* **2001**, *44*, 1195–1198.

(90) Sun, S.; Song, P.; Cui, J.; Liang, S. Amorphous TiO_2 Nanostructures: Synthesis, Fundamental Properties and Photocatalytic Applications. *Catalysis Science and Technology*. Royal Society of Chemistry **2019**, pp 4198–4215. https://doi.org/10.1039/c9cy01020c.

(91) Fatimah, I.; Prakoso, N. I.; Sahroni, I.; Musawwa, M. M.; Sim, Y. L.; Kooli, F.; Muraza, O. Physicochemical Characteristics and Photocatalytic Performance of TiO_2/SiO_2 Catalyst Synthesized Using Biogenic Silica from Bamboo Leaves. *Heliyon* **2019**, *5* (11). https://doi.org/10.1016/j.heliyon.2019.e02766.

(92) Di Paola, A.; Bellardita, M.; Palmisano, L.; Barbieriková, Z.; Brezová, V. Influence of Crystallinity and OH Surface Density on the Photocatalytic Activity of TiO_2 Powders. *J Photochem Photobiol A Chem* **2014**, *273*, 59–67. https://doi.org/10.1016/j.jphotochem.2013.09.008.

Appendix

A.1. Membrane holder 1 cm², membrane and solutions

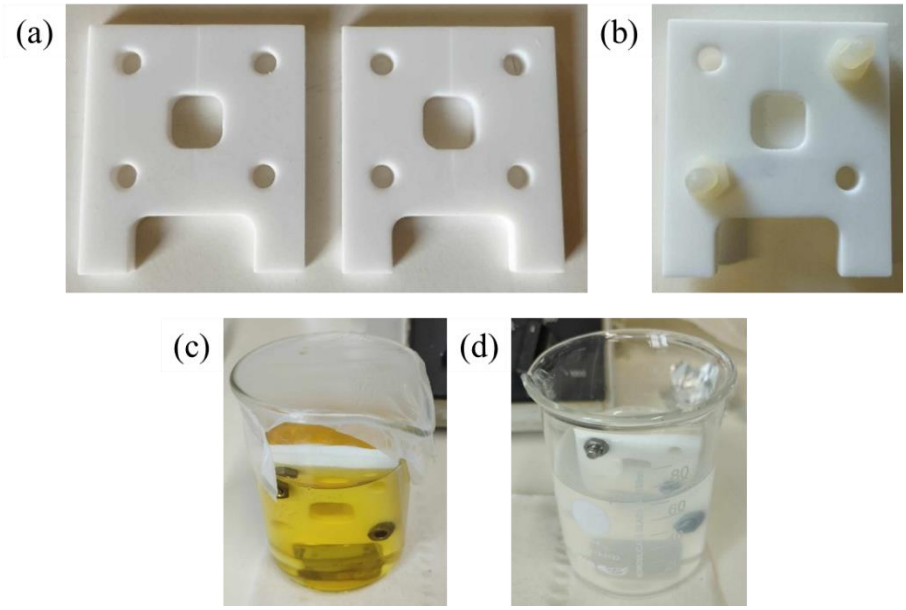

Appendix 1*: (a) Membrane holders for 1 cm² membranes, (b) Membrane holder with PC membrane inside, (c) Membrane holder with membrane in a solution containing the TiO_2 precursor and (d) Membrane holder with membrane in a solution containing the SiO_2 precursor.*

A.2. Membrane holder 25 cm² (5 cm x 5 cm)

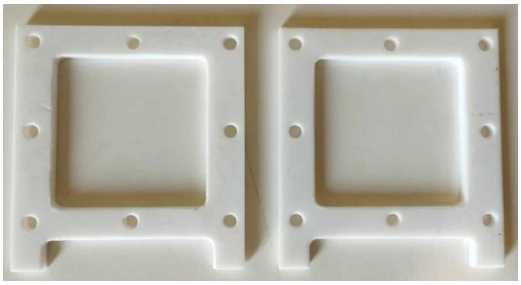

Appendix 2*: Membrane holders for 25 cm² (5 cm x 5 cm) membranes.*

A.3. Spectrum of the lamp (OSL2IR) used for catalytic tests

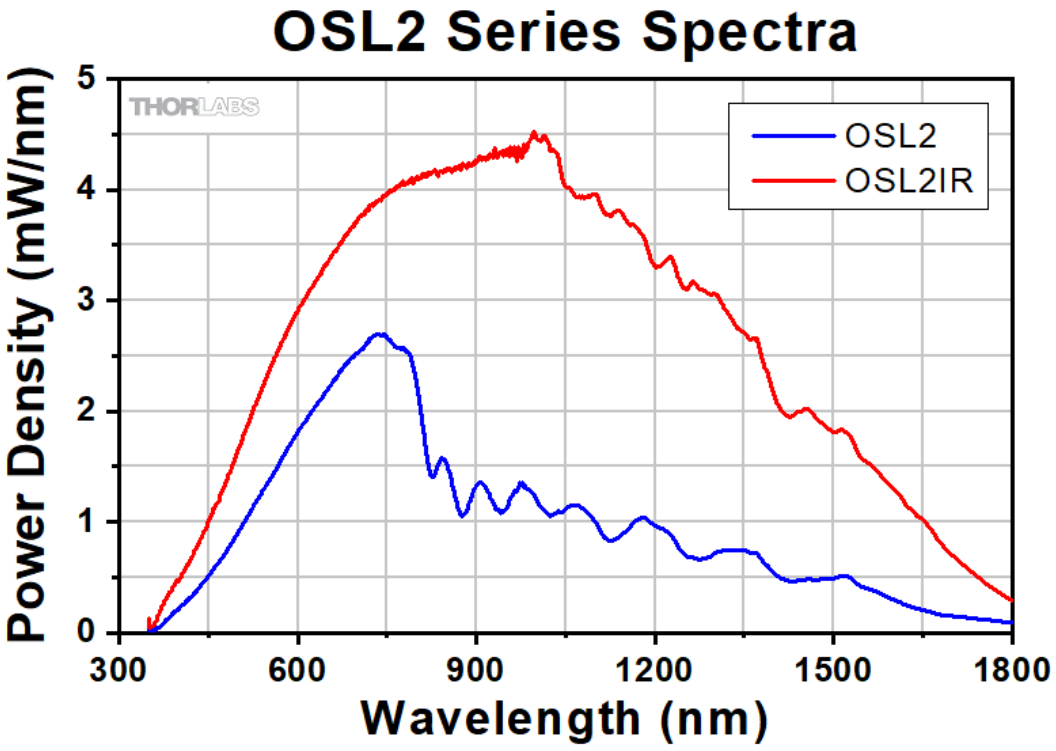

µ

***Appendix 3**: Spectrum of the OSL2IR lamp used for the catalytic tests (red line).*

A.4. SEM image of the filled PC membranes on which the thickness of the TiO_2 nanotubes was measured for different impregnation times

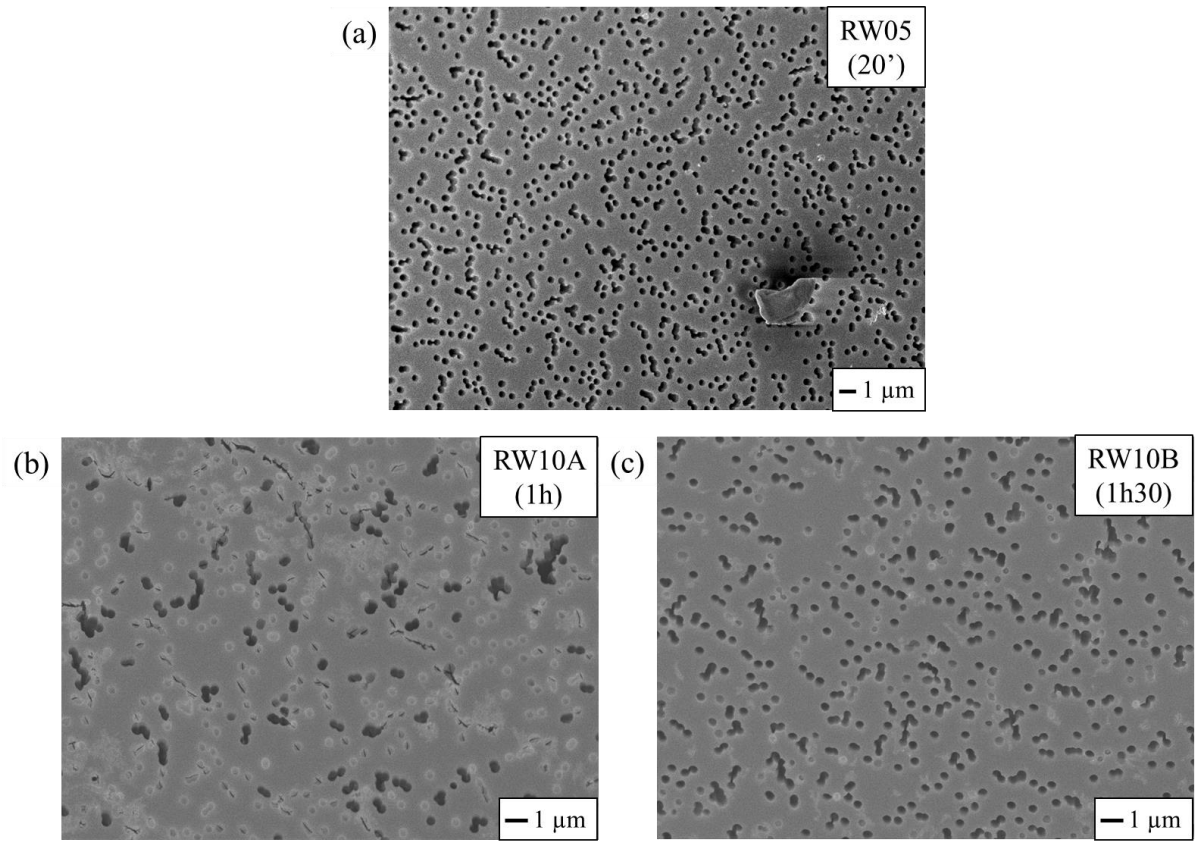

Appendix 4*: SEM images of PC membranes filled with TiO_2 nanotubes for reaction conditions consisting of 2 h ageing of the solution to form the gel and (a) 20 min., (b) 1 h and (c) 1 h 30 impregnation of the template in a solution of molar ratio: EtOH:ACAC:TTIP:H_2O=20:1:1:5.*

A.5. Refinement between the experimental pattern and the sum of the theoretical patterns for anatase and rutile

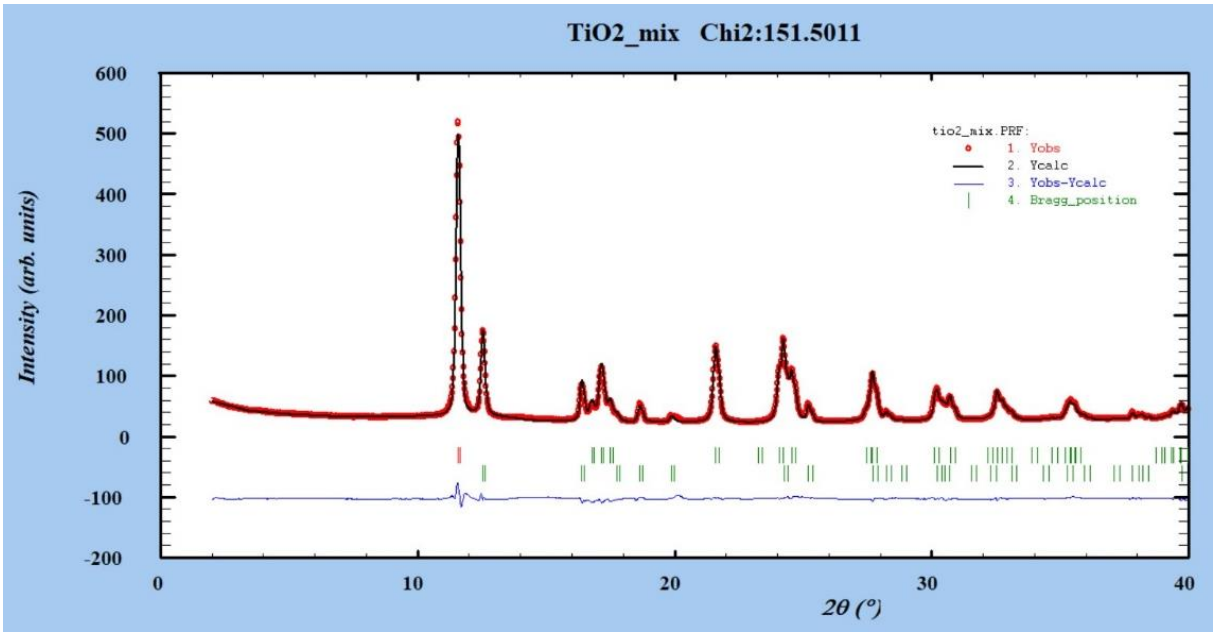

***Appendix 5**: Red = experimental diffractogram obtained on calcined TiO_2 NTs powder, black = theoretical diffractogram obtained from refinement by varying the percentage of anatase and rutile in the TiO_2 compound, green = position of the diffraction peaks (Bragg position) and blue = difference between the experimental data and the predicted refined diffractogram.*

A.6. EDX on 1D NTs of 3 different SiO_2:TiO_2 mixed oxide ratios synthesised by synthesis method 1 (ageing of the two solutions containing the two precursors independently of each other)

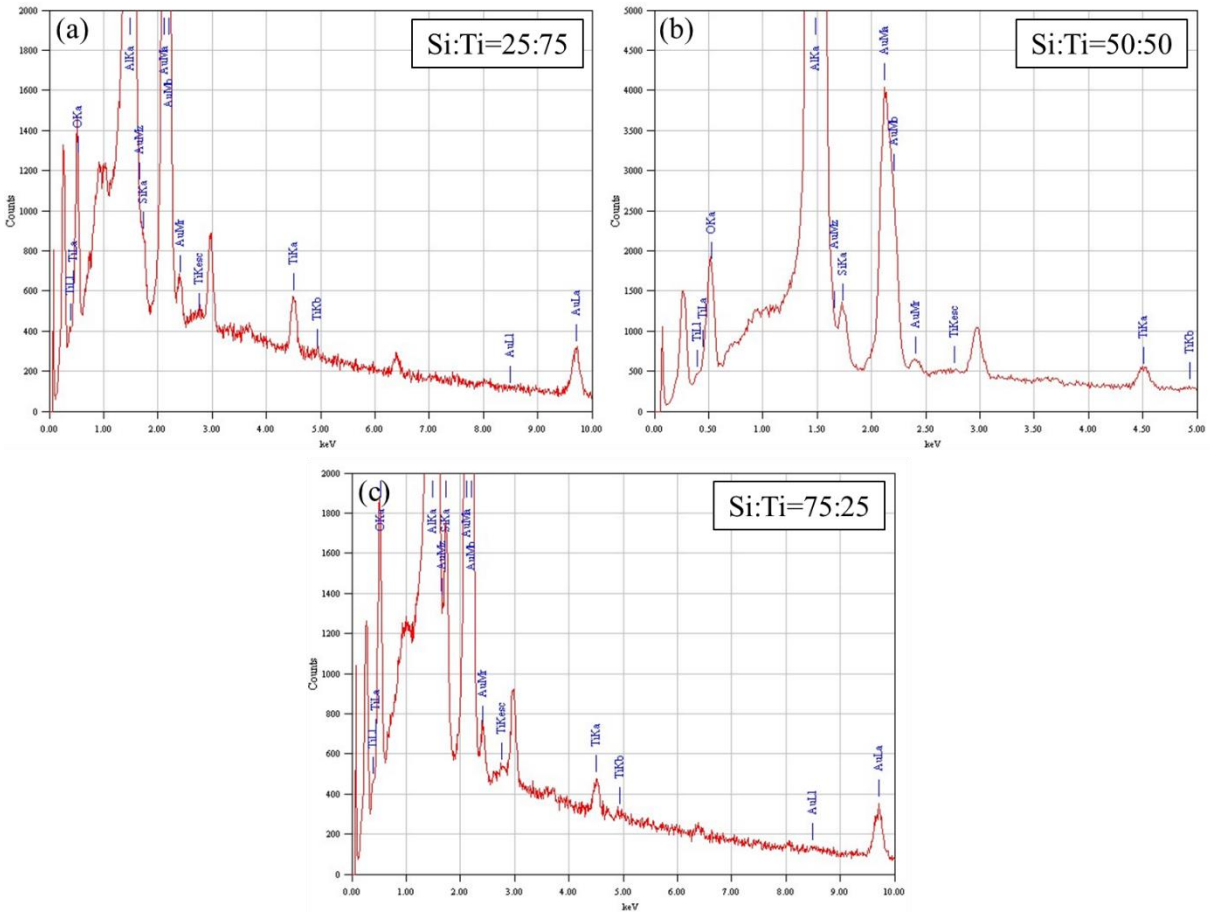

Appendix 6*: EDX results for mixed oxide 1D NTs prepared using synthesis method 1: (a) Si:Ti=25:75, (b) Si:Ti=50:50 and (c) Si:Ti=75:25.*

A.7. XPS analysis of TiO_2 and the different mixed oxides with different compositions

The decomposition of the O and C peaks was used to determine the number of oxygen atoms bound to Si and Ti. The calculated ratio between O and Si + Ti (based on atomic percentages) is equal to 1.5-1.7, varying according to the mixed oxides considered. This ratio, close to a value of 2, is consistent with the formation of a Si and Ti oxide network of the SiO_2-TiO_2 type.

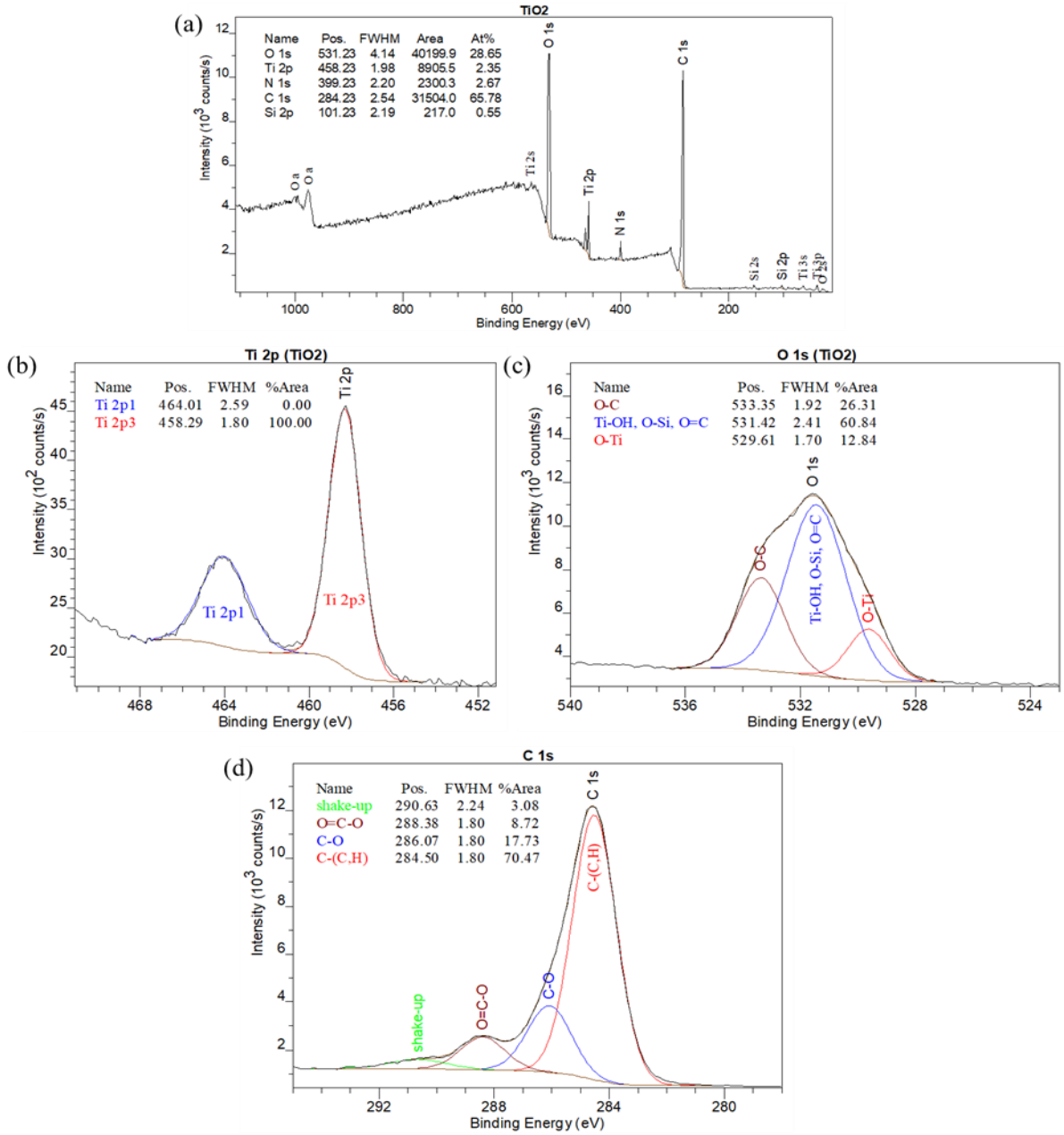

***Appendix 7.(A)**: (a) XPS spectrum of TiO_2, (b) zoom on the Ti 2p peak and zoom + decomposition of the (c) O and (d) C peaks.*

Ti is quantified on the basis of the Ti 2p3 peak using a RSF (Relative Sensitivity Factors) of 5.22, taking into account the fact that we are only taking into account the Ti 2p3 peak and not the Ti 2p1 peak.

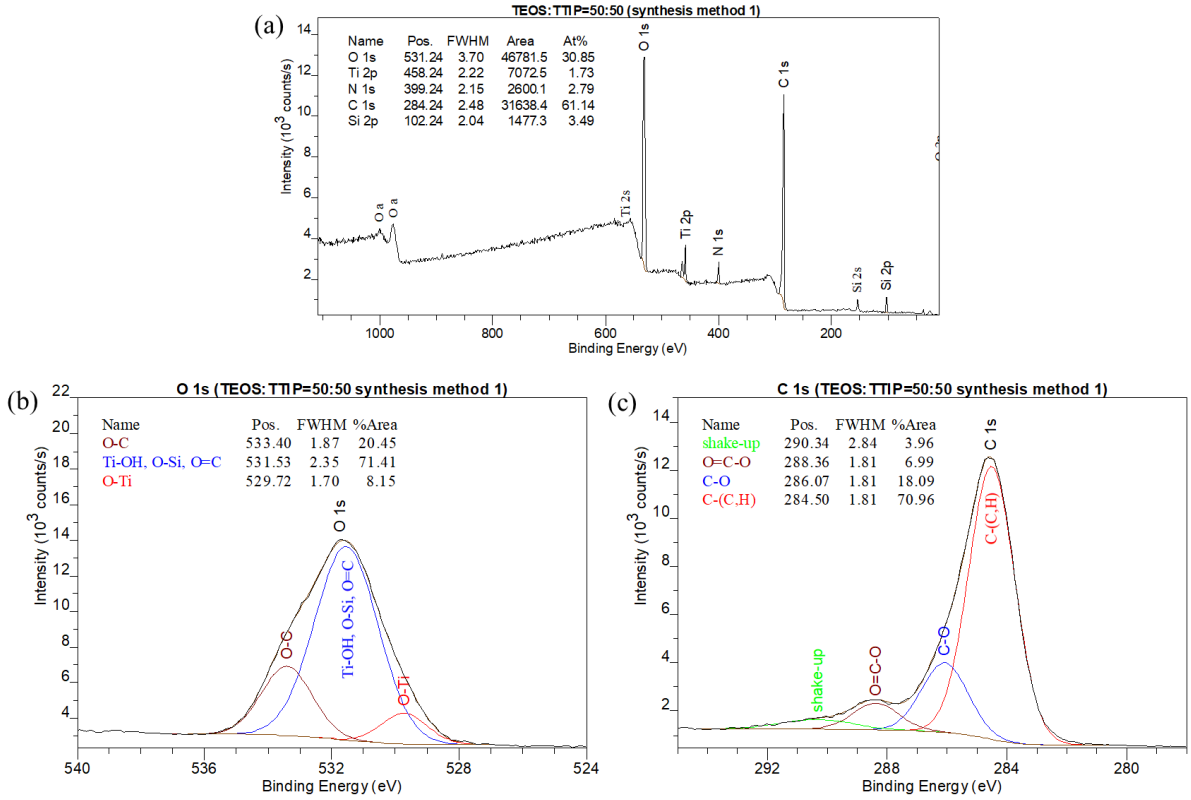

***Appendix 7.(B)**: (a) XPS spectrum and decomposition of the (b) O and (c) C peaks for the mixed oxide TEOS:TTIP=50:50 using synthesis method 1.*

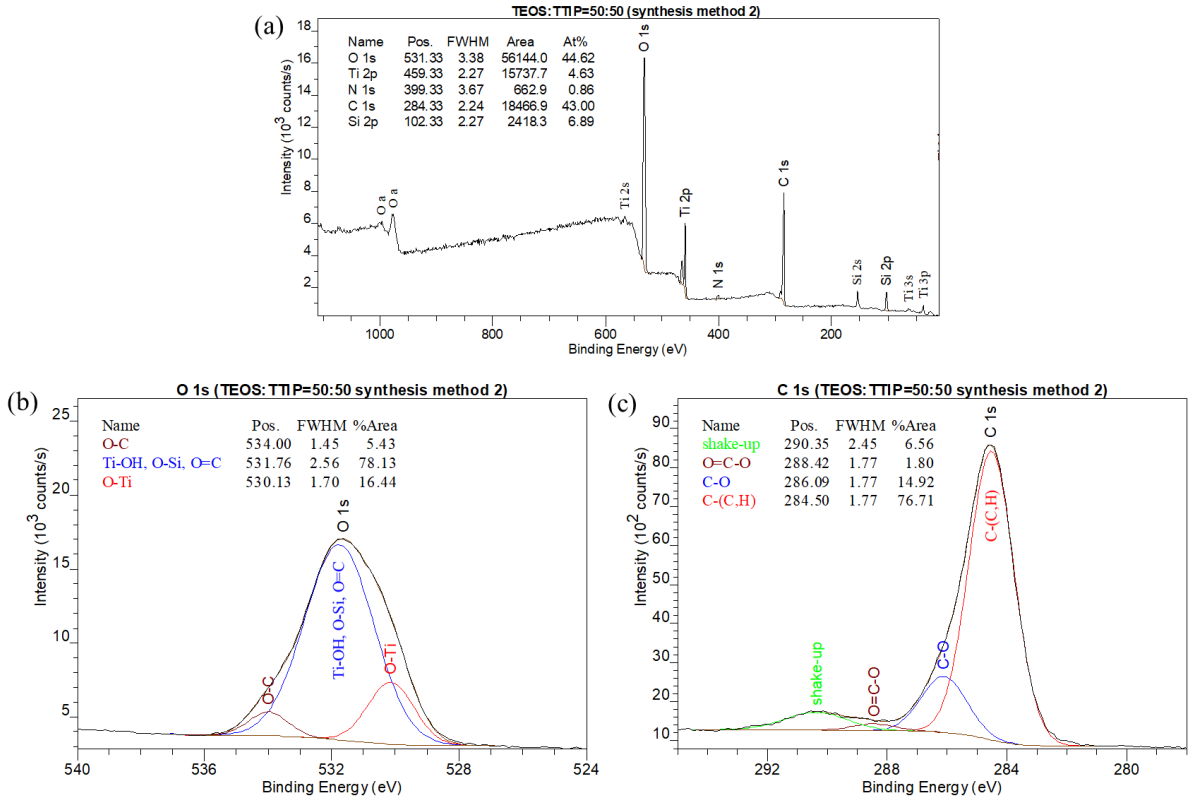

***Appendix 7.(C)**: (a) XPS spectrum and decomposition of the (b) O and (c) C peaks for the mixed oxide TEOS:TTIP=50:50 using synthesis method 2.*

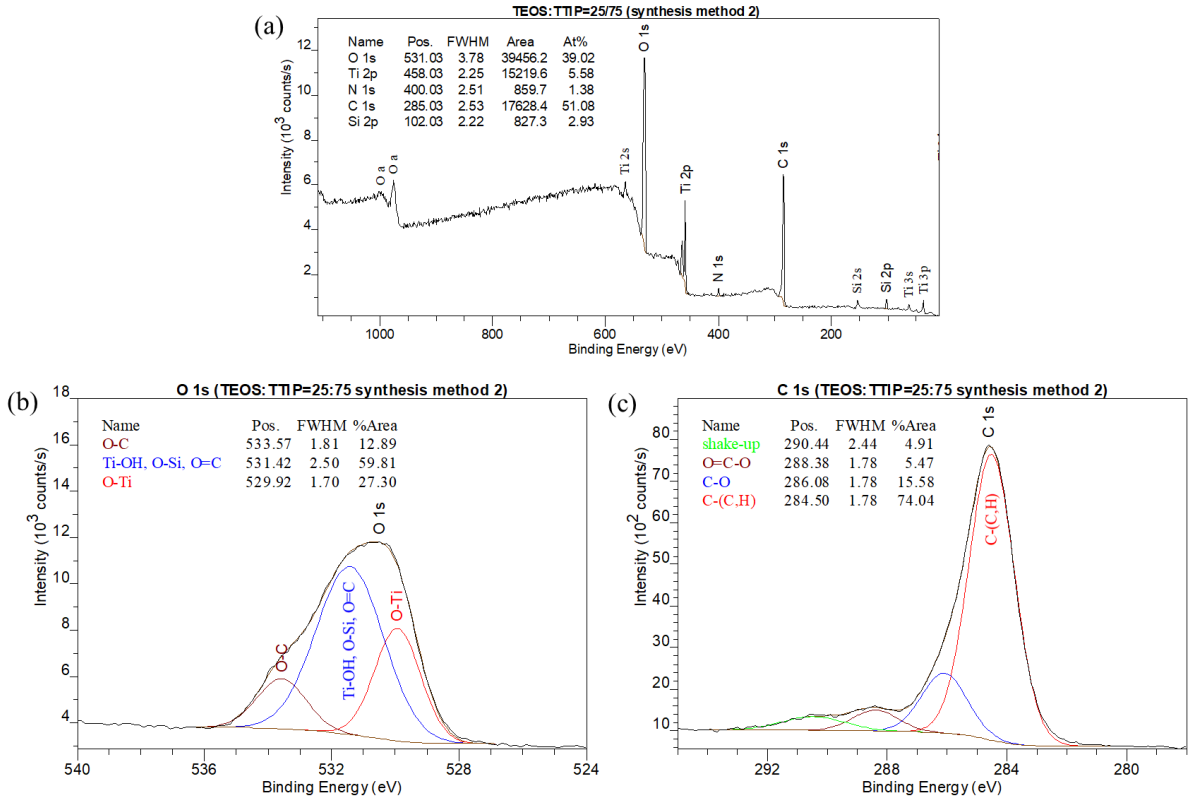

***Appendix 7.(D)**: (a) XPS spectrum and decomposition of the (b) O and (c) C peaks for the mixed oxide TEOS:TTIP=25:75 using synthesis method 2.*

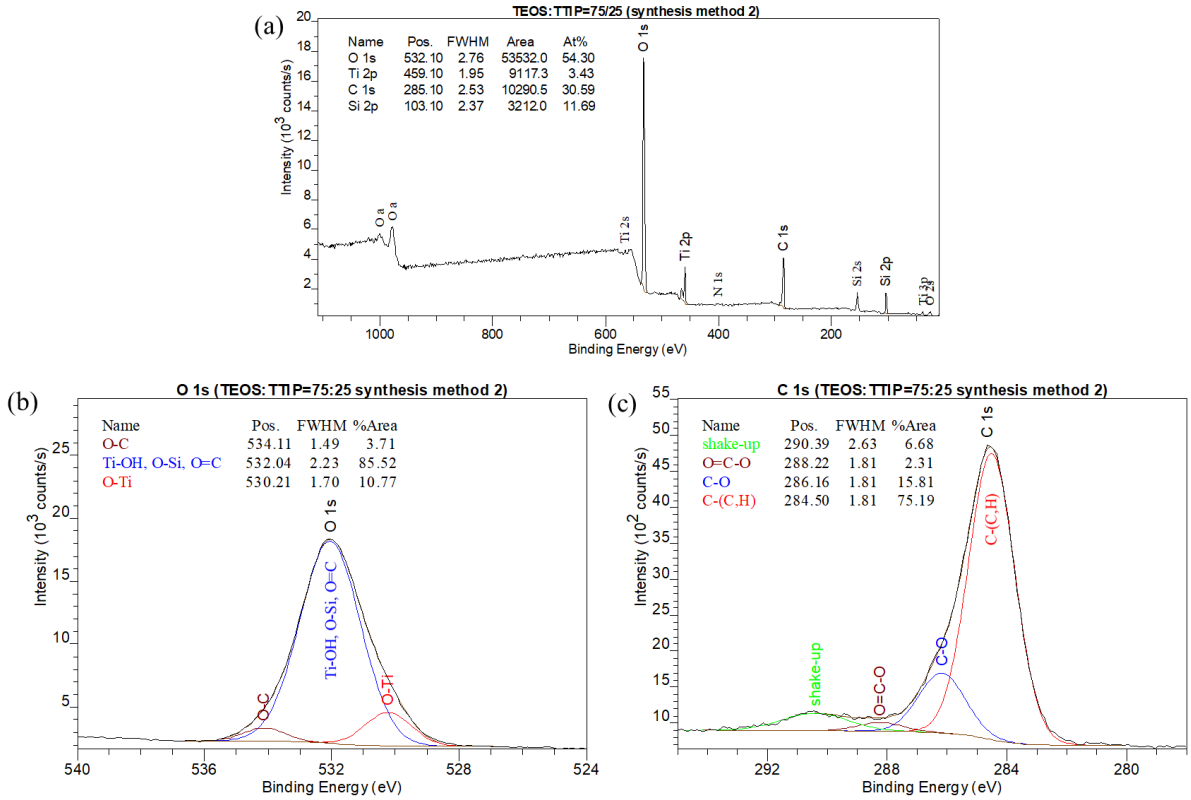

***Appendix 7.(E)**: (a) XPS spectrum and decomposition of the (b) O and (c) C peaks for the mixed oxide TEOS:TTIP=75:25 using synthesis method 2.*

The nitrogen present in all the analyses comes from the PVP treatment carried out on the PET used to release the nanotubes for analysis.

A.8. EDX on 3D membranes of interconnected NTs for 4 different compositions of synthesised SiO_2:TiO_2 mixed oxides

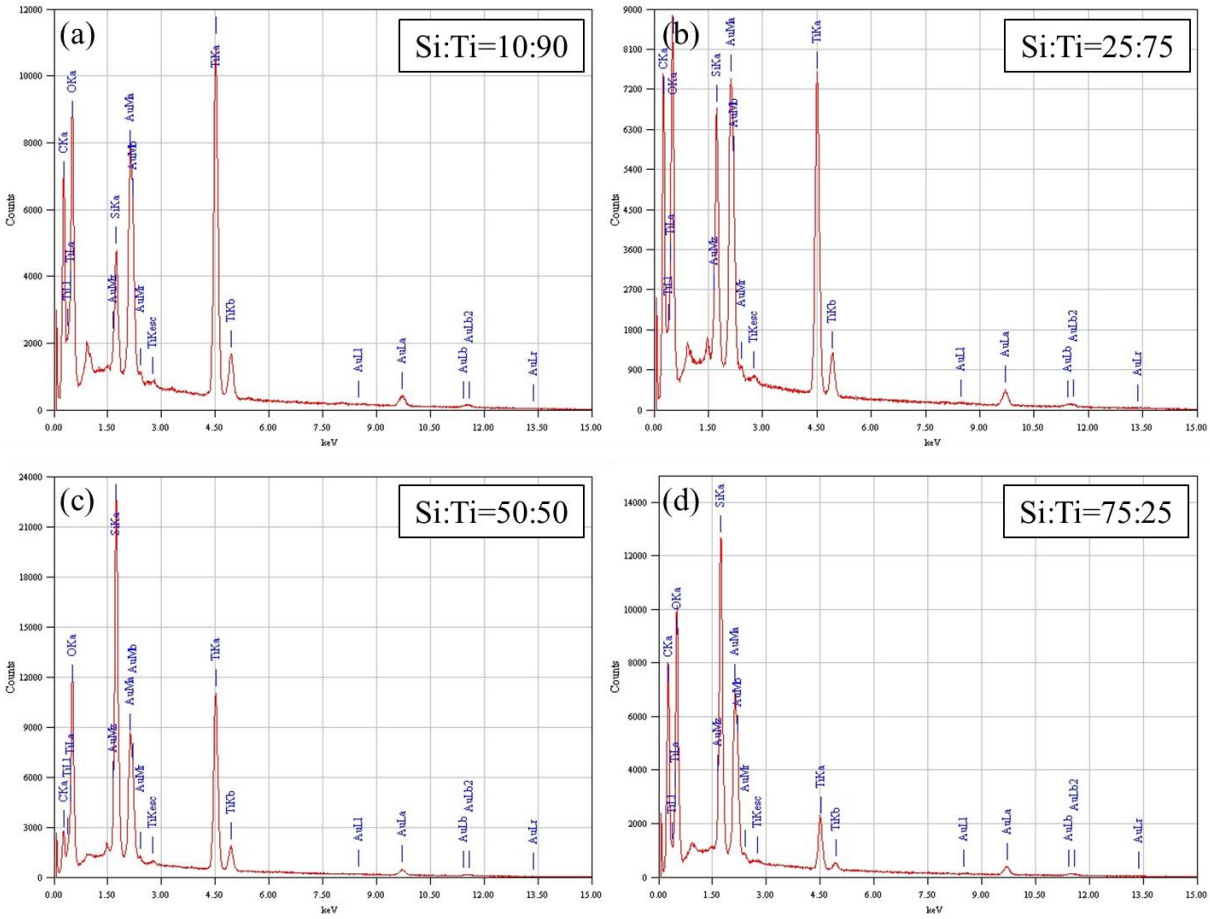

***Appendix 8**: EDX results for 3D membrane of interconnected NTs for different mixed oxide ratios: (a) Si:Ti=10:90, (b) Si:Ti=25:75, (c) Si:Ti=50:50 and (d) Si:Ti=75:25.*

A.9. Graphical construction for the determination of 3D materials bandgaps

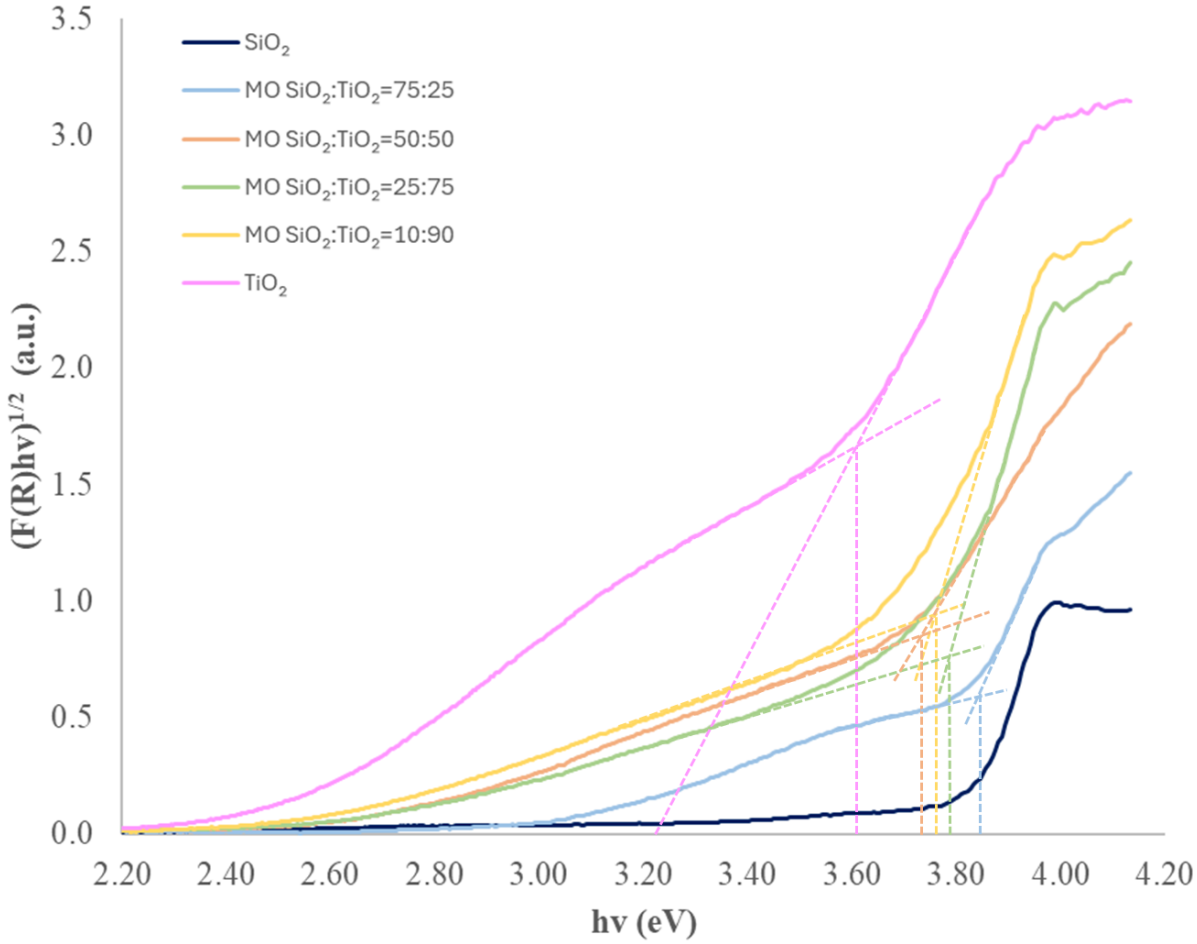

***Appendix 9**: Transformed reflectance spectrum of SiO_2, MO SiO_2:TiO_2=75:25, MO SiO_2:TiO_2=50:50, MO SiO_2:TiO_2=25:75, MO SiO_2:TiO_2=10:90, TiO_2 samples and graphical construction for bandgap determination.*

A.10. Reproducibility test for continuous flow catalytic tests

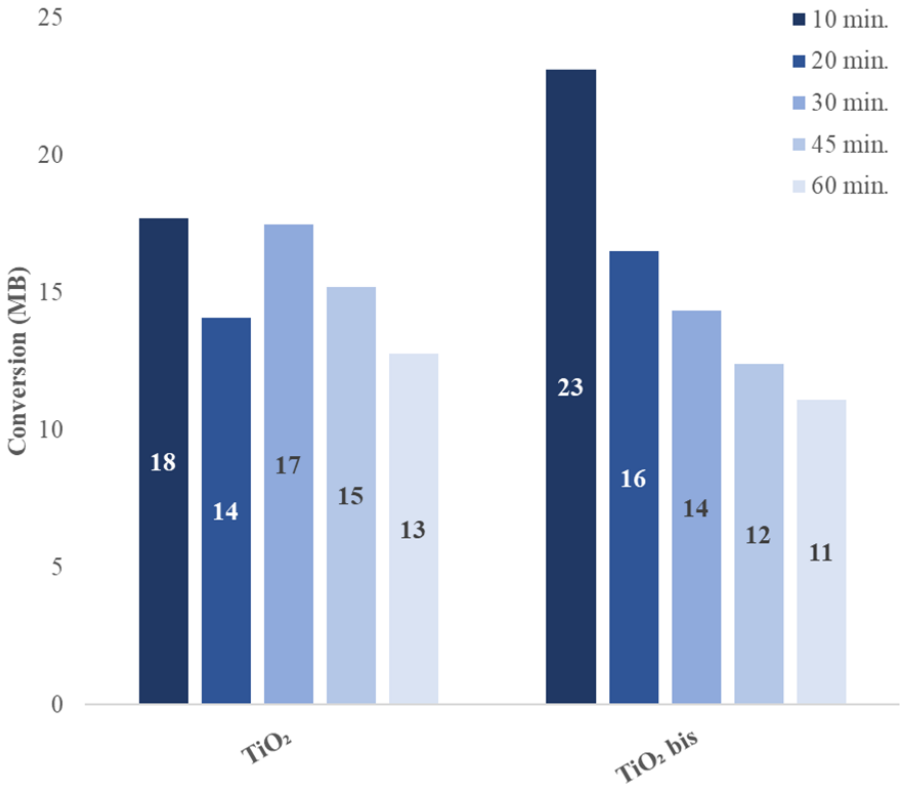

***Appendix 10**: MB conversion (%) after 10, 20, 30, 45 and 60 min. for two tests carried out in continuous flow using identical conditions on pure TiO_2 NTs released on PET and with an aqueous MB solution of 5 mg.L^{-1}.*

UNIVERSITÉ CATHOLIQUE DE LOUVAIN
Faculté des sciences
Place des sciences, 2 bte L6.06.01, 1348 Louvain-la-Neuve, Belgique | **www.uclouvain.be/sc**